

# **LIGHT STRUCTURING FOR MASSIVELY PARALLEL OPTICAL TRAPPING**

THÈSE N° 3939 (2007)

PRÉSENTÉE LE 9 NOVEMBRE 2007

À LA FACULTÉ DES SCIENCES ET TECHNIQUES DE L'INGÉNIEUR  
LABORATOIRE D'OPTIQUE APPLIQUÉE  
PROGRAMME DOCTORAL EN PHOTONIQUE

ÉCOLE POLYTECHNIQUE FÉDÉRALE DE LAUSANNE

POUR L'OBTENTION DU GRADE DE DOCTEUR ÈS SCIENCES

PAR

**Johann ROHNER**

ingénieur en microtechnique diplômé EPF  
de nationalité suisse et originaire de Teufen (AR)

acceptée sur proposition du jury:

Prof. O. Martin, président du jury  
Prof. R. Salathé, Dr J.-M. Fournier, directeurs de thèse  
Prof. K. Dholakia, rapporteur  
Dr T. Grzegorzczuk, rapporteur  
Prof. P. Jacquot, rapporteur



ÉCOLE POLYTECHNIQUE  
FÉDÉRALE DE LAUSANNE

Suisse  
2007



---

# Abstract

## Abstract

Optical trapping, discovered in the 70's, allows moving and stabilizing small objects which sizes varies from atoms to particles of several microns. This technique, based on momentum conservation, is particularly well suited for manipulating biological matter (cells, organelles, vesicles, functionalized particles, etc.) and offers interesting potentialities for research in biotechnologies and biochemistry. The possibility to individually immobilize large numbers of microscopic objects opens new ways for the downscaling of analysis tools for drug screening, particles sorting or assessing statistical data. The combination of optical trapping with microfluidics greatly increases the prospect of the method.

This PhD work takes place in a research aiming at creating large arrays of optical traps compatible with microfluidic devices in order to realize so-called *lab-on-a-chip*. These miniaturized systems allow recreating at smaller time scale, reduced resources and lower cost, experiments usually performed in a macroscopic environment. This study proposes solutions based on light interference and on landscaping of light intensity. Setups combining several laser beams are proposed to create **interference patterns** and various configuration of light potential wells. Increasing the number of interfering beams, in particular by using a **multiple beams interferometer** (Fizeau-Tolansky interferometer) leads to a raise of the light intensity gradient, further increasing the trapping efficiency. The quality of the optical traps is studied and discussed in comparison with conventional laser tweezers. More complex and original solutions using interference of electromagnetic fields are suggested. Namely, the light diffracted by the objects themselves is used to form new potential wells. Diffractive structures are devised to generate three-dimensional arrays of traps. The periodicity of those planar structures creates a self-imaging phenomenon, known as **Talbot effect**. The modulation of the field in the Fresnel zone, i.e. some tens of micrometers behind the diffractive element, reveals interesting properties for optical trapping, in particular local intensity amplification and gradient enhancement.

When several particles are simultaneously immersed in an electromagnetic field, interaction effects arise, that link the particles. This phenomenon of **optical binding**, is studied and demonstrated here in the case of bi-dimensional optical crystals.

# Keywords

## Optical Forces

- Optical trapping
- Laser tweezers
- Multiple Traps
- Optical traps arrays
- Optical Binding
- Optical matter
- Self-assembly
- Optical crystals

## Interference

- Interference pattern
- Multiple beam interferometer
- Fizeau-Tolansky fringes
- Light modelling

## Diffraction

- Fresnel diffraction
- Talbot effect
- Self-imaging
- Diffractive structures

## Lab-on-a-chip

- Lab-on-a-chip
- $\mu$ -TAS (micro-Total Analysis System)
- Microfluidics
- PDMS chip (Polydimethylsiloxane)
- Bio-chemical reactions

## Résumé

Le piégeage optique, découvert en 1970, permet de déplacer et de stabiliser des objets très divers allant de l'atome à des particules de plusieurs micromètres, en se basant sur la conservation du moment. Cette technique est particulièrement adaptée pour la manipulation d'objets biologiques (cellules, organelles, vésicules, particules synthétiques fonctionnalisées,...) et offre de séduisantes potentialités pour la recherche en biotechnologie et en biochimie. La possibilité d'immobiliser individuellement un nombre important d'objets microscopiques à analyser ouvre la voie à une miniaturisation des systèmes d'analyse pour le triage de particules, le dépistage de produits pharmaceutiques ou la collection d'informations statistiques. L'association du piégeage optique et de la microfluidique augment considérablement les atouts de la méthode.

Ce travail de doctorat s'inscrit dans une recherche visant la création de larges réseaux de pièges optiques compatibles avec des systèmes de microfluidique dans le but de réaliser des *"laboratoires sur puce"*. Ces systèmes miniaturisés permettent de recréer, dans des gammes de temps, de ressource et de coût nettement inférieures, des expériences exécutées aujourd'hui à l'échelle macroscopique. Cette étude propose des solutions basées sur les phénomènes d'interférence de lumière cohérente et sur l'idée d'utiliser la lumière elle-même pour créer des modulation du champ. Des montages combinant plusieurs faisceaux lasers produisant des **interférences** de formes diverses sont proposés pour créer des puits de lumière. En augmentant le nombre de faisceaux, entre autre par l'utilisation d'un **interféromètre à ondes multiples** (interferomètre de Fizeau-Tolansky), les gradients d'intensité lumineuse sont augmentés et ainsi l'efficacité de piégeage. La qualité des pièges optiques ainsi créés est étudiée et discutée en comparaison d'une pince optique classique. Des solutions plus complexes et originales mettant à profit l'interférence de champs électro-magnétiques sont avancées, notamment l'utilisation de la lumière diffractée par les objets eux-mêmes pour former de nouveaux puits de potentiel. Des structures diffractives sont élaborées pour réaliser des réseaux de pièges tridimensionnels. La périodicité de structures planes permet de générer des phénomènes d'auto-imagerie, connus sous le nom d'**effet Talbot**. La modulation du champs dans le régime de Fresnel, c'est à dire quelques dizaines de microns derrière l'élément diffractif, révèle des qualités intéressantes pour le piégeage optique, en particulier l'amplification locale du champ et l'augmentation du gradient.

Dès que plusieurs particules se trouvent immergées simultanément dans un champ électro-magnétique des effets d'interaction apparaissent liant les particules entre elles. Ce phénomène de **cohésion optique** est étudié et démontré expérimentalement dans le cas de cristaux optiques bi-dimensionnels.

# Mots Clés

## Forces optiques

- Piégeage optique
- Pinces optique
- Pièges multiples
- Réseaux de pièges optiques
- Liaisons optiques
- Matière optique
- Auto-assemblage
- Cristaux optiques

## Interferences

- Motif d'interférences
- Interféromètre à ondes multiples
- Franges de Fizeau-Tolansky
- Structuration de la lumière

## Diffraction

- diffraction de Fresnel
- Effet Talbot
- Auto-imagerie
- Structures diffractive

## Lab-on-a-chip

- Laboratoire sur puce
- $\mu$ -TAS (micro-Total Analysis System)
- Microfluidique
- Puce en silicone
- Réactions biochimiques





---

# Contents

<b>Abstract</b>	<b>iv</b>
Abstract in English . . . . .	iv
Keywords . . . . .	v
Version abrégée en français . . . . .	vi
Mots Clés . . . . .	vii
<b>Table of content</b>	<b>viii</b>
<b>1 Introduction</b>	<b>1</b>
1.1 Optical trapping . . . . .	2
1.2 State of the art . . . . .	5
1.3 Motivation . . . . .	5
1.4 Optical forces . . . . .	7
<b>2 Optical trapping in interference patterns</b>	<b>11</b>
2.1 Introduction . . . . .	12
2.2 Various types of interference . . . . .	12
2.2.1 Intensity pattern formation . . . . .	13
2.2.2 Beam configurations and optical templates . . . . .	14
2.2.3 Optical trapping in interference pattern . . . . .	17
2.2.4 Numerical simulations and trap shape optimization . . . . .	18
2.2.5 Experimental setup . . . . .	21
2.2.6 Trapping polystyrene particles . . . . .	26
2.2.7 Radiation pressure compensation . . . . .	28
2.2.8 Trapping in microfluidics . . . . .	31
2.3 Variation of trap size . . . . .	34
2.3.1 Setup modulation . . . . .	36
2.3.2 Beads behavior in various fringe sizes . . . . .	36
2.3.3 Influence of fringe's size on trapping efficiency . . . . .	38
2.3.4 Discussion on force measurements . . . . .	40
2.4 Multiple beam interference . . . . .	42
2.4.1 Generation of Fizeau-Tolansky fringes . . . . .	42
2.4.2 Experimental configurations . . . . .	45
2.4.3 Bead steering in microfluidic channel . . . . .	49
2.4.4 Discussion on multiple beam interference trapping . . . . .	50
2.5 Conclusion . . . . .	52

<b>3</b>	<b>Optical trapping in Fresnel diffraction</b>	<b>55</b>
3.1	Introduction . . . . .	56
3.2	Trapping in diffraction patterns . . . . .	56
3.2.1	Trapping in diffraction rings . . . . .	56
3.2.2	Two levels optical trapping . . . . .	57
3.3	Trapping in Talbot lattices . . . . .	60
3.3.1	The Talbot effect . . . . .	60
3.3.2	Self-imaging effect of an array of trapped particles . . . . .	64
3.3.3	Numerical simulations and creation of periodic light templates . . . . .	66
3.3.4	Three dimensional trapping in Talbot lattices . . . . .	76
3.4	Conclusion . . . . .	80
<b>4</b>	<b>Optical binding</b>	<b>83</b>
4.1	Introduction . . . . .	84
4.2	Optical binding forces and optical matter . . . . .	84
4.3	Study of self assembly . . . . .	85
4.3.1	Experimental setup . . . . .	85
4.3.2	Creation of optical crystals . . . . .	86
4.3.3	Generation of various sizes of crystals . . . . .	90
4.3.4	Beads spacing in self assembly . . . . .	91
4.4	Conclusion . . . . .	95
<b>5</b>	<b>Conclusion and Perspectives</b>	<b>97</b>
5.1	Summary and Conclusions . . . . .	98
5.2	Perspectives . . . . .	99
	<b>Acknowledgements</b>	<b>102</b>
	<b>Appendix</b>	<b>104</b>
A	Lab-on-a-chip . . . . .	106
A.1	State of the art . . . . .	106
A.2	Microfluidic chip fabrication . . . . .	107
A.3	Lab-on-a-chip concept . . . . .	108
B	Fresnel calculations . . . . .	110
C	Diffractive plate fabrication . . . . .	119
	<b>Bibliography</b>	<b>122</b>

*Esse ea quae rerum simulacra uocamus ;  
Quae quasi membranae summo de corpore rerum  
Dereptae uolitant ultroque citroque per auras,  
Atque eadem nobis uigilantibus obuia mentes  
Terrificant atque in somnis, cum saepe figuras*  
Lucretius - De rerume natura - Liber IV (v. 30-34)

There exist those somewhats which we call  
The images of things: these, like to films  
Scaled off the utmost outside of the things,  
Flit hither and thither through the atmosphere,  
And the same terrify our intellects,  
Coming upon us waking or in sleep  
Lucretius (98-54 BC) - Of the Nature Of Things - Book IV (v. 30-34)  
Translation: William Ellery Leonard

---

# Introduction

In the Antiquity, common believe by the philosopher -who at that time were also scientists- was that images and light could only be mechanical media, wether by the Greeks, like Aristotle, who explained the vision by a ray going out of the eye to touch and scan the objects, or by the Romans with Lucretius, who considered that images are thin physical crusts hitting the eye. Even if the theoretical explanations of physics have since changed, this poetical idea took a concrete form in 1970 when light beams were used to levitate, move, accelerate and even trap particles. Since then the technique known as *optical trapping* spread out, offering a tool to manipulate small objects, in particular biological matter. This thesis constitutes a part of a research in multiple trapping and in manipulating particles for biological and biochemical applications. Different ways to create atypical light template using interference properties are studied and presented in this dissertation. Combination of beams, use of diffracted waves in the Fresnel diffraction regime and self arrangement effects are exploited for structuring light field. All these solutions take advantage of the constructive and destructive interference effects to generate new distributions of the electromagnetic field in order to create multiple optical wells for trapping particles, differing from commonly employed optical tweezers system which require high numerical aperture microscope objectives.

## 1.1 Optical trapping

By providing an easy source of coherent light, the advent of laser in the sixties' modified in depth investigations on light properties and Physics. Thus, in 1970, Arthur Ashkin demonstrated what Kepler had predicted more than 300 years before, as well as Maxwell and Lebedew. In the 17th century, Johannes Kepler deduced from his observations of comets that sunlight exerts a force on matter, explaining why the dust tail of comets is turned away from the sun. The first demonstration of the existence of radiation pressure was realized at the beginning of the XX<sup>th</sup> century by Nichols and Hull [1]. In 1970 Arthur Ashkin evidenced the possibility to use pressure exerted by light first to levitate, then to accelerate and to trap small dielectric objects [2]. In 1986 he proposed a solution for trapping particles in a single highly focused laser coining the term *optical tweezers* [3]. This still refers today to a laser beam focused by a high numerical microscope objective to create a single optical trap. In 1987, Ashkin and co-workers demonstrated the use of opti-

cal tweezers for biological elements [4] opening the way to new manipulation techniques. Then the importance that those could take for biologists and chemists quickly realized. The possibility to individually trap single cells, cell fragments or DNA molecules with optical forces presents major advantages. Particles can be trapped, displaced and put in contact with each other or with chemicals in a non-invasive way, without contamination and avoiding sticking or mechanical damaging. Main applications that emerged in the domain of biology and chemistry are: single molecule and DNA stretching [5, 6, 7], cell manipulation [4, 8], cell analysis [9, 10], and cell sorting [11, 12, 13]. Nevertheless, a particular attention to the wavelength and the power density of trapping electromagnetic wave has to be taken, in order not to induce optical damages [14, 15]. Commercial products based on optical trapping for cell or particles manipulation are available<sup>1</sup>.

Another wide application of optical forces lies in the field of atomic physics, particularly in atom cooling and atom trapping [16]. The restriction of the spatial motion of atoms by laser light was mentioned by Letokhov in 1968 [17], two years before Ashkin proposed to trap atoms [2]. Atom cooling was suggested by Hänsch and Schawlow in 1975 [18] and has been realized by Wineland et al. in 1978 [19]. The Nobel Prize in Physics was attributed in 1997 to Steven Chu, Claude Cohen-Tannoudji and William D. Phillips for their works on "development of methods to cool and trap atoms with laser light"[20, 21].

The potential of optical trapping can be widely enhanced by multiplying the number of traps in an experimental setup. Since the beginning of laser trapping, many ingenious solutions have been put forward to generate multiple traps. In 1985 Chowdhury and co-workers arranged particles in interference fringes [22, 23]. The idea was first mentioned some years before by Labeyrie who suggested in 1979 to trap particles to make pellicle telescopes for astronomy [24]. In 1991, a time sharing solution was presented by Misawa et al. using galvano mirror to scan the laser beam between several traps [25]. Further scanning systems used piezoelectric mirrors [26] or acousto-optic deflectors [27]. Prentiss et al. proposed in 1993 to trap particles between two

---

1<http://www.arrayx.com><http://www.cellrobotics.com/workstation/ltws.html><http://www.elliotscientific.com><http://www.molecular-machines.com><http://www.palm-mikrolaser.com>

opposing optical fibers, opening the way to integrated optical traps without the need of microscope objectives [28, 29, 10]. The next innovation came with the demonstration by Kawata and Tani of trapping in the evanescent field of a waveguide [30], leading to studies on many body effect and on gradient field in absence of radiation pressure [31, 32] and to sorting of biological cell [33]. The use of a diffractive optical element to generate multiple spot out of one single beam for optical trapping was proposed by Fournier et al. in 1995 [34]. It opened the way to holographic optical tweezers. The introduction in 1999 by Tiziani of spatial light modulators (SLM) led to the most common system of multiple optical tweezers [35, 36, 37, 38, 39]. This system presents the advantage to be dynamically configurable, computer controlled and implementable in conventional optical microscopes. The acronym HOT, for Holographic Optical Tweezers, is conventionally used to refer to systems based on reconfigurable holographic optics. An alternate use of phase modulators for trapping proposed by Glückstad et al. relies on a generalized phase contrast (GPC) method to generate multiple optical traps [40, 41]. In 1998 Fournier and co-workers took advantage of the Talbot effect to trap atoms in 3-Dimensional arrays [42]. Static arrays of traps have also been generated by VCSEL [43], microlenses [44, 45, 46] or high numerical aperture micro-mirrors [47]. A non all-optical scheme for particles trapping has been recently proposed by Chiou et al. [48, 49] based on a combination of optical images and dielectrophoresis.

In the range of techniques using non optical forces for particles confinement, we find solutions based on electrokinetic forces (dielectrophoresis [50, 51], electrophoresis [52]), magnetic forces [53], hydrodynamic flows [54], acoustic waves [55] or gel trapping [56]. Among these techniques, dielectrophoresis is widely used for particles transport. However electrokinetic based systems require chips and containers with built-in electrodes and electrical circuits as well as special cell media for electrophoretic transport.

optical trapping has also been used as a tool for investigation of physical phenomenon. Brownian motion can for example be analyzed and measured in optical tweezers [57]. On a larger scale, multiple optical tweezers could extend the analysis to fluctuation of mesoscopic systems out of equilibrium and to optically induced forces [58].



## 1.2 State of the art

Today, the most commonly used system for optical manipulation of multiple objects is certainly the spatial light modulator in conjunction with a high numerical aperture microscope objective to create holographic optical tweezers. It offers not only the possibility to generate arrays of traps [35, 37, 59] and to dynamically change the position of the optical traps [36] but also the mean to create beams with particular functionalities like vortices which can carry an orbital angular momentum [60, 61, 62, 63], or non diffractive Bessel beams [64, 65]. Both advantages can be combined to create for example arrays of vortices [66]. The principal benefit over concurrent techniques is the possibility to dynamically change the vertical position of a trap and to create three dimensional arrays of traps [38, 67, 39]. Arrangements of up to 400 traps [68] have been reported, but traps number is limited due to the insufficient diffraction efficiency of digital holograms and to limited phase modulation systems affordable in SLM's. Comparable results have been obtained with an acousto-optic deflector (AOD) creating an array of 20x20 traps [69]. In 1995 however Fournier et al. already presented a solution to create 300 traps by the mean of interference [34]. Interferometric traps can be generated over large areas only restricted by the initial intensity of the interfering beams. Interference traps have been created in evanescent wave [32, 70] or through objective lenses [71, 72, 73, 74] but the largest arrays presently reported are created by direct formation of the interference fringes inside the sample [22, 23, 34, 75, 76]. The possibility to create large arrays presents a great potential for life sciences. We present here among the largest optical traps arrays for particles greater than the wavelength and new solutions for trapping in the Fresnel diffraction regime which is not often exploited in the conventional optical trapping experiments. We also report experimental results adding to the comprehension of optical mechanisms.

## 1.3 Motivation

The need for biologists to be able to manipulate large numbers of particles and to perform massively parallel experiments led us to develop schemes for large arrays of traps. This thesis dissertation will focus on the control of light for building optical traps, and on the patterning of light through interference. Chapter 2 proposes various solution based on interference of two, three or

more beams and particularly an original use of a Fizeau-Tolansky multiple beam scheme for optical trapping. Chapter 3 concentrates on trapping in the Fresnel regime and specially in self-images due to Talbot effect creating multilevel 3D optical traps. Finally, chapter 4 presents an analysis of optical binding and the first study of 2D self-arrangement of micron-size objects in an electromagnetic field.

In order to achieve our goal to create massively parallel optical trapping, we will be led throughout this dissertation to a better understanding of the behavior of particles in optical wells weaker than conventional high numerical aperture optical tweezers. Indeed, when generating high numbers of traps out of the same laser source, the initial power distributed in all the traps can be very weak in each single optical well. It is then necessary to optimize each parameter of the traps, mainly the intensity gradient (section 2.2), the size (section 2.3) and the shape of the trap (section 2.4), as well as the influence of other forces (scattering and contact forces) (chapter 3) and the collective effects of many body present in the system (chapter 4).

Superimposition of coherent complex amplitude distributions emanating from external optical elements (beam splitters, diffraction gratings) or from the particles themselves lead to unconventional intensity landscapes. Such light distribution presents interesting properties, like sharp gradients and variable trap sizes, having a high potential for strong optical trapping.

In addition to the manipulation tool provided by optical forces for biological experiment, a microfluidics environment allows for large scale experiments and parallel investigations on biomaterial such as cells, vesicles, organella or synthetic particles coated with functional molecules. Simultaneous analysis in a chamber with controllable medium can give access to statistical information and synchronous diagnosis while permitting sorting of large numbers of objects. The concept of lab-on-a-chip, illustrated in figure 1.1 is detailed in the appendix A.

In order to work in microfluidic flows, optical traps need to be stronger than what is required in a still environment. The whole work of this thesis dissertation is sustained by the idea to provide multiple traps strong enough to be compatible with microfluidics, i.e. able to sustain flows speed of several tens of micron per second. The study of traps characteristics and the design of new optical trapping schemes presented in this work aim at lab-on-a-chip applications.

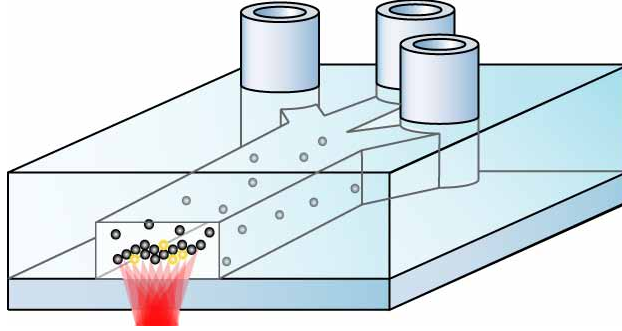


**Figure 1.1:** Lab-on-a-chip concept. Principle of microfluidics chip with optical traps array inside a microchannel where three different inlet channels merge.

## 1.4 Optical forces

Optical forces can be divided into three components all due to the conservation of momentum when photons interact with matter. The literature usually distinguishes the **scattering force** or radiation pressure that tends to push the particle in the direction of propagation of light, the **gradient force**<sup>2</sup> that acts as a spring to pull the particle towards the highest intensity area and the **binding force** that is due to the interaction of many particles inside an electromagnetic field. Optical trapping in two- or three-dimensions is due to an equilibrium between these three components acting on a particles. Generally used to explain optical trapping, the gradient force is in many other cases not the highest of the three ones. The optical forces are in the order of some piconewtons.

Different models are employed to describe optical trapping depending on the size of the particle with respect to the wavelength. When the particle diameter is much larger than the wavelength, the geometrical optics model applies and ray tracing method can be employed. On the contrary, when the particle is very small with respect to the wavelength, it can be assimilated to a dipole in a constant electrical field and behaves accordingly to Rayleigh scattering theory. The last case covers the range where the particle and the wavelength are in the same order of magnitude. In that case, referred as the Lorentz-Mie scattering regime, the field is not constant over the particle; none of the above mentioned models applies and rigorous calculations through Maxwell's stress tensor are necessary. The three models are detailed in the next paragraphs.

<sup>2</sup>The gradient force is also called the "dipole force", particularly in atomic physics

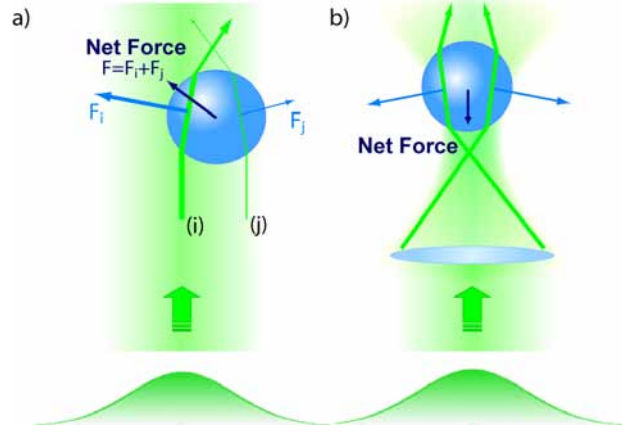


**Figure 1.2:** Geometrical representation of optical forces in the ray optics model. a) in a collimated Gaussian Beam and b) in a strongly focused beam as used in conventional single optical tweezers.

## Ray Optics Model

In the geometrical optics model, light is represented as a sum of individual rays. Let us consider one ray impinging on a single non absorbing particle with a refractive index different from the one of surrounding medium. Due to refraction, each ray changes its direction of propagation and thus photons change their momentum. To defer to momentum conservation a part is transferred to the particle. The calculation of the resulting optical force exerted on a dielectric sphere is made by integrating the effects of all beams including their own reflections and refraction over the whole sphere [77, 78, 79, 80]. Figure 1.2 illustrates the case of a sphere trapped in a collimated Gaussian beam (a) and in a highly focused beam (b). In the first scheme, the particle is attracted towards the center of the beam due to intensity gradient over the particle. This illustrates the action of the gradient force. At the same time, the particle is pushed in the direction of propagation of the beam due to the kicks given by each photon hitting the sphere. To keep the latter in an axial equilibrium, conventional optical tweezers use a high numerical aperture optical element to strongly focus the beam. The direction of the external rays depicted in figure 1.2 (b) illustrates the forces that are acting to stabilize the sphere in the vicinity of the focal area.

### Rayleigh Regime

In the Rayleigh diffraction regime, the particle is represented by a dipole and the field is considered constant over the size of the particle. The Lorentz force exerted on it by the electromagnetic wave can be analytically calculated [81, 82, 83, 84]. In the case of a single dipole immersed in an electromagnetic field of intensity  $I$ , the total force  $F_{tot}$  can be expressed as:

$$F_{tot} = F_{grad} + F_{scat} \quad (1.1)$$

with

$$F_{grad} = \frac{1}{2}\alpha\nabla I \quad (1.2)$$

$$F_{scat} = \frac{1}{3}\alpha^2 k^4 I \quad (1.3)$$

where  $\alpha$  is the polarizability

$$\alpha = a^3 \frac{n^2 - 1}{n^2 + 2} \quad (1.4)$$

$n$  is the relative refractive index,  $a$  the particle's radius and  $k$  the wave number.

Unfortunately most of the particles handled in this opus are too big to behave according to this Rayleigh model. Likewise they are too small to be correctly treated by the geometrical model. However those simple models are often used in the literature to explain optical trapping and guide us in the understanding of optical trapping mechanisms.

### Lorentz-Mie scattering regime

The Mie scattering theory, or more precisely the Mie solution to Maxwell's equations, also referred as Lorentz-Mie or Lorentz-Mie-Debye theory, is rigorous and is valid for any value of  $d/\lambda$  where  $d$  is the diameter of the considered particle and  $\lambda$  the wavelength [85]. It is the only model suitable for the particles that we currently use, but it requires rigorous calculation of either the Maxwell's stress tensor or the Lorentz force. The present study concentrates on experimental work and cannot include such tedious calculations. Solutions have already been calculated for strongly focused beams [85, 86, 87, 88, 89, 90, 91, 92] and for wide electromagnetic fields

[93, 94, 95, 96]. We will further refer to several partners' calculations for simulations of the experimental conditions presented in this work.

---

# Optical trapping in interference patterns

## 2.1 Introduction

The developments in biochemistry and biotechnology tend to downscaling materials and products and the performance of bioanalytics can be considerably augmented by the parallelization of operation and Analysis. Optical tweezers offer the possibility to manipulate single biological elements, considerably limiting the quantity requirements in expensive and rare reactant and biomaterials. However, most of multiple optical traps system are limited to a few tenth of traps. The possibility to generate very high number of traps is obviously of great interest. In this chapter solutions for creating very large arrays of optical traps by the interference of several beams are presented. Trap arrays generated this way cover very large fields of view and fine light patterns can be achieved for the confinement of small objects. The principle of trapping in interference is presented and different schemes creating intensity gradient by interference are studied. The optimization of the intensity gradient is essential for the trapping efficiency, since the optical forces are proportional to it<sup>1</sup>. The advantages of the presented solutions are emphasized by numerical simulations. An experimental setup allowing the creation of different light pattern configurations is presented and studies of optical trapping are reported and discussed. In a second part, a more sophisticated interference trapping scheme is studied. Multiple beam interference, also known as Fizeau or Tolansky fringes, are generated by multiple reflections inside an interferometer. These fringes provide a high flexibility and sharper intensity gradients interesting for optical trapping.

## 2.2 Various types of interference

Light interference was first evidenced by Thomas Young in 1801 when he established the wave theory of light with his double-slit experiment. The invention of the laser in the 60's brought a convenient source of coherent light. Since then, interference has been a powerful tool for e.g. distance and shape measurements, phase measurement (holography) or light structuring. Meanwhile, when arising through spurious reflections, unwanted interference pattern can also be a serious drawback. Interference occurs when at least two spatially or temporally (or both) coherent monochromatic waves overlap

---

<sup>1</sup>This assessment is valid in the Rayleigh regime and also in most situations in the geometric optics



and when both wave vectors and polarization states of the two waves are not perpendicular. The first utilization on interference fringes for optical freezing was reported by Chowdhury et al. in 1985 [22]. Optical trapping in interference has been used also for the study of optical crystallization and optical binding [23, 34, 70], for optical trapping of mesoscopic particles [71, 73, 97, 74] and for sorting of particles [98, 99].

### 2.2.1 Intensity pattern formation

Let us consider two waves of complex amplitude  $E_1$  and  $E_2$  with

$$\vec{E}_j = \vec{A}_j e^{-i\omega t} \quad (2.1)$$

$\vec{A}_j$  ( $j = 1, 2$ ) being the complex amplitude,  $\omega$  the pulsation and  $i^2 = -1$ . The intensity is given by

$$I_j = \langle E_j^2 \rangle \quad (2.2)$$

Where  $\langle \cdot \rangle$  indicates the temporal mean. The total electric field at a point where  $E_1$  and  $E_2$  are overlapping is

$$E = E_1 + E_2 \quad (2.3)$$

and the total intensity is given by

$$I = I_1 + I_2 + I_{12} \quad (2.4)$$

where

$$I_{12} = 2 \langle E_1 \cdot E_2 \rangle = 2\sqrt{I_1 I_2} \cos \Delta\phi \quad (2.5)$$

is the interference term with  $\Delta\phi = \phi_1 - \phi_2$  being the phase difference between the two waves. If the intensity  $I_1$  and  $I_2$  are the same ( $I_1 = I_2 = \frac{I_0}{2}$ ), the total intensity is expressed as

$$I = I_0[1 + \cos(\Delta\phi)] = 2I_0 \cos^2 \left( \frac{\Delta\phi}{2} \right) \quad (2.6)$$

The intensity of the signal being a  $\cos^2$  function, it presents a total extinction when  $\Delta\phi = (2N + 1)\pi$ ,  $N$  being an integer. The  $\cos^2$  form provides a spatial distribution of the potential with maxima in which dielectric particles, whose

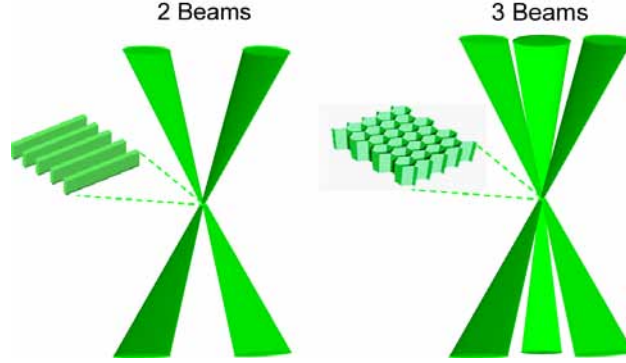


**Figure 2.1:** Schematic representation of the interference of (a) two and (b) three beams focused on their overlapping area.

index of refraction is higher than the one of the surrounding medium, can be trapped.

The quality of the traps depends on the interference characteristics, particularly on the fringe contrast, described by the visibility function  $V$ :

$$V = \frac{I_{max} - I_{min}}{I_{max} + I_{min}} = \frac{2\sqrt{I_1 I_2}}{I_1 + I_2} \quad (2.7)$$

Optical forces are proportional to the intensity gradient in the Rayleigh regime and also, to some extent, according to geometrical optics; considering this also for particles of size in the range of the wavelength, we will try to maximize the gradient by varying the beams configuration. Besides, gradient optimization can also be achieved by increasing the number of interfering beam.

In the case of three plane waves the total intensity distribution is given by:

$$I = I_1 + I_2 + I_3 + 2\sqrt{I_1 I_2} \cos(\phi_2 - \phi_1) + 2\sqrt{I_2 I_3} \cos(\phi_3 - \phi_2) + 2\sqrt{I_3 I_1} \cos(\phi_1 - \phi_3) \quad (2.8)$$

and presents a three-fold symmetry. Its characteristics will be discussed later.

### 2.2.2 Beam configurations and optical templates

We will study different configurations with two and three beams. Let us first examine the case of two interfering Gaussian beams. We consider them as two plane waves at the interference zone since we are working within the Rayleigh distance  $z_0$  ( $z_0 = \frac{\pi w_0^2}{\lambda}$ ,  $w_0$  being the minimal radius of the beam) around the

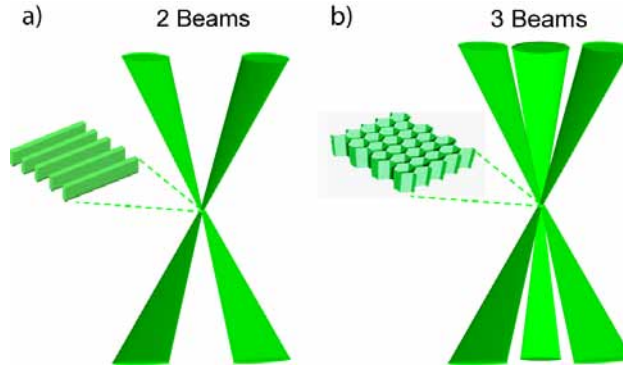


**Figure 2.2:** Definition of interference fringes parameters

focal area of a slightly converging Gaussian beam. The two beams come from the same laser source with sufficient coherence length to allow interference over the whole area under investigation. The laser beam is separated in two beams after the focusing element and these two beams are crossing each other at an angle to generate interference. The beam path-lengths have to be rigorously the same to ensure that both beams have the same divergence and the same size at the interference area and that the path-length difference is within the coherence length of the light source. The constructive and destructive interference of the electrical field creates sinusoidal fringes that persist in the  $z$  direction along the whole overlapping area of the beams. The interference pattern can be considered as "wall" of light as shown in figure 2.1 a).

The pitch of the interference fringes  $p$ , as defined in figure 2.2, depends on the angle between the two interfering beams and on the wavelength  $\lambda$  in the medium, and is given by

$$p = \frac{\lambda}{2 \sin \frac{\theta}{2}} \quad (2.9)$$

Adding a third beam to the system allows the possibility of creating three sets of fringes as shown in figure 2.3. The intensity pattern of the interference of the three beams presents hexagons (figure 2.1 b)). The expected superposition of the three sets of fringes in a incoherent way would produce hexagons as shown in figure 2.4 a). Meanwhile, the coherent superposition of all three plane waves gives rise to the structure of figure 2.4 b) where the hexagons are tilted by  $30^\circ$  in reference to the incoherent scheme. The size of

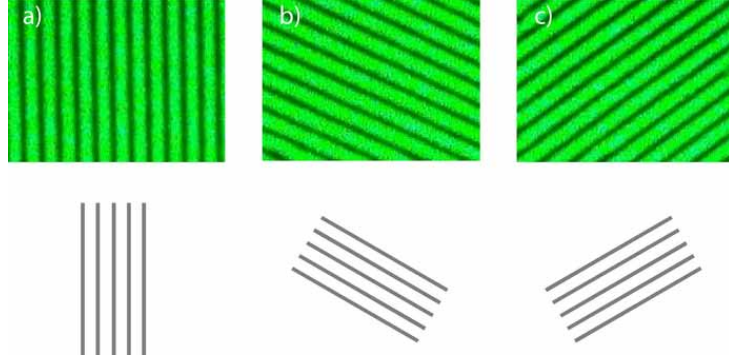


**Figure 2.3:** Achievable interference patterns direction depending on the pair of interfering beams.

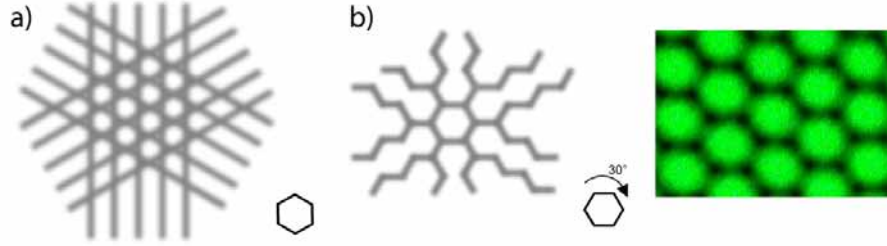


**Figure 2.4:** Schematic representation of a) incoherent and b) coherent superposition of three sets of interference fringes.

the paved hexagons created by three sets of fringes with a pitch  $p$  is given by (see figure 2.5)

$$H = \frac{2p}{\sqrt{3}} \quad (2.10)$$

and

$$A = \frac{4p}{3} \quad (2.11)$$

The pitch  $p_{hexa}$  between two hexagon is then equal to  $H$ . Let us remark that such hexagons represent the area over which the optical wells are centered.

When three beams of wave vectors  $\vec{k}_1$ ,  $\vec{k}_2$  and  $\vec{k}_3$  are regularly disposed along the ridges of a symmetrical tetrahedron of base (ABC) and converge to the same point O (see figure 2.6), the interference creates a three dimensional honeycomb-like structure stretched all over the overlapping area of the beams along the z-axis.

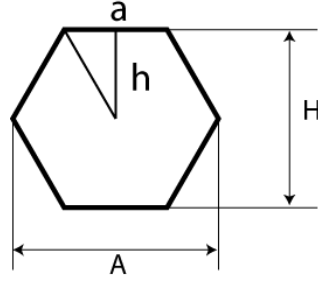


**Figure 2.5:** Dimension of the hexagonal interference pattern.

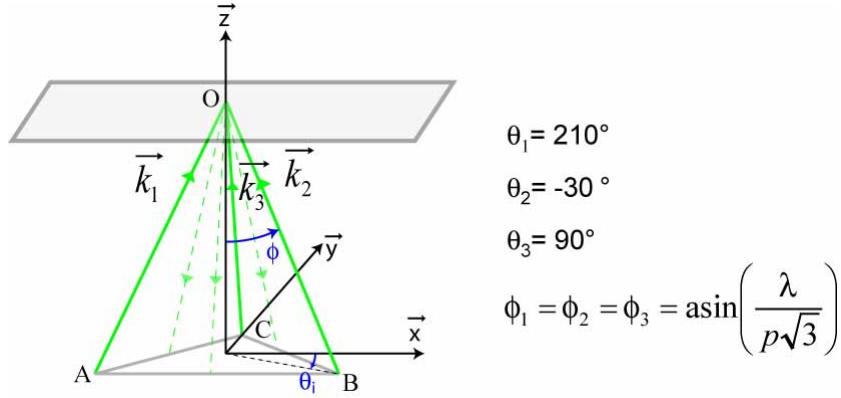


**Figure 2.6:** Configuration of the three interfering beams of wave-vector  $k_i$ . The dashed arrows represent the reflected beams when a mirror is placed at the level of the gray plane (trapping plane)

For convention, the z-axis is defined as the axis of the pyramid and the xy planes is perpendicular to it at the level of the intersection of the three beams.

### 2.2.3 Optical trapping in interference pattern

The intensity distribution in the interference area generates potential wells in which particles can be trapped. The gradient force creates a lateral arrangement in any plane perpendicular to the z-axis. Optical binding forces also contribute to the lateral arrangement as we will discuss in the chapter 4. The scattering force however pushes the particles along the z-axis. In order to get a z-confinement, the solution of particles is contained within a closed chamber and the top wall stops the particles in its plane. This plane will be referred hereafter as the trapping plane.

### 2.2.4 Numerical simulations and trap shape optimization

The above mentioned configuration gives us the possibility to create various types of light templates based on a basic sinusoidal shape of intensity. We are now interested in finding the optimal shape for a trap of a defined size assuming that the optical forces are proportional to the gradient of intensity for Mie particles as in the Rayleigh regime (see equation (1.2) in section 1.4) and as in the ray optics model. The following numerical simulations let us predict the intensity gradient depending on the beam configuration.

The simulations are based on the scheme presented in the latter paragraph where three beams are uniformly distributed around an axis and equally tilted with respect to it. The tilt angle is determined by the desired size of the interference fringes according to equation (2.9). The beams are considered as waves with a planar phase and a Gaussian intensity distribution whose waist is 50 to 100 times larger than the beads diameter. Figure 2.7 represents the intensity level in a plane perpendicular to the z-axis. The optical traps are 2 microns wide, created by coherent beams forming an angle  $\theta$  of  $15.42^\circ$  in air (figure . The field is represented over 6 by 6 microns and the gray level scale is the same for each image. The initial intensity  $I_0$  is set to 1 and is distributed evenly in each beam. The simulation is intended to analyze the optimal beam configuration, i.e. when the intensity gradient inside an optical well is maximal. The initial power can be split in two of the three beams or in three equivalent parts. The gradient is calculated in x and y directions. The maximal value of the gradient for each plot is summarized in table 2.1.

In the literature, there is no particular criteria for defining the size of a non Gaussian optical well. One could relate the distance  $g$  between two symmetrical intensity gradient maxima to the trap's size. In that case  $g_{sin} = \frac{p}{2}$  for a sinusoidal fringe paving and  $g_{hexa} \cong \frac{6p}{5}$  for an hexagonal paving,  $p$  being the pitch of sinusoidal fringes. Figure 2.8 gives the absolute value of the intensity gradient along the x-axis corresponding to the cases presented in figure 2.7 b) and c).

#### Recycling light

To increase the gradient and also to reduce the effect of radiation pressure, a mirror can be placed at the beams intersection area. Reflecting the three in-

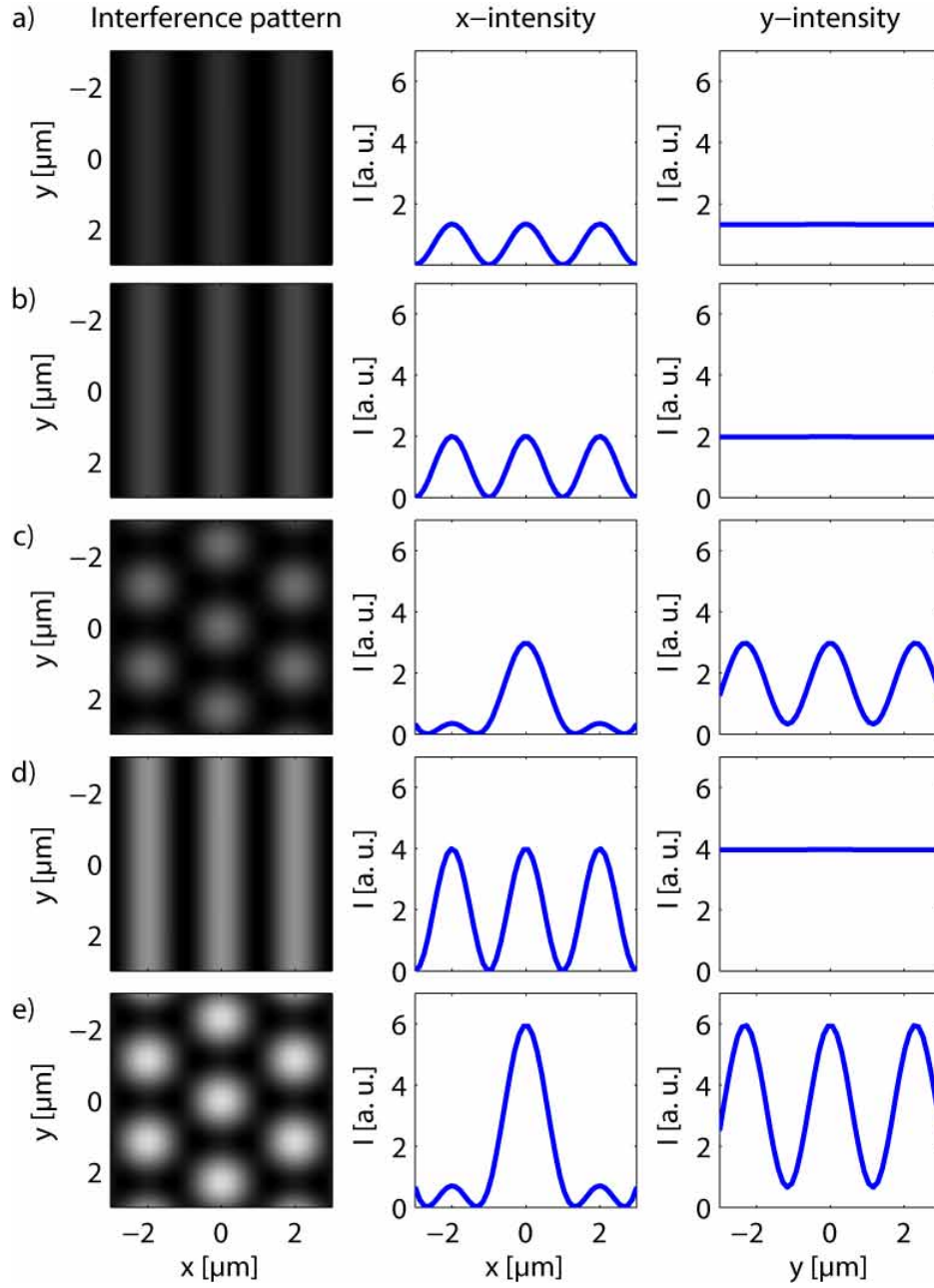


**Figure 2.7:** Intensity distribution for different beam ratios and for various beam configurations (see table 2.1)

	Intensity repartition in beams	Max gradient x	Max gradient y
a)	$I = 1/3 - 1/3 - 0$	1.12	0.00
b)	$I = 1/2 - 1/2 - 0$	1.67	0.00
c)	$I = 1/3 - 1/3 - 1/3$	1.96	1.93
d)	$I = 1/2 - 1/2 - 0$ - mirrored	3.32	0.00
e)	$I = 1/3 - 1/3 - 1/3$ - mirrored	4.88	4.80

**Table 2.1:** Maximal Intensity gradients of the interference pattern of three beams along x and y axis depending on the intensity distribution in each beam for an initial intensity  $I_0 = 1$  and a fringe's pitch of  $2 \mu\text{m}$ . The gradient is expressed in multiple of  $I_0 = 1$  per  $\lambda$ . The configurations are the one presented in figure 2.7. The two last rows correspond to the case where the beams are reflected by a mirror placed in the interference plane.

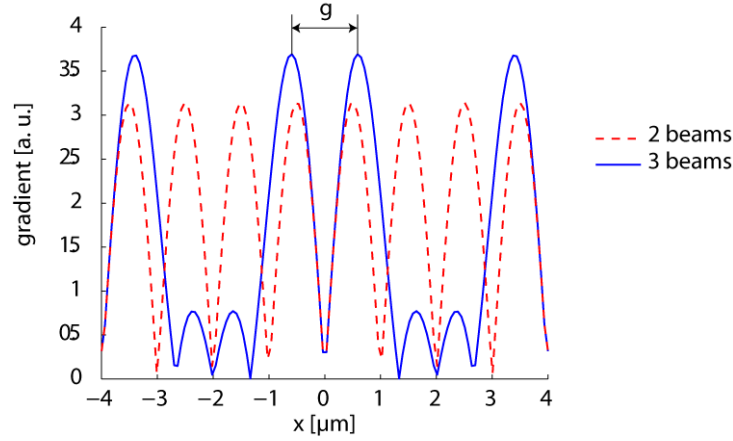


**Figure 2.8:** Comparison between the absolute value of the intensity gradient along the x-axis for 2 and 3 beam interference (figure 2.7 b) and c)) for a  $2 \mu\text{m}$  fringe's pitch.

coming beams creates three beams with counter-propagating direction, tilted by  $180^\circ$  with respect to the incoming beams. The radiation pressure that tended to push the trapped object towards the wall is locally compensated. In the ideal case, an equilibrium is reached on the central axis as shown in figure 2.9. The figure was obtained by calculating the radiation pressure effects without taking interference into account. The two last lines of table 2.1 present the calculated intensity gradient for the configuration with reflected beams. The intensity gradient is increased by a factor of almost three by adding a mirror while keeping the same initial power. Moreover, minimizing the scattering force by cancelling the radiation pressure effects allows dimin-



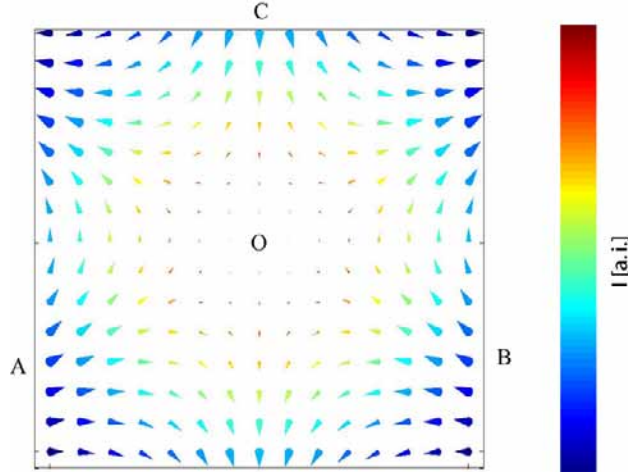


**Figure 2.9:** Simulated radiation pressure due to the sum of three interfering beams and of the their reflections on the mirror. The simulated plane is perpendicular to the  $z$ -direction and located at the level of the gray plane of figure 2.6. The size of the cones is proportional to the radiation pressure, the direction of the cones is the one of the resulting vector of the sum of the three wave vectors and their color represents the local intensity level according to the color bar. The simulation does not take interference into account.

ishing the friction in the system; objects are now trapped in the bulk of the cell instead of touching the upper wall.

### 2.2.5 Experimental setup

The basic setup divides the output beam of a laser in three beams whose intensity and polarization are individually controlled and allows directing them along the ridge of a pyramid. The laser source is a diode pumped solid state Neodymium:Vanadate laser manufactured by Coherent (Verdi V-5 #A1450) delivering up to 5W in cw mode at 532nm (intra cavity frequency doubled). It is linearly polarized and delivers almost a  $TEM_{0,0}$  mode ( $M^2 \cong 1.1$ ) with slight ellipticity. The setup has evolved progressively with the undertaken experiments and the principal configuration is shown in figure 2.10. The beam intensity is controlled through a polarization rotator (Fresnel Rhomb) followed by a polarizing beam-splitter. A second polarizing beam-splitter helps cleaning the linear polarization. A positive lens ( $f=1000$  mm) placed before the division system focuses the beam at the trapping area, then reducing its size to about  $150 \mu\text{m}$ . In order to get a smaller spot at the focal

area, the beam is enlarged by a telescope before impinging on the focusing lens.

Another polarizing beam splitter placed after a  $\lambda/2$  zero order waveplate splits the beam with a ratio adjusted by rotating the waveplate.  $1/3$  of the intensity is sent in one beam and  $2/3$  in the other one. The following beam-splitter is non-polarizing and divides the highest intensity beam in two equivalent parts so that the total energy is equally distributed among the three beams. Additional  $\lambda/2$  plates are needed to rotate the polarization of each beam. Since the three beams are not coplanar, a common polarization state cannot be found in the interference area. The polarizations can only be set identical two by two and the difference with the third one has to be minimized. This is more easily achieved when the angle between the beams is small, i.e. for large interference fringes. The polarization state is represented by dark green arrows in figure 2.10.

A particular attention has to be paid to the different path lengths, on the one hand to preserve the same size for each beam at the trapping area and on the other hand to ensure maximum interference contrast in the trapping area. This second criterion is not so critical with the Verdi laser used since this model has a coherent length of several meters but could be important with other types of lasers. The control of the light-path is realized by adjusting the mirrors positions at the basis of the pyramid, taking into account the optical path through elements of higher indices. A piezo electrical element is mounted on a mirror folding one of the beams. The translation of this mirror in the order of the micrometer induces a phase shift on this arm that moves the fringes laterally in the trapping plane.

Because of convection and gravity effects, the sample cell is placed horizontally and the optical axis must be set vertically. A 2" broadband dielectric mirror is placed near the top of the pyramid to fold the apex in a vertical position. A mirror mounted on a flip-flop element and placed before the beam separation gives the possibility to illuminate the sample cell with a single beam along the axis of the pyramid. This beam will be also used for experiments on optical binding reported in chapter 4.

The cell holder is mounted on a motorized stage driven by two DC-motors to laterally move the sample in x- and y-directions. The motors are supplied by a manually controllable voltage generator. The position is given by encoders with an accuracy of 1 micrometer.

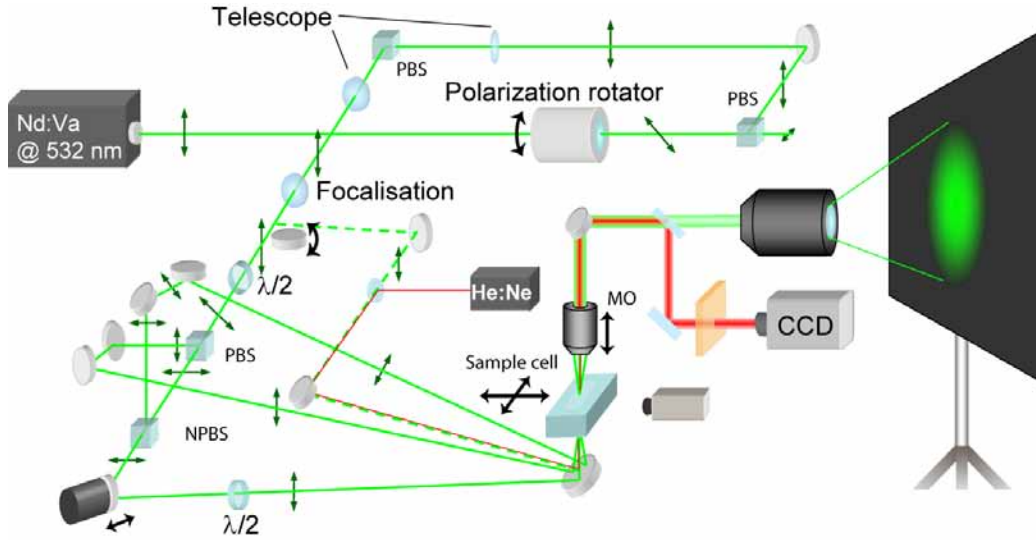


**Figure 2.10:** Basic setup for generation of interference for optical trapping. The output beam of a 5W Nd:Vanadate laser is split in three parts that are combined at the trapping area where a sample cell is placed. Two objective lenses project the image of the trapping area on a screen. The green arrows show the polarization states.

An He-Ne laser emitting at 632.8 nm with a power of 30 mW has been inserted in the setup. Directed along the axis of the pyramid, it offers the opportunity to image the sample independently of the trapping light. It also allows the reading of the particles arrangement by observation in the reciprocal space ( $k$ -space). This latter investigation method will be described in paragraph 2.2.6 and in section 4.3.

An imaging system offers the opportunity to project the image of the trapping plane both on a digital sensor and on a large screen. A long working distance microscope objective (Nachet x 20 infinity corrected, WD 17 mm, NA 0.3, N-20X-LD) makes a real image of the trapping plane which is relayed by a large photographic objective (Pentax 50mm Macro), projecting the image on the large screen. A camera records the projected images. A dichroic mirror placed between the two objectives used for imaging selects a part of the light and projects it directly on a CCD sensor. This latter is positioned at the image plane of the Nachet objective; the image of the trapping plane is focused simultaneously on both displays (CCD and screen). Additional filters discriminate between the residual trapping light and the red illumination, depending on the images that need to be recorded. An-

other imaging system allows side observation of the trapping area. However, it requires a special sample cell with a lateral optical window.

### Sample preparation

Most optical experiments presented in this work are performed with spherical polystyrene microparticles suspended in water. These objects have several advantages.

- Polystyrene (latex) beads have a refractive index of 1.59 or 1.6 depending on the supplier. When immersed in water, they provide a relatively large index modulation (1.2) which constitutes one of the most important parameters for optical trapping as illustrated by equation (1.2) and (1.4).
- The absorption of light by polystyrene in the visible and near infrared domain is very low.
- Microparticles can be found in solutions sold by various manufacturers. Our main providers are Polysciences (polystyrene particles) and Invitrogen-Molecular Probes (fluorescent or reactant coated particles).
- The size of the particles covers a range from a few nanometers to tenths of millimeters with a large choice in the micron range ( $0.5\text{-}20\mu\text{m}$ ) corresponding to the optimal object sizes used in our optical trapping experiments.
- Manufacturer produce polystyrene beads with a narrow size distribution. The coefficient of variation is in the range of 1-3%.
- Polystyrene has a density of 1.05, close to that of water. It allows having colloidal solutions with slow sedimentation.
- The beads are furnished in solution (water) at a high concentration (1-10% w/v) and can then be easily handled and diluted to the desired concentration.
- Beads solutions can be stored for a long time at low temperature ( $4^{\circ}\text{C}$ ).
- Due to the fabrication process, polystyrene microparticles have an almost perfect spherical shape.

Manufacturers supply functionalized polystyrene spheres, electrically charged or not. For the work reported in this PhD dissertation, we only use neutral particles.

Samples are prepared by diluting the high concentration beads suspensions by about a factor 100 in deionized water which results in a concentration of about 0.03% w/v depending on the desired final concentration and on the beads size. Preparations of 2 to 5 milliliters are kept ready for experiments. The test-tubes containing the solutions are shaken in an ultrasonic bath during 15 minutes before each experiment. This degassing operation also breaks up the aggregates of beads.

### Sample cell

Sample solutions have to be contained in a closed cell since 2-dimensional interference trapping configuration requires a surface for the confinement in the third direction. Optical flatness is required in order to avoid phase distortion. The top and bottom of the cell have to be of optical quality for sustaining the high fluence needed for optical trapping and for a good imaging. The height of the cell is critical. A too high container gives rise to convection effects that can seriously disturb trapping experiments. A height of  $200\mu\text{m}$  provides a sufficient volume, meanwhile reducing considerably the convection effects. We employ both commercial cells and home made containers schematized in figure 2.11.

We use cells with detachable windows sold by Hellma, GmbH (catalog Number 106) with a light-path of 0,2 mm. The two windows are clamped by a cell holder. For a more flexible solution, a home-made silicone spacer is squeezed between a standard microscope slide and a coverslip. Such a spacer acts extremely well as an O-ring. The desired spacer shape is cut in a  $170\mu\text{m}$  thick PDMS sheet. This one is realized by molding a two-components polydimethylsiloxane (Sylgard 184, Dow Corning, USA) between two flat surfaces spaced by standard  $170\mu\text{m}$  thick microscope coverslips and then heating up at  $70^\circ\text{C}$  during two hours. This simple solution is flexible, inexpensive and the cells present a much better sealing than the one of the commercial cells. The different components of the cell can easily be cleaned with ethanol.

For side viewing, we use a square Hellma cell (catalog number 131.050) with a  $200\mu\text{m}$  channel.

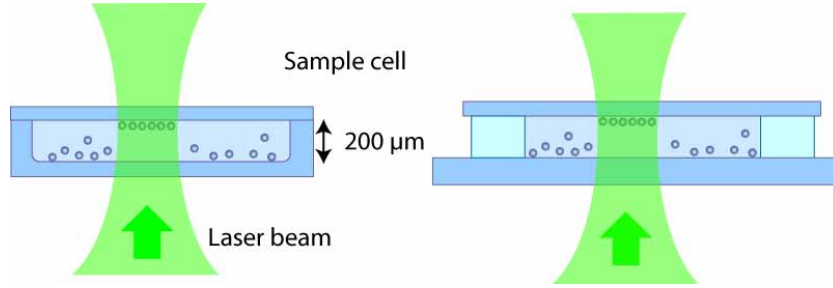


**Figure 2.11:** Two types of cell used for trapping. Particles are confined at the top of the cell due to the radiation pressure.

### 2.2.6 Trapping polystyrene particles

Lets consider particles with a diameter in the micron range, typically 1 to 10 microns. In the case of interference trapping, particles can be trapped as well in bright fringes as in dark fringes depending on the relationship between beads diameter, index modulation and fringes'size. The exact equilibrium position of dielectric object in interference pattern can only be reliably calculated by rigorous implementation of Maxwell's equations and no easy prediction of the trapping of such objects can be made. A few calculation of optical forces on Mie particles in extended electromagnetic fields can be found in the literature [100, 94, 95, 96]. Simulations show that particles will not necessarily be trapped at maxima of light intensity, but they will place themselves at positions such that their volume encloses the maximum of electromagnetic energy density [96].

We first study the behavior of polystyrene beads with a diameter of  $2\ \mu\text{m}$  (Polysciences Inc. Cat# 19814) in 2-micron interference fringes. The Influence of the trap size on optical trapping will be presented later in section 2.3. The setup described in paragraph 2.2.5 allows creating about 70 line traps or 3400 hexagonal traps in the field of view of the objective that contains the major part of the laser intensity. Under such conditions, beads settle down at the highest intensity point in the center of the hexagons or in the center of the bright sinusoidal fringes respectively as shown in figure 2.12.

After the modifications brought to the setup allowing changing the pitch of the interference fringes (as it will be describe later on in paragraph 2.3.1), we could create over 20,000 traps inside the field of view of the objective. Figure 2.13 shows 24,000 traps generated by  $1.26\ \mu\text{m}$  fringes, partially filled with 1 micron beads.



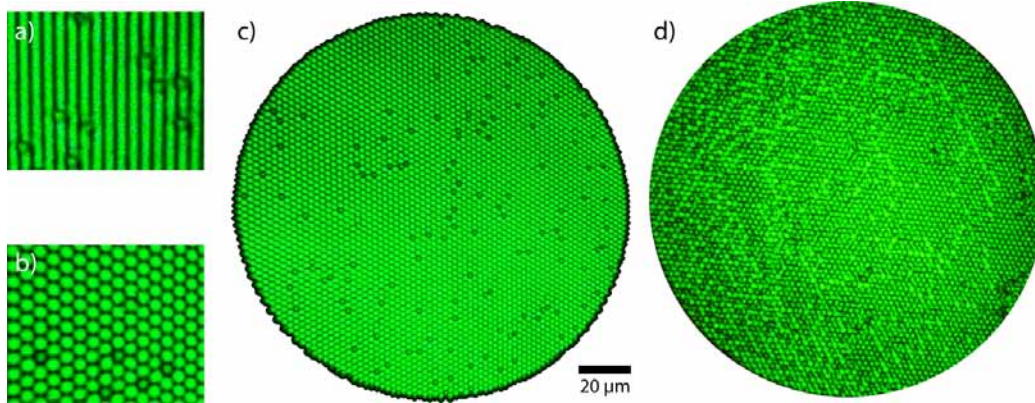


**Figure 2.12:** Two-micron polystyrene spheres trapped in a) two-beam and b) three-beam interference. c) Whole trapping area with 3400 Traps. The beads find an equilibrium at the intensity maxima. d) Same as c) but almost totally filled with  $2\mu\text{m}$  beads

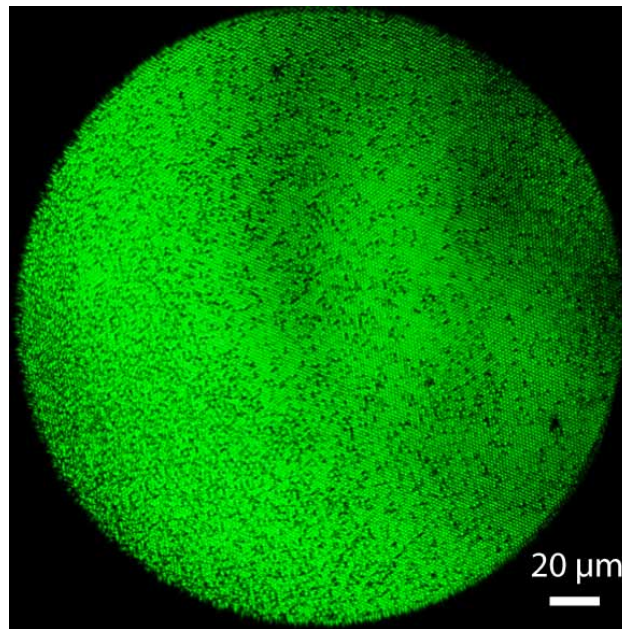


**Figure 2.13:** Over 24'000 traps in an area of  $240\mu\text{m}$  in diameter partially filled with  $1\mu\text{m}$  polystyrene beads

## Force measurements

In order to determine the strength of the traps we use the drag-force method well known in the calibration of optical tweezers and described in [101, 102]. This method relies on the viscous force (Stokes' formula) determined by the fluid velocity that the trapped object can sustain while remaining in the trap. Conversely to the case of conventional 3D optical tweezers, the trapped particles in the present experiments are in the vicinity of a wall of the container. In that case, the influence of the proximity of a surface is difficult to estimate and the exact value of the Stokes force cannot be determined. Multiple factors intervene such as friction, Van der Waals forces or the unknown exact distance between the surface and the particle. However, the trapping strength can be related to the drag speed and relative values can be determined. One must notice that the drag method can be implemented according to two different techniques. When the cell is dragged in a direction perpendicular to the fringes, the optical forces oppose the liquid flux and the influence of the proximity to the wall works against the trapping force. On the other hand, when only the solution is flowing through the cell perpendicularly to the fringes, for example in a fluidic channel, the proximity effects help stabilizing particles in the traps.

## K-space observation

Observing the Fraunhofer diffraction of the ensembles of particles gives an information on the distribution of light in the  $k$ -space. To access this representation, it suffices to place a screen in the far field, i.e. some tens of centimeters behind the interference area. Regularly disposed particles, as trapped in the interference pattern, will diffract light in specific direction according to the pitch of the array. Even partially filled template will diffract in well defined spots as visible in figure 2.14. The smaller the spot, the better the trapping since irregular diffracting element will spread the diffraction spots.

### 2.2.7 Radiation pressure compensation

In order to compensate for the radiation pressure that pushes the trapped particles against a wall, a dichroic mirror has been added at the top of the cell to reflect the incoming beams. The coated surface of the mirror is placed



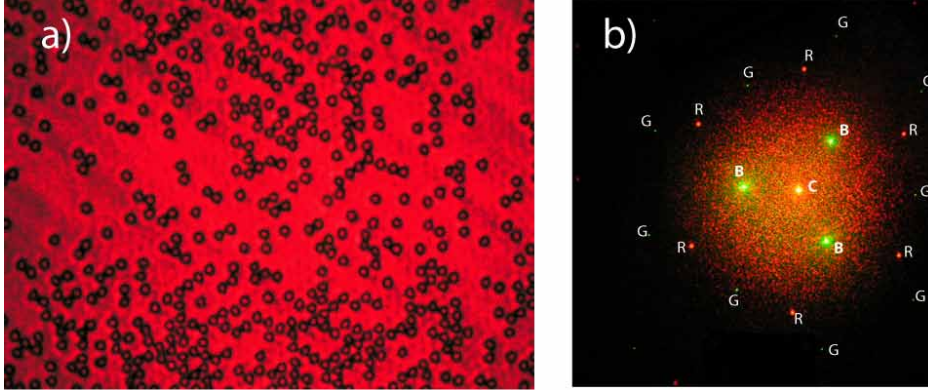


**Figure 2.14:** a) Partially filled crystal of two-micron polystyrene beads trapped in three beam interference pattern at 532 nm observed with red He-Ne light. b) Diffraction pattern observed on a diffuser placed 252 mm behind the trapping plane. The three bright green spots (B) are the propagating trapping beams. The central red spot (C) is the illumination He-Ne beam and the small red (R) and green (G) spots are the first diffraction order due to the illumination and trapping beams respectively.

in contact with the solution. Each beam is specularly reflected; this produces a six beam interference as shown on the simulations presented in paragraph 2.2.4. Experiments with  $2\mu\text{m}$  beads show that effects of radiation pressure can be minimized and beads can be stabilized for the time of experiment (about 10 to 15 minutes) and stay at different depths in the cell. In comparison, without back reflection, the same beads would reach the top of the cell in several seconds (5 to 15 sec. depending on the laser power). The radiation pressure compensation works better for a small concentration of beads in the cell. Indeed, each bead scatters some of the light impinging on it; this scattered light is lost from the incoming beams and therefore the reflected beams are less intense than the forward beams entering the cell.

For  $2.06\mu\text{m}$  spheres in  $2\mu\text{m}$  fringes, a dragging speed of  $37.3\mu\text{m/s}$  could be reached when the mirror is used. This should be compared to the dragging speed of  $13.3\mu\text{m/s}$  reached when the beams are not reflected. For this experiment the power incident on the cell was 2 Watts. This increased trapping efficiency is due to the following reasons:

1. The presence of the mirror doubles the intensity in each trap (excepted for the losses of the mirror and for effect of diffusion)
2. The gradient of the intensity pattern is theoretically almost three times higher, as explained in paragraph 2.2.4.

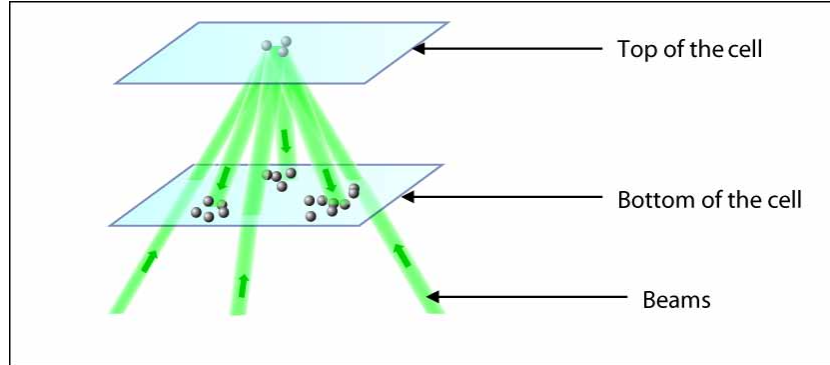


**Figure 2.15:** Schematic representation of the formation of clusters of beads where the radiation pressure is only partially compensated.

3. The beads are not in contact with the walls of the cell, therefore they only experience the viscous force.

Bigger  $3\mu\text{m}$  beads are more sensitive to radiation pressure and gravitation. This is why they have been used to find the final equilibrium position of trapped particles inside the volume of the cell. The beams have an angle  $\phi$  of  $8.8^\circ$  in air with respect to the  $z$  axis ( $6.6^\circ$  in water) as represented in figure 2.6. Beads amass at four different places in the cell as shown in figure 2.15. A first accumulation occurs at the top of the cell on the  $z$ -axis. Three other concentrations of beads are found where the three reflections exit the trapping volume. Due to their inclination, the incoming beams and their respective reflections only overlap at the surface of the mirror (see figure 2.9). At the bottom of the cell, a particular beam and its reflection present a shift of over  $40\mu\text{m}$ , leaving space where the radiation pressure is not totally compensated (see figure 2.16). Even if the radiation pressure would be uniformly compensated, this would not suffice for a 3D trapping; a gradient in the  $z$  direction is necessary. However, for short experiments, beads could be trapped in the bulk of the cell. Creating a gradient in  $z$  over a large area in the  $xy$  plane is not trivial. We will present a solution in the chapter 3.

An ingenious solution for radiation pressure effects compensation was experimented by Chiou et al. [103, 104], using photorefractive crystals to get phase conjugation in a four wave mixing configuration.

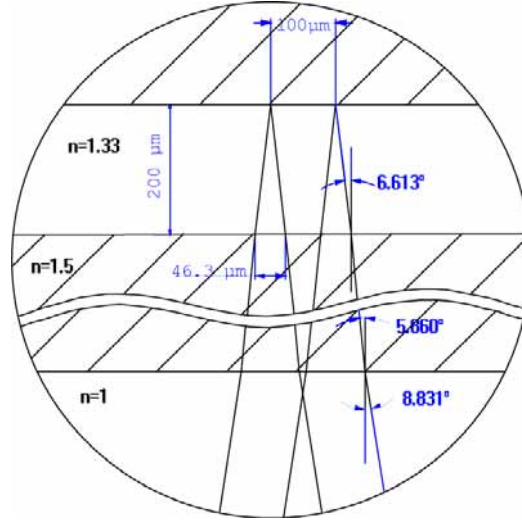


**Figure 2.16:** Schematic path of a beam with a waist of  $100 \mu\text{m}$  impinging on the cell and its reflection at the top of the cell. The beam slant corresponds to a fringe pitch of  $2 \mu\text{m}$ . The drawing shows area with lack of radiation pressure compensation at the none overlapping area at the bottom of the cell. The beam size variation is neglected over the thickness of the cell since the Rayleigh length is  $60 \text{ mm}$ .

### 2.2.8 Trapping in microfluidics

In biology, many experiments call for the reduction of consumption of matter and of reactants. Optical tweezers provide a suitable tool for the manipulation of small amounts of objects and microfluidic systems are excellent complement for dealing with small quantities of products [105, 106, 107]. The concept of lab-on-a-chip also known as  $\mu\text{TAS}$  (Micro Total Analysis System) is now particularly appreciated for biological studies. Low reagent consumption, short reaction time, low cost, customizable design and possibility for parallel operation are the major advantages of those systems. Informations on those systems are provided in appendix A. If a single optical tweezers in microfluidics has been often used for biological applications [108, 109, 110, 111, 112], the combination of multiple optical trapping and microfluidics is more powerful but difficult to implement. To our knowledge, as of today, no biochemical experiment has ever been published using the conjunction of microfluidics and multiple optical trapping. To some extent, this is due to the high strength needed for optical traps to sustain microfluidics flows. Indeed many systems for creating arrays of optical traps generate also important loss of power and are limited to a few number of traps (see paragraph 1.2). More powerful schemes have been demonstrated when do-

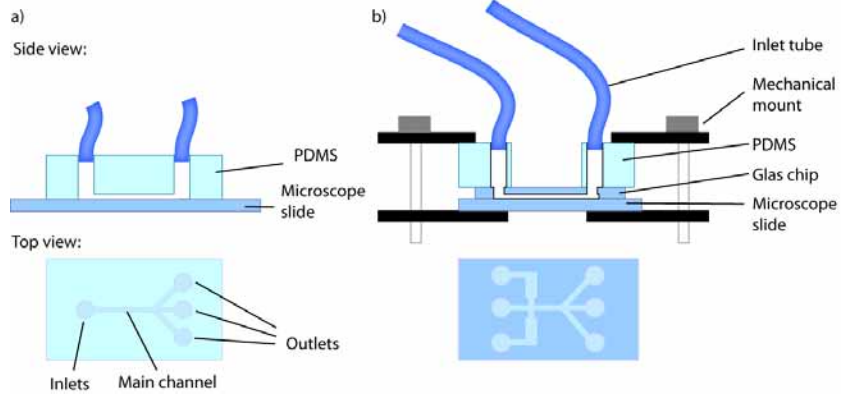


**Figure 2.17:** Two constructions of microfluidic chips. On a), channels are molded in PDMS and bonded to a glass microscope slide. Holes for connecting tubes are punched into the PDMS layer. The channels of the chip drawn on b) are engraved in glass and the PDMS layer only acts for sealing the tubes connection. The assembly is pinched with mechanical clamps.

ing sorting in optical landscapes without total confinement of particles [13]. Our goal is to generate interferometric traps inside microfluidics capable to sustain flows and immobilize particles.

## Microfluidic Chip

Microfluidic chips are characterized by fluidic channels having at least one dimension in the sub-millimeter range, typically between 30 and 200 microns. In a basic design, several inlet channels merge in one central channel that lead to one or several outlets. The small dimensions allows fluids to flow in a laminar regime at low Reynolds numbers. With sufficient flow velocities, several different fluids can be flown parallel to each other over a long range with little diffusion.

Two types of microfluidic chips have been used for experiments presented in this dissertation. One sort is made out of silicone while the other one is a glass component. For the first type silicone is molded on a master made by photolithography (figure 2.17). The fabrication process is detailed in the appendix A.

Some experiments required a chip with glass top and bottom to withstand higher fluences than PDMS. In that case, Microchannels are engraved in a glass plate. Connection holes are drilled and the plate is mounted on a 1mm

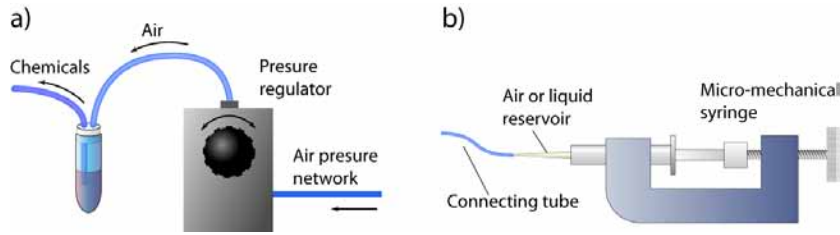


**Figure 2.18:** Microfluidic flows are controlled a) by regulators connected to an air pressure network and b) by a syringe mounted on a manually controlled precision screw.

microscope slide with a PDMS block for fluidic connections. The whole ensemble is pinched between mechanical clamps as shown in figure 2.17 b).

Microfluidic flows are either driven by external pressure regulators (Bellofram type 70) connected to the air network or by a manually controlled micro-mechanical syringe. Pressure regulators can be multiplied and control constant flows in several inlets independently. On the contrary, the manual syringe can not deliver a constant flow over a long period of time but offers the possibility to quickly control flow changes. Teflon tubes allow direct plugging to the holes punched in the PDMS layer. Beads solutions or chemical reactants are sucked at the end of the tube (figure 2.18 b)) or put in a reservoir under pressure (figure 2.18 a)).

The generation of interference fringes, not requiring bulky optics in the vicinity of the sample, allows the use of a wide range of chips or containers. In our setup, the microfluidic chips do not specifically need to have a thin bottom, as is generally necessary for trapping through high numerical microscope objectives. The bottom layer of the chip must nonetheless be of optical quality and supporting high fluences.

## Experiment

A microfluidic chip is placed inside the interference volume. The optical lattice covers a field larger than the channel's width so that the colloidal solution is flowing through the highest intensity zone of the template, which is created by superimposing beams with Gaussian intensity distribution. Figure 2.19 shows a sequence of images taken by a CCD camera illuminated by a red He-Ne laser at 633 nm. Green trapping light is filtered but is shown on b). The array pitch is two microns and polystyrene beads have a diameter of 2.06 microns. Beads flowing at velocities higher than  $100 \mu\text{m/s}$  could be

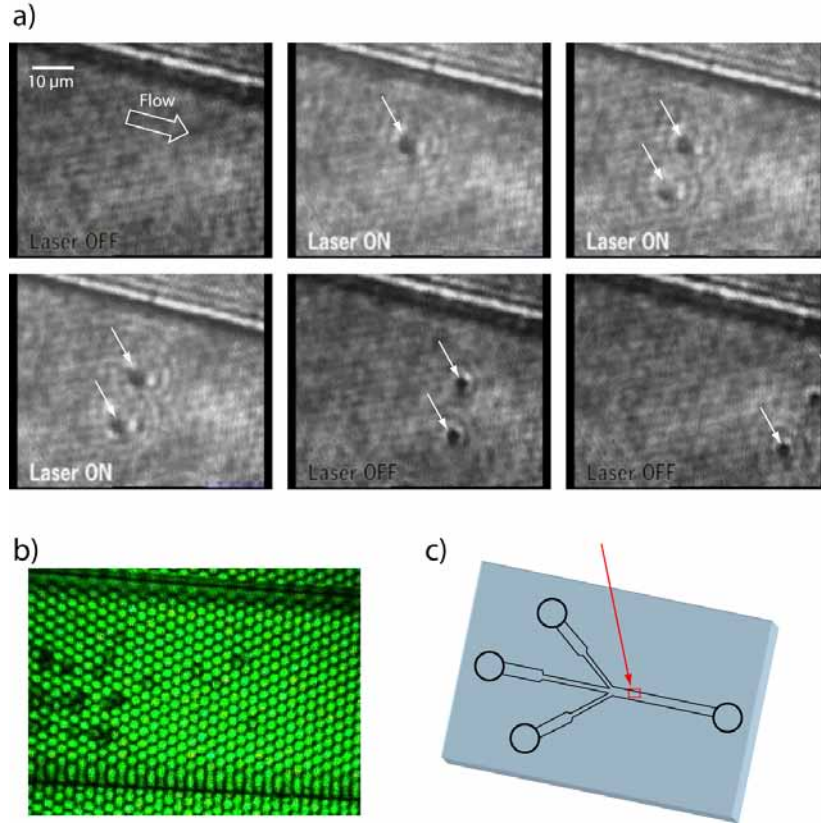


**Figure 2.19:** Polystyrene Beads ( $\varnothing 2.06 \mu\text{m}$ ) flowing in a microchannel and trapped in interference pattern. a) Sequence of images taken at 1 seconds intervals recorded on CCD through a red He-Ne illumination. The trapping laser at 532 nm is turned on between the first and the second image and is filtered before the camera sensor. b) Optical template recorded without filtering. c) Schematic representation of the microfluidic chip and the region of interest.

stopped by the optical traps. The initial power of the laser is 3.5 W. When the laser is turned off, released beads flow away with a slower speed due to their proximity to the top of the channel and due to Poiseuille flow speed distribution.

## 2.3 Variation of trap size

A key issue when generating very large number of traps is the individual efficiency of each trap, since the initial power is distributed all over the traps. We have seen in paragraph 2.2.4 how to increase the intensity gradient of each potential well. In this section we are interested in studying the



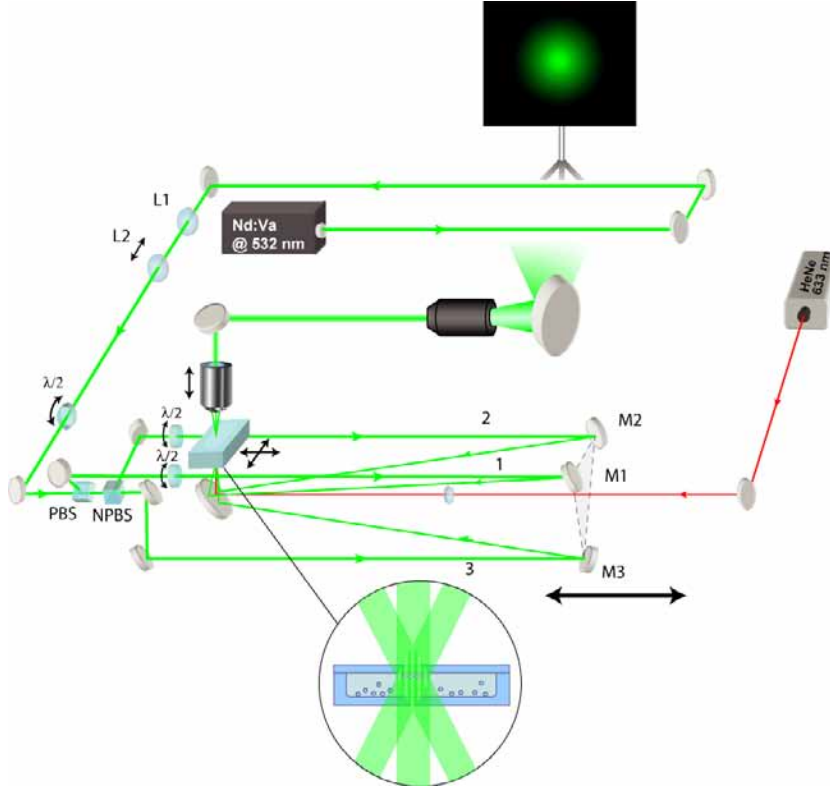


**Figure 2.20:** Enhanced experimental setup for fringe modulation when compared to the setup in figure 2.10. The three mirrors M1, M2, M3 can be translated to change the angle between interfering beams.

optimal trap size for a fixed size of particle of given index. For the considered particles' sizes no simple analytic predictions can be made to determine the optimal trap size. The resonance effects have important influence on the trapping forces as theoretical works predict [86, 87, 89]. Several groups are studying the comportment of particles in large optical landscape [93, 94, 95, 96]. Zemanek et al. have studied the behavior of sublambda particles in standing-wave showing the influence of the size on the trapping effects [84, 113, 114, 32]. They demonstrated how particles can be dragged or not in travelling standing waves depending on their size. We are interested in micrometric particles (typically 2 to 6  $\mu\text{m}$ ) whose sizes are comparable to the ones of targeted biological elements (some microns for prokaryotic cells and 10-20 microns for eukaryotic cells). We present here under the first experimental results of the influence of varying the sinusoidal trap sizes on the trapping efficiency for a given size of particle.

### 2.3.1 Setup modulation

The experimental setup is based on the scheme presented in paragraph 2.2.5 but requires to have an adjustable angle between interfering beams. Figure 2.20 presents an overview of the modified experimental setup. The initial beam is divided into three beams propagating parallel to each other and impinging on three mirrors (M1, M2, M3) placed at the apex of an equilateral triangular basis of the pyramid formed by the interfering beams. The three mirrors are on a common mechanical base that can be translated along the axis of the pyramid. Mirrors are mounted on kinematic mounts for fine adjusting of the reflecting beams onto the sample which remains at a fixed position. The interference pitch  $p$  can be varied as a function of the position of the three mirrors:

$$p = \lambda \sqrt{\left(\frac{L}{a}\right)^2 + \frac{1}{3}} \quad (2.12)$$

where  $a$  is the distance between the parallel beams and  $L$  the distance between the cell and the mirrors, corresponding to the height of the pyramid. The easy positioning of the mirrors M1, M2 and M3 allows a relatively quick adjustment of fringe spacing between 1 and 10  $\mu\text{m}$  with a accuracy of 20nm. The symmetry around the axis of the pyramid leads to similar optical path-length for each beam for every longitudinal position of the three mirrors basis. The telescope system composed of lenses L1 and L2 is also adjustable in order to focus simultaneously the three beams into the sample cell.

### 2.3.2 Beads behavior in various fringe sizes

First observations were performed with beads of 2.061 microns in diameter (Polysciences Inc. Cat# 19814) trapped in arrays with fringes spacing of 6, 5, 4, 3, and 1,74 microns. Beads were not electrically charged. Parallel line traps and hexagonal traps have been studied. A single bead, when not in presence of other particles, will set at the highest intensity peak of traps larger than the beads diameter. However when the size of fringes was set to 1.74  $\mu\text{m}$ , i.e. smaller than the beads diameter, the trapping seemed to disappear. The 1.74  $\mu\text{m}$  pitch value was set according to theoretical calculations performed in the Mie regime with the exact parameters of the experiment<sup>2</sup>. This fringe's size was predicted by the model to achieve the maximal trapping force for

---

<sup>2</sup>O. Moine, April 2006



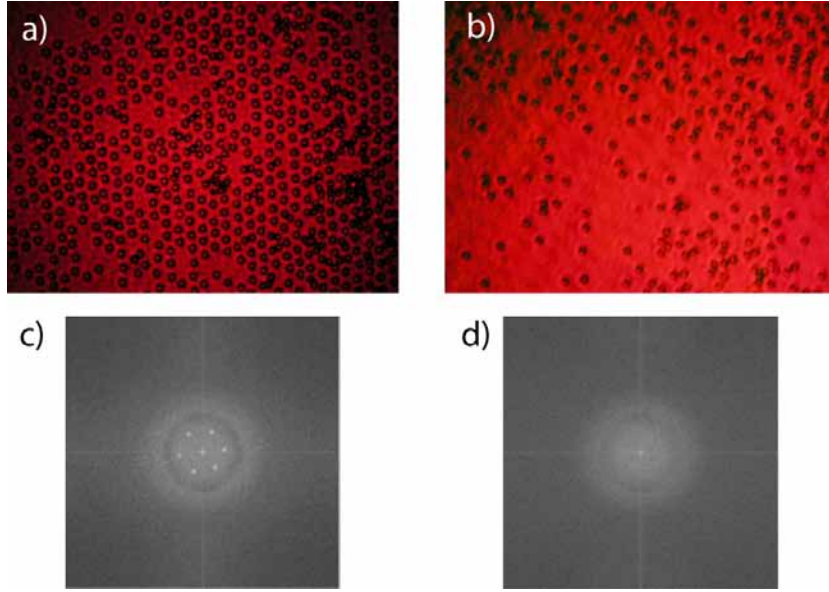


**Figure 2.21:** Polystyrene beads ( $2.06 \mu\text{m}$  in diameter) in hexagonal pattern of a)  $4 \mu\text{m}$  and b)  $1.74 \mu\text{m}$ . c) and d) FFT of images a) and b) respectively. Diffraction spots are not present in d); this is evidenced by the lack of trapping.

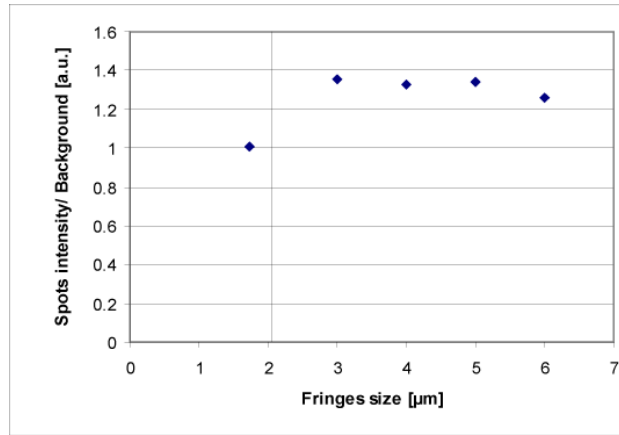


**Figure 2.22:** Intensity of spots in FFT image of beads arrays depending on the pitch of the light template.

$2.06 \mu\text{m}$  spheres. The experiment did not confirm predictions. To check for the trapping quality, we recorded images of beads in a still cell when various traps sizes were applied and we processed the images through a Fast Fourier Transform (FFT). A regular arrangement of the beads in the traps produces more intense spots in the FFT image. Figure 2.21 presents an arrangement of 2-micron polystyrene beads in a 4-micron and a 1.74-micron hexagonal

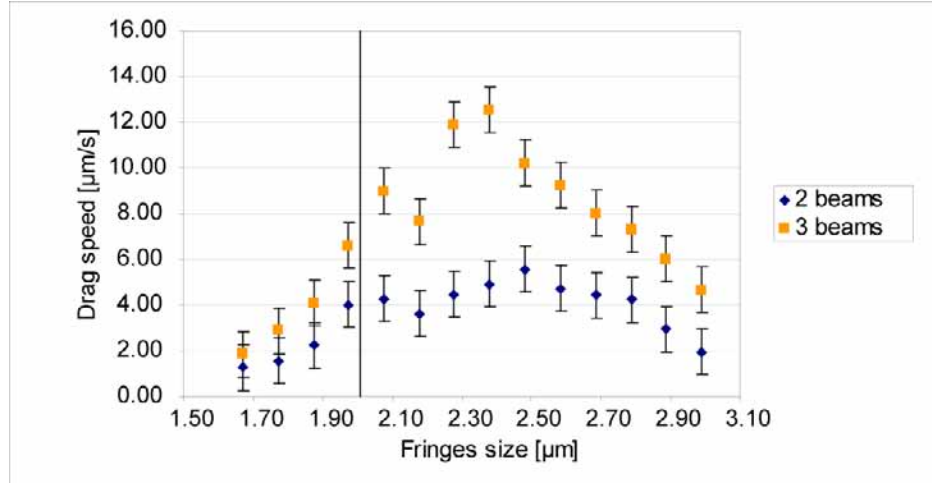


**Figure 2.23:** Optical trap stiffness measurement as estimated with the maximal drag speed sustainable by 2.06 micron polystyrene beads in sinusoidal (lozenges) and hexagonal (square) pattern as a function of the array's pitch. The laser power in the cell is 1.8 W with 3 beams and 1.25 W with 2 beams. The vertical line indicates the particles' size.

2D array generated by the Nd:Va laser at 532 nm and illuminated by an He-Ne light (green light is filtered). The FFT-image of the 4-micron trap array clearly shows the arrangement of the beads in the hexagonal pattern. Oppositely, no organization was observed with the 1.74  $\mu\text{m}$  trap array. The intensity of the peaks as a function of the fringe's pitch is illustrated in figure 2.22. The analysis of the diffraction spots in the FFT (intensity of the peaks over the background) shows a decrease in the sharpness of the spots with the increasing fringe sizes. At this stage, no external force was added and particles' movement is due to Brownian motion. One can notice the presence of Debye-Scherrer rings in figure 2.21 indicating the size dispersion of the beads.

In the next paragraph, the dragging method will be employed to emphasize the influence of the pitch of fringes on the trapping stiffness.

### 2.3.3 Influence of fringe's size on trapping efficiency

Investigations were performed with two different sizes of beads (2.061  $\mu\text{m}$  and 5.854  $\mu\text{m}$ , Polysciences, inc Cat#19814 and Cat#7312 respectively). For each bead type, the fringe's pitch (distance from peak to peak) was modified in steps of 100 nm in a range between -0.5 micron to + 1 micron around the

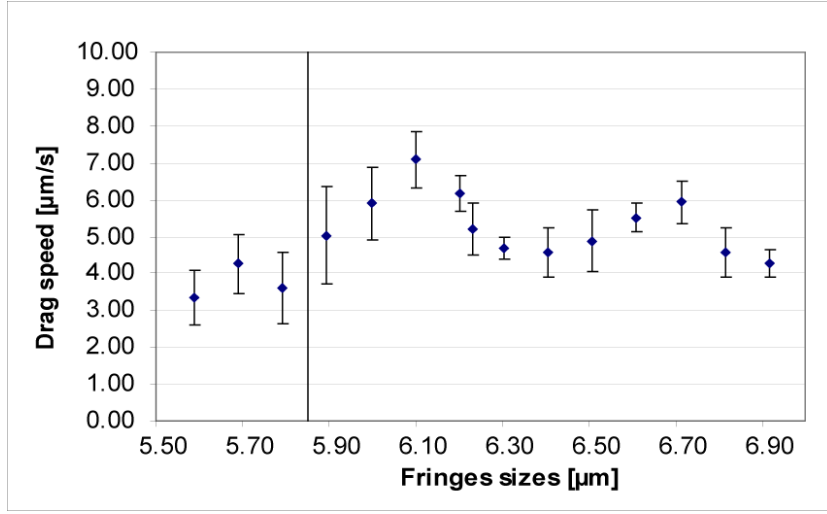


**Figure 2.24:** Same experiment as in figure 2.23 performed with 5.8  $\mu\text{m}$  polystyrene beads in sinusoidal fringes only.

value of the beads' diameter. The initial power at the laser output was set to 3 W corresponding to an effective total power of 1.8 W in the trapping area, divided in the three interfering beams. For experiments with sinusoidal traps, when just two of the three interfering beams are used, only two third of this power was available. Beads were observed at the top of a 200  $\mu\text{m}$  thick cell made by two glass slides separated by a PDMS spacer. The light template is fixed and the cell was laterally translated. Trapped beads stayed in the template while other ones were dragged with the fluid. The maximal speed at which the cell could be moved while particles remained trapped was defined as the maximal trapping speed. In the case of sinusoidal fringes, the dragging direction was set perpendicular to the fringe's direction. In the case of three beams, the dragging direction was perpendicular to the fringe's set created by the two beams whose polarization were collinear (see paragraph 2.2.5). The cell was dragged by one of the DC motor and the encoder permitted precise recording of the stage speed.

Figure 2.23 presents the maximal trapping speeds for 2-micron beads as a function of the fringes' pitch in the center of the gaussian shape of the template's intensity profile. This experiment is always performed with very dispersed solutions of beads to avoid optical interactions between neighboring spheres and to stay away from hydrodynamic effects. Every experiment was repeated six time for each fringes' size. The values illustrated in figure 2.23 and 2.24 correspond to the average of those six measurements.

One-dimensional (sinusoidal fringes) and 2-D (hexagonal) configurations were studied. Figure 2.24 presents the result for  $5.8 \mu\text{m}$  beads in sinusoidal fringes only.

### 2.3.4 Discussion on force measurements

A first intuitive reasoning leads to the thought that a bead with a diameter equal to a half of the fringes' pitch will be trapped in a bright fringe; when its size can covers two bright fringes it should sit in between, i.e. on a dark fringe. This is also confirmed by theoretical calculation [96]. Between the two cases (trapping in bright fringes or in dark fringes) there is one ratio of beads' size over fringes' size where optical forces cancel. According to our measurements there can be several fringes' size for which the trapping force is maximal.

In both studies ( $2.06$  and  $5.85 \mu\text{m}$  beads), we observe two force maxima for fringes' size slightly larger than the beads diameter. Although our trapping scheme does not allow determining the effective optical force because of the proximity between trapped particles and cell wall, the trapping speed recorded is nonetheless directly proportional to the trapping efficiency. The variation of trapping efficiency for both studied spheres' sizes could be explained by resonance effects. One must notice that no reciprocity should be expected with this curves. They give the trapping efficiency for one given size of bead as a function of the fringe's size, which differs from the efficiency for particle varying in size in a fix interference pattern.

The graph of figure 2.23 also reveals the variation in trapping efficiency due to the addition of a third beam. Although the template with three beams is implied with 1.5 times more power than the template with two beams, the trapping speed is indeed increased by a factor of about 1.95. This gain in efficiency can be attributed to several reasons. The increase of intensity gradient in the optical well created by three beams is higher than the one formed with two beams (see Table 2.1). The ratio of the intensity gradients between both cases is 1.75. Secondly, in the three beams configuration a stable trapping is reached, whereas in the two beams configuration particles are slightly pushed along the fringes due to the inclination of both beams with respect to the trapping plane. Even though the force measurement direction (dragging direction) is perpendicular to the fringes' direction in which the beads move, the lack of stability can lead to reduced efficiency.

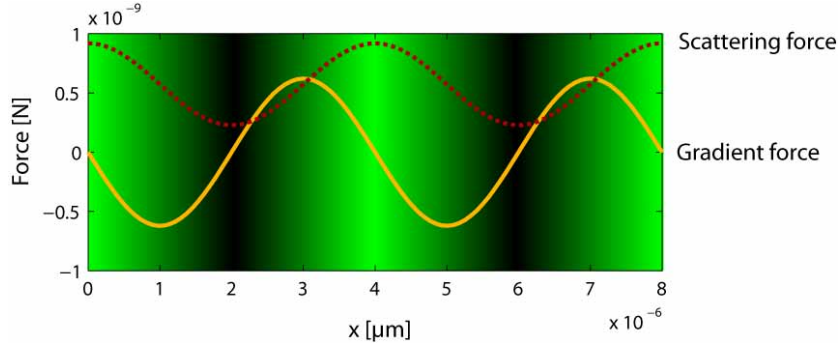


**Figure 2.25:** scattering (dotted line) and gradient (plain line) force acting on a 2-micron polystyrene sphere depending on its position in sinusoidal fringes with a pitch of 4 microns (background). The average laser power over the particle is 1 W. Calculation have been made according to the geometrical optics model. Results courtesy of F. Merenda.

The highest maxima of the two curves in figure 2.23 are not reached for the same fringe's pitch. To understand this shift, one must keep in mind that the distance between the intensity gradient maxima in an optical well is bigger for the 3-beam interference than for the 2-beam interference as we have seen in paragraph 2.2.4. Obviously the optimal trap's size in the 3-beam configuration is then reached for a smaller fringe's pitch than in the 2-beam configuration. The sampling of the measurement do not allow to see a similar discrimination between the position of the two first maxima of the curves in figure 2.23.

At rest, the equilibrium position of a trapped sphere is located at the peak of the bright sinusoidal fringe. When the cell is dragged, the particle finds a new equilibrium position, influenced by the viscous force. The effective trapping force is measured for beads located at this position. It theoretically corresponds to the maximal intensity gradient. In that position, the scattering force is also modified if compared to the one exerted at the center of a bright fringe. The variation of the scattering force as a function of the lateral position of the particle is shifted by  $\pi/4$  with respect to the gradient force. Figure 2.25 presents the value of the scattering force and of the gradient force for a 2-micron polystyrene sphere depending on its position in 4-micron pitch sinusoidal fringes, according to the geometrical optics model. A force measurement method based on the Brownian motion would allow to determine the stiffness of the traps close to the equilibrium position

but the dragging method is more representative of the working conditions in a microfluidic environment.<sup>3</sup>

## 2.4 Multiple beam interference

In most interferometric trapping setups, the intensity gradients are generated by the interference of a few beams (most often 2 to 6). Whereas the interference of two plane waves creates fringes with a sinusoidal profile, increasing the number of interfering waves sharpens the intensity gradient. As stipulated in paragraph 2.2.4 trapping forces can be increased by raising the intensity gradient of the optical trap. Multiple-beam interference, like the one produced in a Fabry-Pérot interferometer, provides very high intensity gradients and can therefore constitute an interesting basis to generate templates for optical trapping or guiding of particles. Their use was first suggested for atom trapping in the 90's [116] but, to our knowledge, was never used for micron-sized particles. In this chapter, we report on the first experimental trapping in multiple beam interference for mesoscopic objects [117]. Here, a solution to create high gradient fringes for trapping polystyrene spheres is presented. Multiple-beam interference trapping gives access both to massively parallel trapping and to the generation of high intensity gradient traps, and can be used in combination with microfluidics systems.

### 2.4.1 Generation of Fizeau-Tolansky fringes

Multiple interference fringes are generated by many passes of a coherent light beam through an interferometer [118, 119, 120, 121, 122]. Let us consider an interferometer composed of two reflecting plates, one being semitransparent and the other being highly reflective (figure 2.26).

---

<sup>3</sup>After the submission of this thesis manuscript, Mu et al. published an experimental study on the measurement of the trapping force for different bead sizes in fringes of various sizes [115]. For the beads they investigated (sizes 1.5, 2 and 3 microns), no local minima was found for fringe sizes bigger than the beads diameter; Also, their results fit the theoretical models. Several parameters differ between their experiment and the ones we performed: the trapping area is much wider in our setup, which causes the force to be one order of magnitude smaller. Our results are then more sensitive to the influence of other forces. Moreover the beam focus adjustment in our experiment can perhaps also cause some variations that are avoided in the scheme presented by Mu and co-workers. Nevertheless, our measurements are made in the same practical conditions than the ones used to perform all experiments reported along this thesis.

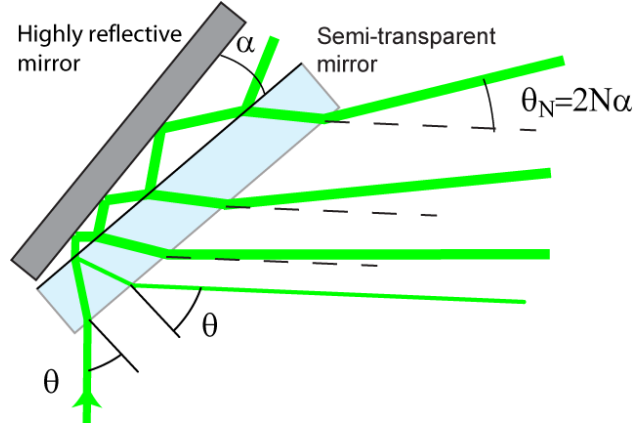


**Figure 2.26:** Multiple beam interferometer principle. Through a partially transparent mirror, an incoming light beam is divided in many sub-beams with different intensities and propagation directions.

The two plates form a dihedron with a small angle  $\alpha$ . A coherent laser beam incident on the system is first reflected on the semi-reflective interface and then reflected many times between the mirror and the semitransparent surface. Each transmission through the semi-reflective plate creates a "new" outgoing beam. Interference between the beams emerging from this system generate fringes. Each passage between the two plates induces a phase shift  $\Phi$ . A bright fringe is created when  $\Phi = m2\pi$ ,  $m$  being an integer.

Let us consider how the system evolves when the angle  $\alpha$  between the mirror and the semitransparent plate is modified. The evolution of the fringes has been studied in depth in [123, 124]. Two different cases can be distinguished depending on whether  $\alpha = 0$  or not. The first case, when  $\alpha = 0$ , produces multiple beams having the same tilt: this corresponds to the well-known Fabry-Pérot rings. In this case, the two mirrors are rigorously parallel and a lens is placed after the interferometer. The phase shift is given by

$$\Phi = \frac{2\pi}{\lambda} 2Ne \cos \theta + \Psi_{r1} + \Psi_{r2} \quad (2.13)$$

$e$  being the distance between the two layers;  $\Psi_{r1}$  and  $\Psi_{r2}$  are the phase shifts due to the reflections on the two reflecting surfaces,  $\theta$  is the angle of the incoming beam and  $N$  the number of reflections on the mirror. The system is working in air. The interference creates concentric circular fringes whose radius grows as the square root of the order number  $k$ . The  $k^{th}$  fringe is at

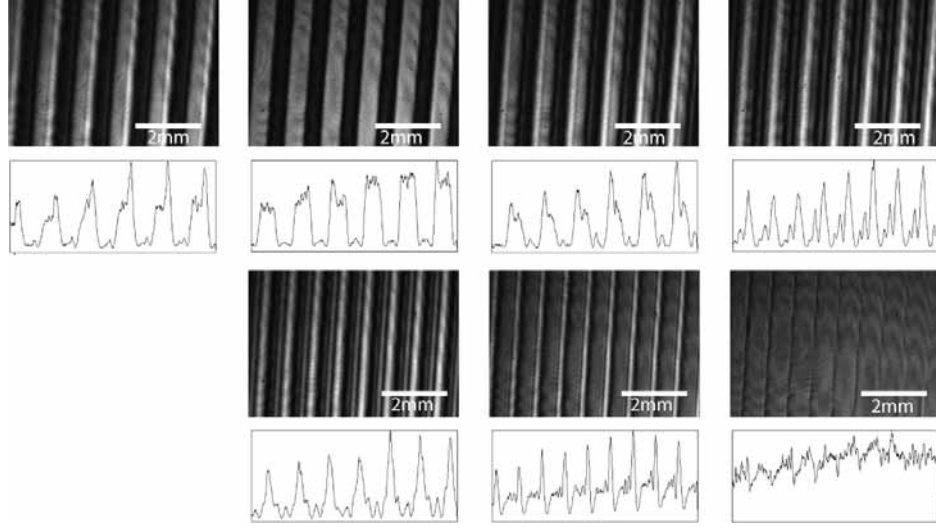


**Figure 2.27:** Variation of the profile of Tolansky fringes when angle  $\alpha$  between the two mirrors varies by successive steps of 0.05 degrees. Images are recorded by a CCD camera placed in the vicinity of the interferometer.

an angle

$$\theta_k = \sqrt{k} \sqrt{\frac{\lambda}{Ne}} \quad (2.14)$$

In the second case, the semitransparent plate makes a small angle  $\alpha$  with the mirror. Let us study the practical condition where the distance  $e$  between them is as small as possible. Each outgoing beam will propagate with an angle  $[-\theta - 2N\alpha]$ . This produces fringes sometimes called "of equal thickness" to refer to the optical path difference being the same at each step. Such fringes are known as Fizeau fringes or called also Tolansky fringes. They are produced both in transmission and in reflection; obviously, their intensity and profile depend on the reflecting coefficient of both plates and on the angle  $\alpha$ . Figure 2.27 shows some profile variation for different values of  $\alpha$  at a fixed plane located just after the interferometer.

According to Holden [125], the analytic expression of the profile in reflection is given by<sup>4</sup>:

$$I_R(\Phi) = r_0^2 + \frac{(t_1^2 r_2)^2 + 2t_1'^2 r_2 r_0 \cos(\Phi + \varphi') - 2t_1'^2 r_2^2 r_1 r_0 \cos \varphi'}{1 - 2r_1 r_2 r_0 \cos \Phi + r_2^2 r_1^2} \quad (2.15)$$

<sup>4</sup>This equation corresponds to the limit given by an infinite number of reflections



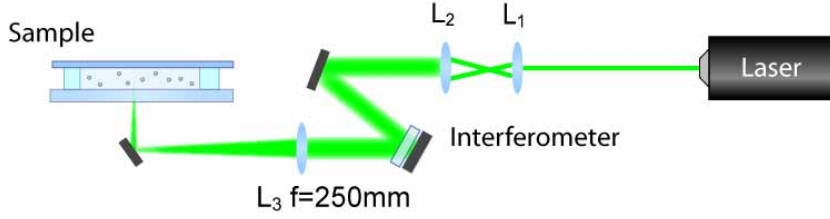


**Figure 2.28:** Output beams of the interferometer are focused on the sample cell. The trapping plane is imaged on a large screen.

$r_i$  being the amplitude reflection coefficient at the interface  $i$  and  $t'_i$  the amplitude transmission coefficient.  $\varphi' = \Psi_{r0} + \Psi_{r1} - 2\Psi_{t1}$  where  $\Psi_{t1}$  is the phase shift in transmission.

### 2.4.2 Experimental configurations

Two solutions have been tested to generate multiple fringes inside the trapping area of a cell. On a first example, fringes are generated far away from the trapping area and are projected to it by a relay optics. This system has been combined with a microfluidic chip and results are presented in paragraph 2.4.3. The other way out is to have the sample in contact with the interferometer, to generate fringes directly in the cell where trapping occurs. In that case, a converging beam is impinging on the interferometer. Eventually, a system composed by a double interferometer for generating of arrays is proposed in the last paragraph.

#### a. Projection of multiple-beam fringes

An interferometer generating fringes of equal thickness that are projected by a relay lens onto the sample is shown in figure 2.28.

The output of a the laser used in 2.2.5 is first expanded by an afocal system. The size of the collimated beam at the output of the telescope slightly overfills the aperture of the 1 inch interferometer mirrors. Multiple interference can occur only on the overlapping areas of the various beams which exit the interferometer; the wider the beams, the higher the number of overlaps, then the higher the interference number. The interferometer is composed of a 1 inch dielectric mirror and a 1 inch semitransparent plate which has an intensity reflection coefficient of 50% at  $45^\circ$  incidence at 532nm. The incoming beam impinges on the system at an incidence angle  $\theta$  set to  $11^\circ$ . At

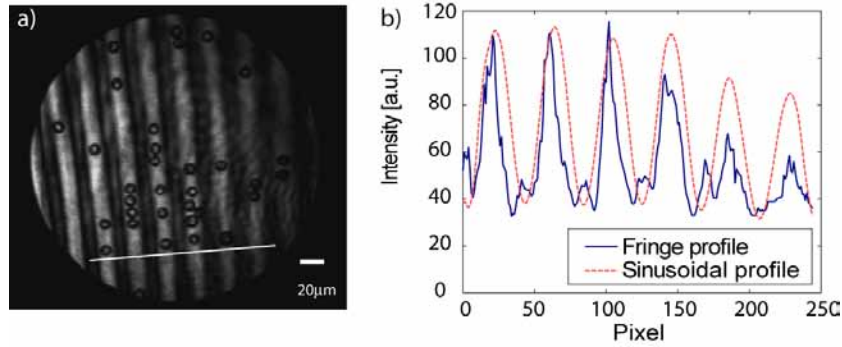


**Figure 2.29:** a)  $10\mu\text{m}$  beads optically trapped and aligned on multiple-beam interference fringes. Beads are at the top of a  $200\mu\text{m}$  thick cell. b) Intensity profile along the white line in a) compared to a sinusoidal shape.

this incidence angle, the reflection coefficient of the semi-transparent plate is 40%. The interference pattern generated at the output of the interferometer is projected by a large plano-convex lens ( $f=250\text{mm}$ ,  $\varnothing=2''$ ) onto the cell described on page 25 containing polystyrene beads suspended in water. The lens can be moved in the  $z$  direction for adjusting its distance to the sample. This distance should be slightly smaller than the focal length to allow overlapping of all beams on the trapping area. Obviously, at the focal plane of the lens the beams are focused at distinct focal points corresponding to the various directions of the individual beams: those are geometrically separated in the focal plane, then forbidding any interference. The imaging system is similar to the one exposed in the paragraph 2.2.5

The trapping area is  $240\mu\text{m}$  wide. Beads are laterally trapped by the gradient force and align in the bright fringes as they are pushed by radiation pressure towards the upper coverslip. They lay in a plane located at the top of the cell, called hereafter the trapping plane. Figure 2.29 a) shows the alignment of  $9.6\mu\text{m}$  polystyrene beads (Polysciences, Inc. polybeads CAT# 17136) in multiple-beam fringes. The comparison in figure 2.29 b) between the profile of the interference and a sinusoidal shape illustrates the gain on intensity gradient.

The two plates of the interferometer are mounted on kinematic mounts, facilitating a fine tuning of the angle  $\alpha$  and of the distance between the two mirrors. Small variations of these two parameters rapidly change the pitch and orientation of the fringes. This characteristic is of particular interest when used in conjunction with microfluidics as it will be presented in paragraph 2.4.3.

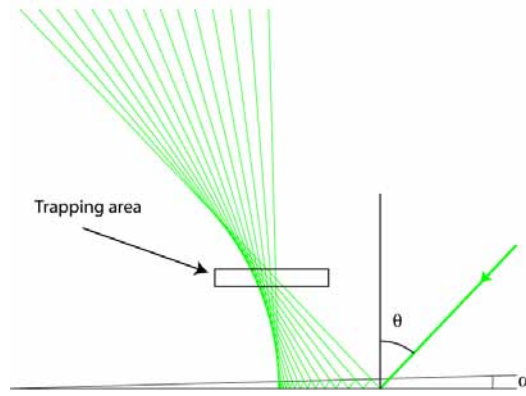


**Figure 2.30:** Crossing area of multiple reflections occurs in the sample. The use of a lens focusing in the same region concentrates energy inside of the sample area and leads to fringes' sizes in the micron range.

#### b. Generation of multiple-beam fringes in the sample

High optical gradients are due to the large number of interfering beams generating high order interference. Using a focusing element after the interferometer generating multiple beams however blocks higher spatial frequencies. Also, as mentioned previously, each beam focuses to distinct points separated from each other in the focal plane, preventing the formation of interference fringes in that particular area. These constraints add to the physical limitation of the system, when one attempts to decrease the fringe sizes within a restricted area. Indeed, to reduce the pitch of the fringes, the angle  $\alpha$  must be increased. However, the larger the angle, the larger the separation of the focus points in the focal plane.

The configuration presented in figure 2.30 allows increasing the interference order and avoids the use of relay optics between the interferometer and the sample. By choosing a negative angle  $\theta$ , the absolute value of  $\theta_N$  decreases as  $\alpha$  increases and the beams are crossing in a defined area whose size can be comparable to the beam cross-section. When the incoming beam is focused and the intersection area of multiple reflections coincides with the focal area, intense fields can be obtained without sacrificing the contribution of high spatial frequencies, overcoming the problem presented in the former paragraph. Obviously, the focal length and the numerical aperture of the focusing element should be appropriately chosen to produce a sufficiently long Rayleigh range in order to produce small variations of the beam radius between the intersecting reflected beams. Figure 2.31 shows the intensity

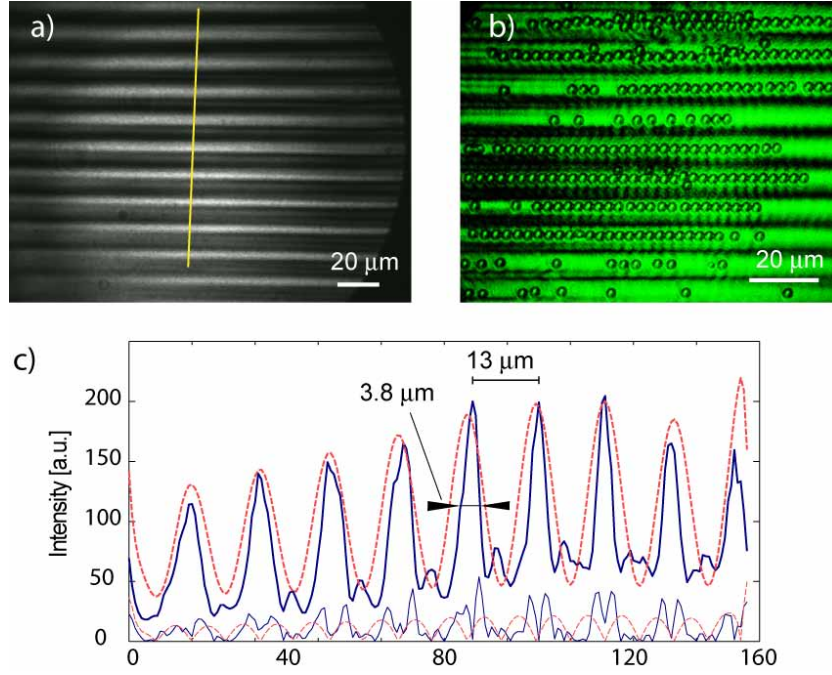


**Figure 2.31:** a) Multiple fringes generated directly at the output of the interferometer with a converging beam. b) 5-micron polystyrene beads trapped in multiple-beam interference fringes. c) Fringe intensity profile (bold continuous line) along line cross section in a) compared to a sinusoidal function with a similar envelope (bold dashed line). Thin lines at the bottom of c) show the absolute values of the gradient of the intensity profile (continuous) and of the sinus function (dashed).

profile of the fringes obtained with this scheme. The beam is focused by a 200mm focal length lens and the interference area covers about  $200\mu\text{m}$ . The intensity gradients shown in figure 2.31 c) (thin lines) has been raised up to a factor of 2.5 compared to a sinusoidal function. The width of the fringes has also been reduced by a factor of  $\sim 2$  with respect to the pitch of the pattern. When an optical landscape of such multiple-beam fringes is applied, polystyrene beads with a diameter of 5 microns are trapped laterally and can sustain a flow of few microns per second. Meanwhile they are pushed axially towards the top of the cell by radiation pressure.

### c. Two dimensional lattices

Combining two multiple-beam interferometers allows creating 2D light patterns as illustrated in figure 2.32 a) and b). The experimental configuration resembles a Michelson interferometer with two multiple-beam interferometers

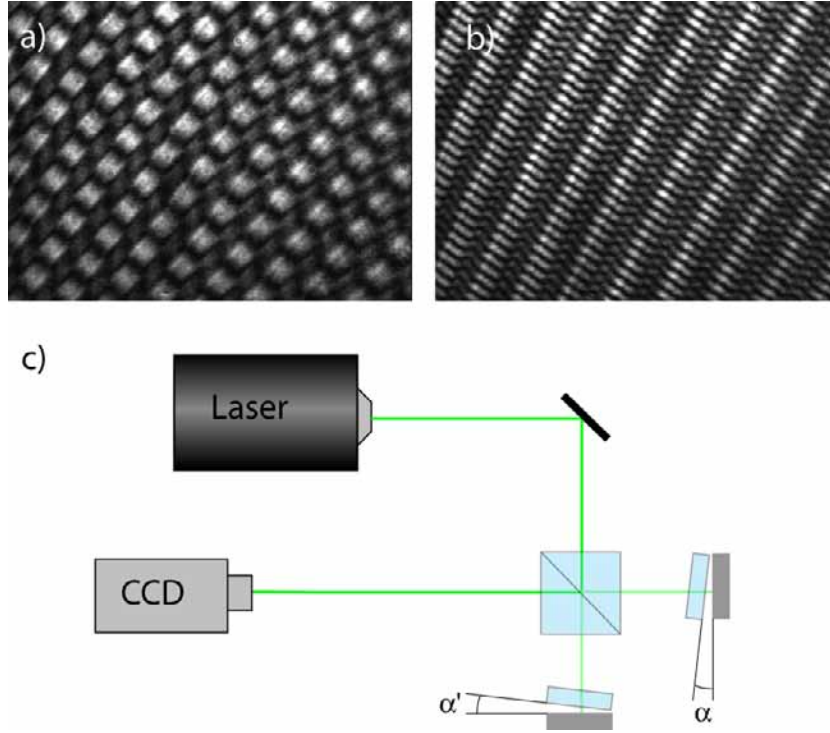


**Figure 2.32:** a) and b) Multiple interference fringes at the output of a double interferometer for different values of tilt angles  $\alpha$  and  $\alpha'$ . c) Setup scheme.

replacing the mirrors (figure 2.32 c)). This system could offer the opportunity to create asymmetrical traps of distinct shape and pitch in the  $x$ - and  $y$ -directions, since the parameters  $\alpha$  and  $e$  of both crossed interferometers can be adjusted independently. Figure 2.32 a) shows a regular pattern when the angle  $\alpha$  of both interferometers is set at the same value in two perpendicular planes. In contrast, in figure 2.32 b) the angle  $\alpha$  of one interferometer is bigger than in the previous system and fringes spacing gets smaller only in one direction.

### 2.4.3 Bead steering in microfluidic channel

The fringes generated by the setup presented in figure 2.28 have been projected into a microfluidic channel to deflect particles in a flow. A glass chip as presented in figure 2.17 b) is used and flows are regulated by a micromechanical syringe (figure 2.18 a)). The solution of polystyrene beads is contained in a polymer tube used as a reservoir and plugged to one entrance of the chip. Other inlets are blocked. Once injected in the chip, the solution of beads

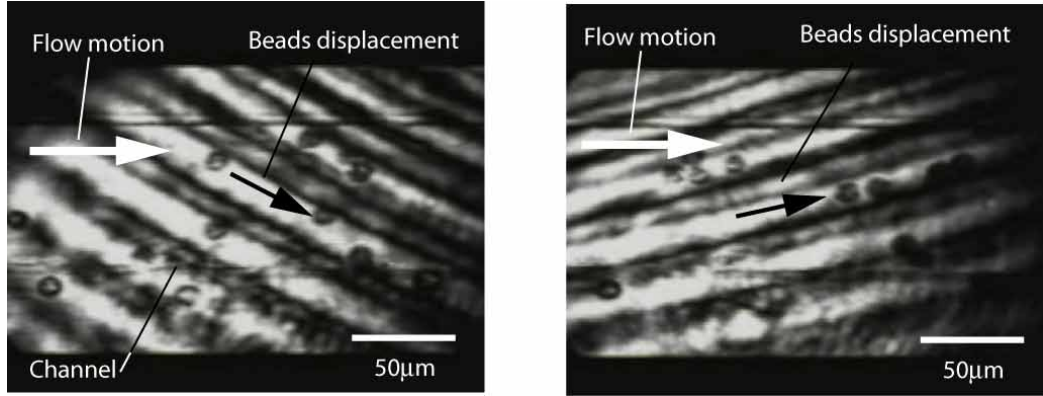


**Figure 2.33:** Ten micron polystyrene beads flowing in a glass microchannel and deflected by structured light shaped by multiple interference

flows through the main channel toward the outlets. The interfering beams create vertical "walls" of light inside the channel. A slight change in the orientation of the interferometer's semitransparent plate not only changes the width of the interference fringes but also modifies their orientation. The two parameters can be controlled independently. When the fringes' orientation is neither parallel nor perpendicular to the flow direction, the beads trajectory gets deflected due to the optical gradient force. Such guiding is shown in figure 2.33, highlighting two different directions of beads deflection. In this experiment fluid flows from 10 to 20 microns per second were used to carry particles. The simple control of the orientation of the fringes allows a quick and dynamic change of particles' trajectory.

#### 2.4.4 Discussion on multiple beam interference trapping

The results presented in paragraph 2.4.2 show how multiple-beam interference can sharpen the intensity gradient profile of fringes compared to the interference produced by two beams only. The implementation of Fizeau-Tolansky fringes by multiple beam interferometers generates fringes with high intensity contrast and gradient. However, "square" profiles obtained at a macroscopic scale (see figure 2.27) can not be replicated for fringes whose size is in the order of the wavelength. Indeed, the width of the fringe's edge always extends over a distance  $\geq \lambda$ . It seems essential here to remember that this work relates to mesoscopic sized spheres. In case of Rayleigh particles,



the optical field can be considered uniform over the entire spheres. For large objects one must consider variations of the field (gradient) all over the particle. Compared to a sinusoidal fringe which has a local flat intensity at its maximum, multiple beam fringes present a high gradient also at the center of the trap which provides a high gradient force at the equilibrium position. The sharp profiles presented in figure 2.27 are measured just behind the interferometer where the interference pattern area is several millimeter wide and the corresponding fluence is far too low for efficient optical trapping. Increasing the fluence by focalization is difficult due to the intrinsic separation of individual beams at the focal plane of the focusing lens. Figure 2.29 shows that, despite some loss in gradient sharpness due to the diminution of the number of crossing beams, the fringes' profile presents better characteristics for trapping than the sinusoidal shape of Young's fringes. The physical limits of the system prevent reducing the size of the fringes without reducing the intensity gradient. However, the forces are sufficient to deflect particles in microfluidic flows.

The approach described in 2.4.2 b significantly reduces the limitations of the precedent configuration. It presents two main advantages: smaller fringe pitches can be produced and many outgoing beams can overlap within the same area. This system is not aperture limited. The size of the trapping area depends directly on the beam size and convergence at the entrance of the interferometer. Although the light-path inside the interferometer is different for each outgoing beam, the difference in beam size can be neglected with respect to the focal length of the focusing lens and the beams have a comparable size in the overlapping area. One must notice that the solid state laser used in experiments has a coherence length of several meters. Therefore, coherence is not an issue in our experiments (except for the fact that we have to prevent undesired reflections which could create unwanted interference). Moreover, the superposition of spatially displaced beams modifies the intensity over the whole light field. One could take advantage of this feature to flatten the envelope of the overall intensity distribution. This would lead to a more uniform trapping efficiency over a large field, compared to the pseudo-gaussian shapes more often encountered in trapping.

As seen in section 2.3, the width and the profile of fringes are two key parameters for trapping mesoscopic objects. Multiple interference devices can control the fringe width with a very fine sensitivity, by adjusting the tilt

angle between the two reflectors and by modifying the incident angle. This can be taken into consideration to modify considerably the trapping efficiency of mesoscopic particles, with potential applications in sorting and in trapping. Alternatively, the fringes may be directly generated in the microfluidic system if the interferometer were integrated at the bottom of the chip.

## 2.5 Conclusion

Interference presents a great potential for multiple optical trapping, especially for very large number of traps (up to thousands) since the number of optical wells that can be created only depends on the width of the beam and on the relative width of the traps. Optical templates created by interference have been used to trap polystyrene spheres in a static environment and to stop particles flowing in a microfluidic flow. The traps' shape and size can be optimized for the particles to be trapped. The width of the interference trap for a particle of a given size can dramatically influence the trapping efficiency. Numerical simulations have shown the interest of increasing the number of interfering beams, confirmed by experimental results and led to the creation of Fizeau-Tolansky fringes. The implementation of a multiple beam interferometer allowed a simple control over the width and the orientation of the fringes. Multiple beam fringes have been successfully used to deflect particles in a microfluidic channel. Interferometric traps are not aperture limited and do not require bulky optics. They can be generated in a wide range of containers, including cells with thick bottom, microfluidic chips and commercial fluorescence and absorption cells. Trapping schemes presented in this chapter allow creating two-dimensional arrays of objects. The confinement in the third direction is realized by mechanical contact to a wall of the container. The influence of the vicinity to the surface is still poorly understood and needs to be the subject of further investigations.

The high number of traps achievable is obviously energy costing. Indeed, the total available laser power is spread out over all individual traps. Although weak traps can even generate an arrangement of particles in a static environment, in fluidic system strong traps are required to sustain flows. A laser power of several watts (3-4 W) is needed for about 500 traps in a microfluidic environment to allow micron-size particles sustaining flows of some tens of micrometer per second. However, the generation of traps array by interference can be done with minimal loss of energy since no microscope



---

objective with very limited transmission, nor diffractive elements producing unwanted diffraction order are used. Losses can occur due to shape and size mismatches between the optically patterned area and the microchannel containing the sample. Ultimately, interferometric system could be directly embedded in a lab-on-a-chip, e.g. by engraving diffraction gratings directly on the bottom of a fluidic chip [126].



---

# Optical trapping in Fresnel diffraction

## 3.1 Introduction

In the previous chapter, we have seen how to trap particles in interference pattern and we have emphasized the advantages of avoiding the use of high numerical aperture microscope objectives. We have also seen how demagnifying optics can be a drawback when one wants to generate high optical gradients. In the Fresnel diffraction regime, i.e. just behind a diffractive element, wave propagation directions are not filtered and all spatial frequencies can propagate and therefore contribute to enhance intensity gradients. Unlike most optical trapping schemes working in the far field, through a microscope objective, or in evanescent wave, we present original solutions for taking advantages of diffraction in the Fresnel regime.

In this chapter, several cases are treated where particles are trapped in intensity distributions generated in the Fresnel diffraction regime. First observations concern particles trapped in diffraction patterns produced by other colloidal particles, trapped or not. The use of particles to generate optical traps is reported for the first time. In the second section, diffraction is generated by a diffractive optical element especially designed to generate, by Talbot restructuration, periodic fields used as optical templates for optical trapping. We present what is, to our knowledge, a remarkable solution for 3-dimensional multiple optical trapping without the need of microscope objectives. The influence of the diffractive optical element's properties on the self-imaging Talbot effect is studied through numerical simulation according to the Fresnel diffraction theory.

## 3.2 Trapping in diffraction patterns

The field diffracted by particles immersed in an electromagnetic field interferes with the illumination field, creating a new intensity distribution among which one finds optical potentials. Polystyrene spheres are very sensitive to light intensity variations and can be trapped at local maxima or in areas where their volume contains the maximum of electromagnetic energy density.

### 3.2.1 Trapping in diffraction rings

A common diffraction pattern is the one created by a single spherical particle immersed in a plane wave. It creates diffraction rings, as described by Fres-

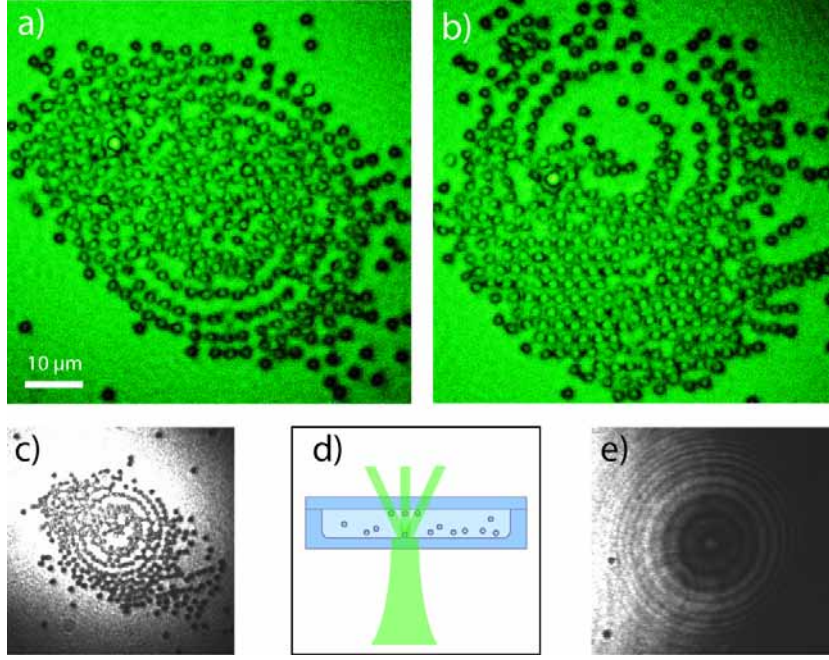


**Figure 3.1:** a)-c) 2.06  $\mu\text{m}$  polystyrene beads trapped in the diffraction of a same bead sticking at the bottom of the cell. d) Schematic representation of the trapping in the diffraction of a single bead. e) Diffraction rings of a single polystyrene beads in Fresnel regime

nel's theory. Figure 3.1 e) shows diffraction rings from a polystyrene particle at the border of a Gaussian beam. In the center of the Gaussian shape, i.e. at the maximal intensity, the intensity variations due to the presence of a particle are hardly visible by human eye. However polystyrene beads are very sensitive to the intensity variation and get trapped along the rings as visible in figure 3.1 a)-c). In a single closed chamber, diffraction rings at the trapping level (top of the chamber) are due to beads sticking at the bottom or rising up because of radiation pressure. In order to control the diffraction pattern, a double chamber with two trapping levels is proposed in the next paragraph.

### 3.2.2 Two levels optical trapping

Various diffraction patterns are created by arrays of trapped particle. Figure 3.2 b) shows the principle of trapping in the light diffracted by a crystal of trapped beads. In order to use the diffracted light as a mean to build optical traps, a second cell is built over the first trapping chamber. We use two

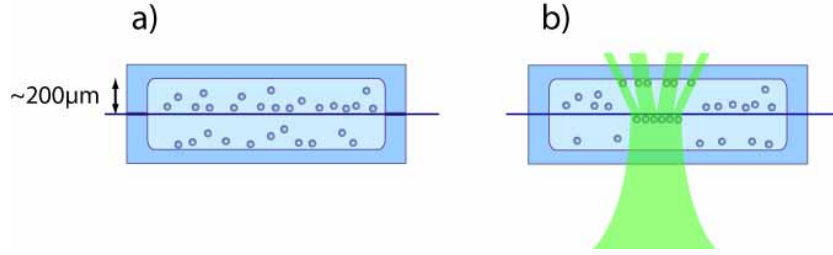


**Figure 3.2:** Schematic representation of two cells separated by a thin film. a) The two chambers are filled with beads at different concentrations. b) Trapping in impinging beam and in light diffracted by trapped beads.

bottoms of commercial cells with detachable window, Hellma # 106 (see page 25). The two etched grooves ( $200\text{ }\mu\text{m}$  deep) face each other and are separated by a thin stretched plastic membrane ( $10\text{ }\mu\text{m}$  thick). The two chambers are filled with polystyrene beads in suspension at different concentrations as schematized in figure 3.2 a).

Figure 3.3 presents the result of three experiments. The images on the first column (inserts a), d) and g)) show the beads at the lower chamber of the cell sketched in figure 3.2. The two columns on the right present beads trapped and/or bound at the top of the upper chamber.

At the lower level, beads are trapped by a large Gaussian trap. The waist of the beam is about 50 microns in diameter. A single bead will sit at the center of the Gaussian distribution and create diffraction rings as described in the precedent paragraph. The Brownian motion of the beads makes the diffraction pattern move slightly, forcing a perpetual rearrangement of the trapped beads at the upper level. Insert of figure 3.3 b) clearly shows the alignment of particles along the curvature of diffraction rings. In the wide central spot, a non perceptible ring (visible only on the graph of figure 3.4) prevents the beads to all accumulate at the center.

Several beads trapped in a single large Gaussian beam ( $> 10 \times$  beads diameter) will self-organize to form a crystal in a close-packed form. This self-organization due to trapping and binding forces will be described in detail in chapter 4. Since the close-packed arrangement has a three-fold symmetry, the light is diffracted in six first order directions. In the Fresnel regime the diffraction pattern forms interference fringes along the six orientations. Particles are trapped in the fringes and hop from one the the other depending on the movement of the pattern (figure 3.3 e) and f)). At the limit of the Fresnel regime, distinct spots characteristic of Fraunhofer diffraction appear.

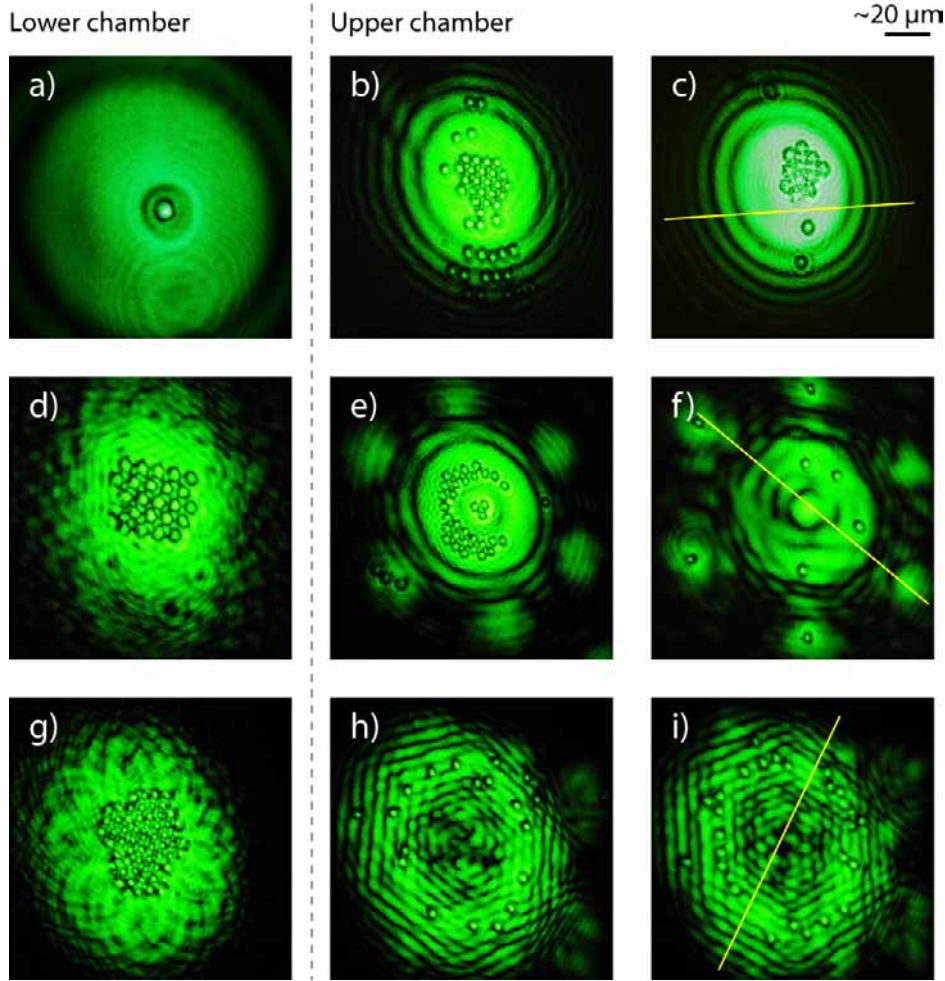


**Figure 3.3:** Trapping in a two-level cell according to scheme of figure 3.2. a), d), g) Trapped beads at the top of the lower chamber (left column) and corresponding diffraction patterns with trapped particle at the top of the upper chamber. Images in the middle column and in the right column are taken at different periods.

Particles are also trapped in these spots (figure 3.3 h) and i)). The flexibility of the separation film between the two chambers allows a variation in the height of the chambers. The images in the second (e, f) and third rows (h, i) are taken at two different heights of the second chamber. The intensity profile shows important variations as plotted in figure 3.4. On graph a) the fringes amplitude is increasing monotonously towards the center. Beads can jump from one fringe to the next. On the contrary, on graph c) potential barriers are too high and beads remain trapped in one fringe.

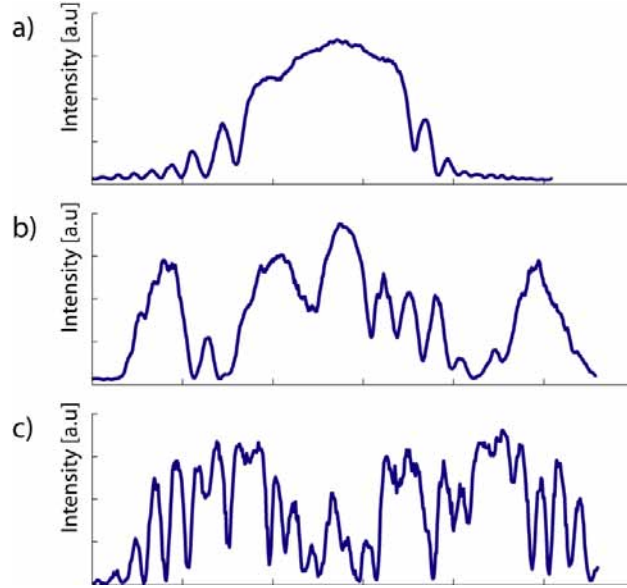


**Figure 3.4:** a)-c) Intensity profiles of diffracted pattern along lines in figure 3.3 c) f) and i) respectively.

### 3.3 Trapping in Talbot lattices

Using a static diffractive optical element (DOE) allows generating fixed 3D light intensity distributions for optical trapping. In optical trapping experiments, they are often used to work in the far field in conjunction with microscope objectives, but they can also be designed to create traps array in the Fresnel diffraction regime, in particular by exploiting the Talbot effect.

#### 3.3.1 The Talbot effect

Self-imaging of periodic structure was first observed by William Henry Fox Talbot in the beginning of the 19<sup>th</sup> century. Talbot is one of the pioneers of photography; he realized the first negative image that could be replicated in many positive images through a process called calotype (also sometimes called talbotype). Working on image propagation, he found that an object presenting periodicity in its lateral dimensions creates, when illuminated, a periodic field in the  $z$  propagating direction. The pattern of the grating is repeated at regular intervals, multiple of the so-called Talbot distance. Talbot published his results in 1836 [127] but did not pursue this research, as he was concentrating on photography. It is only in 1881 that the phenomenon



was explained by Lord Rayleigh [128] as a consequence of Fresnel diffraction. He showed that the Talbot distance  $Z_T$  is given by

$$Z_T = \frac{2d^2}{\lambda} \quad (3.1)$$

where  $d$  is the pitch of the periodic object and  $\lambda$  the operating wavelength.

The periodicity of the object can be either in amplitude or in phase. In the first case, the grating is replicated at integer multiples of the Talbot distance  $Z_T$ , whereas at halves of  $Z_T$  the same modulation occurs but with a contrast inversion; moreover, at a fourth of the Talbot distance a modulation of twice the frequency of the grating is produced [129, 130, 131]. Figure 3.5 presents a simplified schematic superposition of the diffracted pattern of a set of slits emphasizing the reconstruction of the grating pattern. The diffraction order of each slits are represented by a vanishing stroke. Indeed, destructive interference can not be represented on the image, but the presence of pattern with a spatial frequency double of the original one is easily understandable.

In the case of the diffraction by a periodic phase structure, an amplitude modulation is generated at fractions of the Talbot distance as described by Lohmann [132, 133].

$$z = N \cdot Z_T + \frac{P}{Q} Z_T \quad (3.2)$$

Where  $N, P$  and  $Q$  are positive integers and  $P < Q$ .

With a pure phase grating, the whole light is redistributed in the amplitude pattern with some field enhancement. This local increase of intensity will be exploited later for optical trapping. The optical wells are confined laterally according to the periodicity of the structure and axially according to positions of sub-Talbot planes. The technique has been proposed for so-called Talbot array illuminators (TAIL), taking advantage of fractional-Talbot effects, generating Talbot sub-images, sometimes referred as Lohmann images or Fresnel images [134, 135, 136, 137, 138]. The basic principle of a TAIL is schematized in figure 3.6.

The self-image phenomenon occurs also with incoherent light and was described by E. Lau in 1948 [139], and is now coined the "Lau effect" [140]. It has to be noted that speaking of *images* (or *self-images*) for the Talbot effect is actually a misnomer. Indeed, if the reconstructed intensity pattern in the Talbot plane reproduces the one of the illuminated structure, no "images" are produced in the optical meaning of the term; there is no amplitude and

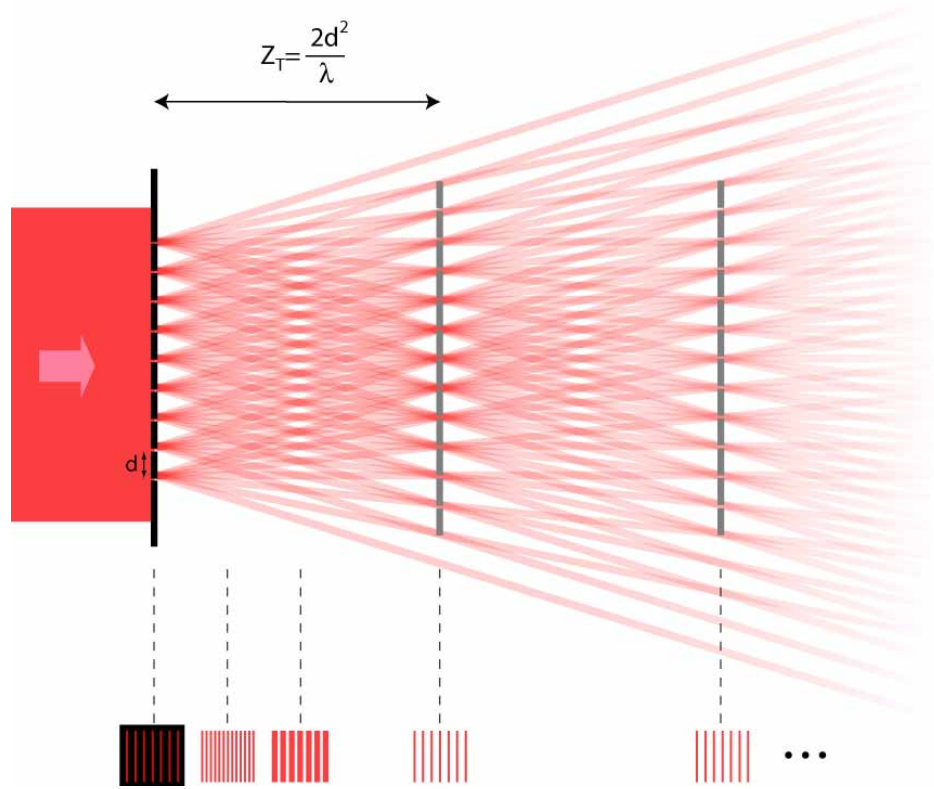


**Figure 3.5:** Talbot Effect: schematic superposition of the diffracted pattern of individual slits distributed along regular intervals. The periodicity in the  $z$ -direction is clearly visible and reconstructions of the initial pattern are manifest.

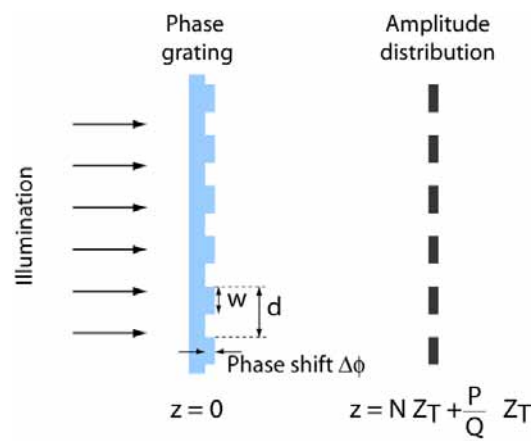


**Figure 3.6:** Principle of a Talbot array illuminator with a two level phase grating.

phase conjugation from one Talbot plane to the other one as described in P. Latimer's article [141]. The term "intensity pattern" are more rigorous than "self-images". We will however sometimes refer to the terms of self-images and self-imaging, since they are commonly used in the literature.

The Talbot effect acts also sometimes as a prejudice creating unwanted outcomes in many applications in optics, when dealing with periodic elements like microlens arrays [142], VCSEL arrays, etc. The effect has however been exploited in different ways for example for imaging [143], phasing of arrays of semiconductor lasers [144] or distance measurement [145, 146]. Three dimensional light patterns generated by Talbot effect have been successfully replicated by photolithography in photopolymer to create physical 3D structures [147].

In the present work, the field created by a two dimensional phase grating illuminated by a plane wave is used to trap dielectric particles. Optical trapping in Talbot lattices was experimented with microspheres by Fournier et al. in the 90's and also used as a tool for selective atom cooling [34, 42]. Walker and al. have carried out several experiments with cold atoms in Talbot structures [148]. Later on we applied the effect to microbeads trapping [76]. Talbot effect is also mentioned as a based for optical trapping due to periodicity of an optical lattice formed by the interference of multiple plane-waves generated by a spatial light modulator [97]. Talbot images have also been recently used to sort polystyrene particles in microfluidics with two dimensional traps [149].

In this report, a simple way to generate Talbot images just by projecting one beam on a diffracting structure is proposed for trapping mesoscopic particles. Three dimensional arrays of traps are generated and, for the first time, particles were trapped at different levels. In a first paragraph, the self-imaging effect is first illustrated by an example of the diffraction by an array of trapped particles. A second part focuses on the study of the diffraction of different structure in the Fresnel regime through numerical calculations. Finally, experiments on optical trapping in Talbot 3D-traps are presented and discussed.

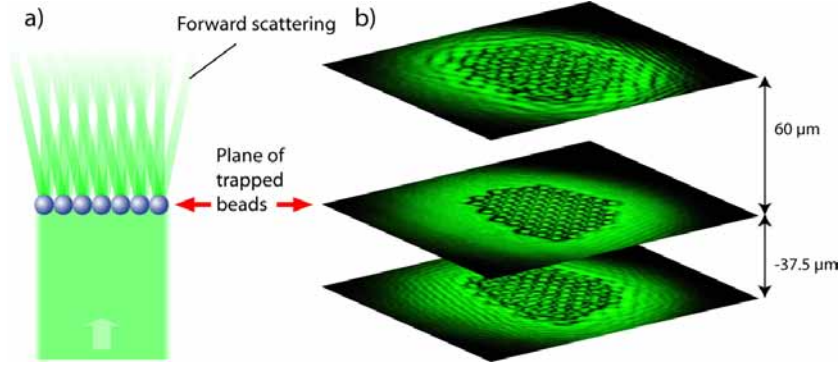


**Figure 3.7:** Self-images of an array of beads over and under the real position of the beads.

### 3.3.2 Self-imaging effect of an array of trapped particles

Spherical particles trapped in a single wide Gaussian beam arrange themselves in a close-packing form as seen previously. As the crystal formed by the spheres reaches a sufficient size, the periodicity created by the alignment of beads in an hexagonal shape generates a Talbot effect such that self-images of beads are present at several levels above the real "physical" array. Since the trapped array is not infinite, edge effects occur and a good reconstruction of self-images only appears above the center of the crystal; the borders get fuzzier as we consider planes further away from the array. The observation of self-images of trapped beads is illustrated in figure 3.7. Measurement have been performed over a range from  $-50 \mu\text{m}$  to  $+100 \mu\text{m}$  away from the physical beads' plane and Talbot images of the beads array are reconstructed over this entire distance. According to theory, the first Talbot plane is located at  $Z_T = 3d^2/2\lambda = 45.9 \mu\text{m}$  for beads with a diameter of  $3.5 \mu\text{m}$ . Figure 3.8 a) shows the evolution of sub-images over 60 microns above the beads' plane. These images are captured through a long working distance microscope objective focused at various planes of observation. It is to be noted that the objective itself makes a spatial filtering preventing the imaging of the real intensity in the observed planes. The progressive restriction of the area displaying a sharp reconstructed image is clearly visible and emphasized on two images with a bold white line.

Talbot effect occurs both above of and below the periodic object. The column b) of figure 3.8 shows the reconstructed pattern under the plane of

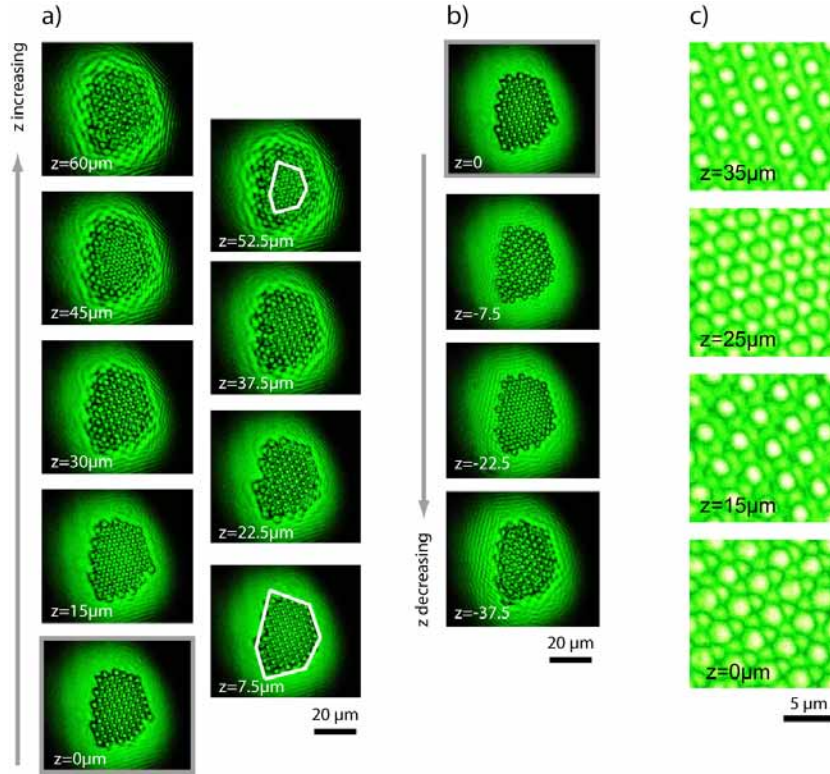


**Figure 3.8:** Self images of a close-pack crystal of 3.5 microns polystyrene beads. a) images taken every 7.5  $\mu\text{m}$  over the beads planes. b) images taken with the focal plane of the objective position under the array. c) evidence of the contrast inversion in the self images.

spheres, where images are taken with the focal plane of the microscope objective below the real array. The large number of diffraction directions above the array, i.e. in the direction of propagation of the beam, can reconstruct a virtual image which "seems" to be behind the real periodic structure.

It should be noticed that for a spherical shape of the individual elements forming the optical crystal, sub-images positions are not as well defined as in step-case phase variation. Indeed, the beads act as microlenses and they create a first array of intensity maxima which is much more intense than the following Talbot sub-images. Several contrast inversions occur between the Talbot planes as visible in figure 3.8 c).

Figure 3.9 presents a simulation of the Fresnel diffraction over 100 microns above the array. Sub-figure b) shows the intensity distribution in the yz planes corresponding to the black line drawn on a). The sphere have a diameter of 3.5 microns and their refractive index is 1.6.

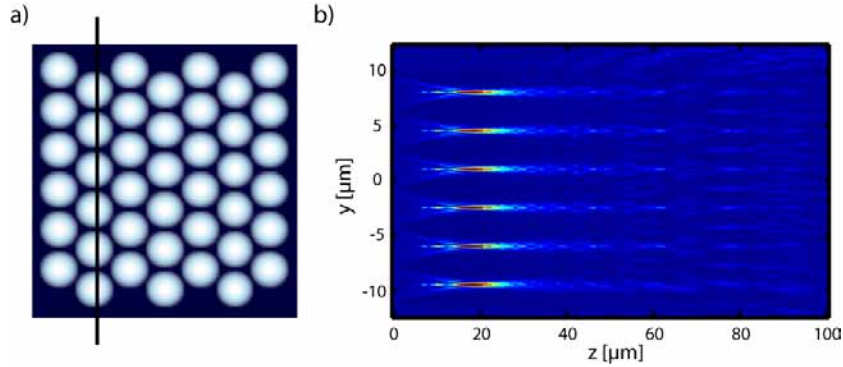


**Figure 3.9:** Simulation of the diffraction generated by an hexagonal array of polystyrene beads. a) Phase shift in the xy plane due to the 3.5  $\mu\text{m}$  diameter polystyrene spheres (false colors). b) Intensity distribution over 100 microns in the yz plane corresponding to the black line visible on a).

### 3.3.3 Numerical simulations and creation of periodic light templates

The Talbot effect presented in the last paragraph occurs from periodic arrays formed by trapped particles. Obviously, the same effect can be generated by a fixed element designed to create a desired light template for optical trapping. A good understanding of the Talbot effect is necessary to predict the position and the intensity pattern of the sub-Talbot images in order to design the appropriate diffractive elements. The next pages present the method used to simulate the light propagation in the Fresnel regime, and the results of the simulation for various diffractive phase structures designed for generating controlled arrays of optical traps.

#### Fresnel propagation algorithm

The diffraction of the electromagnetic field behind a complex amplitude distribution was simulated by calculating the propagation in the Fourier domain and transforming back in the spatial domain by performing fast Fourier transforms (FFT) [150, 151].

The Rayleigh-Sommerfeld formula, giving the diffraction of a wave passing through an arbitrary aperture, is written as:

$$U(x, y, z) = \frac{1}{i\lambda} \int \int_S U(x', y', 0) \frac{e^{ikr}}{r} \cos\theta dx_1 dy_1 \quad (3.3)$$

with  $r = \sqrt{(x - x')^2 + (y - y')^2 + z^2}$ ;  $x', y'$  being in the plane of the diffractive element and  $x, y, z$  in the plane of interest. Let us write  $U(x, y, z)$  as a function of the spatial frequencies distribution:

$$U(x, y, z) = \int \int_{-\infty}^{+\infty} A(f_x, f_y, z) e^{i2\pi(f_x x + f_y y)} df_x df_y \quad (3.4)$$

$f_x$  and  $f_y$  denote the spatial frequencies along both x- and y-axis. Equation (3.3) can be rewritten as:

$$U(x, y, z) = \int \int_{-\infty}^{+\infty} A(f_x, f_y, 0) e^{i2\pi z \sqrt{\frac{1}{\lambda^2} - f_x^2 - f_y^2}} e^{i2\pi(f_x x + f_y y)} df_x df_y \quad (3.5)$$

$e^{i2\pi z \sqrt{\frac{1}{\lambda^2} - f_x^2 - f_y^2}}$  being the Rayleigh-Sommerfeld propagation kernel. The amplitude in the Fourier domain at position  $z$ ,  $A(f_x, f_y, z)$ , is calculated by multiplying the amplitude at  $z = 0$  by the kernel. The value of the field  $U(x, y, z)$  is obtained by calculating the inverse Fourier transform of  $A(f_x, f_y, z)$ . The Fresnel approximation consists in replacing  $r$  by  $z + \frac{(x - x')^2 + (y - y')^2}{2z}$  in the exponential term and  $r$  by  $z$  otherwise. We get:

$$U(x, y, z) = \frac{e^{ikz}}{i\lambda z} \int \int_S U(x', y', 0) e^{\frac{ik}{2z} [(x - x')^2 + (y - y')^2]} dx_1 dy_1 \quad (3.6)$$

and so a function of the distribution in the Fourier plane:

$$U(x, y, z) = \int \int_{-\infty}^{+\infty} A(f_x, f_y, 0) e^{ikz} e^{-\pi\lambda z(f_x^2 + f_y^2)} e^{i2\pi(f_x x + f_y y)} df_x df_y \quad (3.7)$$

where  $e^{ikz} e^{-\pi\lambda z(f_x^2 + f_y^2)}$  is the kernel of Fresnel propagation. One can notice that the propagation is reduced to a simple multiplication in the Fourier domain. Thus, to obtain the field at a desired  $z$  position, the wave amplitude is first calculated in terms of spatial frequencies in the Fourier domain, affected by a multiplication factor in the Fourier domain and then inverse Fourier transformed to get the propagated field in the spatial domain. The program's block diagram is presented in figure 3.10.

In the simulations presented in this chapter, the diffractive element is illuminated by a plane wave with a uniform amplitude distribution. Such simplifications are acceptable since, in the experimental conditions, the diffractive plate is illuminated with a beam focused on it by a low NA lens, and



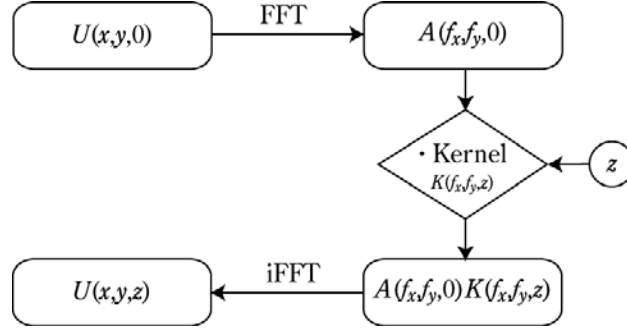


**Figure 3.10:** Block diagram of the propagation algorithm for simulation of the diffraction at a distance  $z$  of a diffractive element with uniform plane wave illumination.

thus observation are made over a distance of about one tenth of the Rayleigh length, which is in the order of the centimeter. The diffractive element is illuminated by a Gaussian beam over a large area (hundreds of microns) and the observed zone is located at the center of the Gaussian shape where intensity variations are neglected for the calculation. In the following simulation, only the Fresnel propagation kernel is employed. Although the results it gives are slightly differing from the one obtained with the more precise Rayleigh-Sommerfeld kernel, they are nevertheless sufficient for our study.

### Simulation for 2D three-level ruling

The simulation algorithm is applied to predict the intensity modulation created by a known diffractive element. The DOE is a three level phase mask made with engraved parallel ridges in two orthogonal directions. It has been etched over an area of 2 x 2 cm, in two steps, on a 1 mm thick and 2 inches diameter quartz wafer at M.I.T. Lincoln Labs (USA) by M. Holz and co-workers. The corresponding phase profile is represented in figure 3.11. The plate was designed for use with an Argon laser at 514.5 nm. The grooves in each direction are 3.6  $\mu\text{m}$  wide and have a height of 0.560  $\mu\text{m}$  which provides a  $\pi$  phase shift for this wavelength when immersed in air. The quartz substrate has a refractive index of 1.462 (@ 514.5 nm). The zones that have been etched twice during the two successive steps of the process generate a  $2\pi$  phase shift (see illustration in figure 3.11 c)). The light passing through these zones is in phase with the one passing through the non graved zones. The grating can be considered as binary for the designed wavelength.



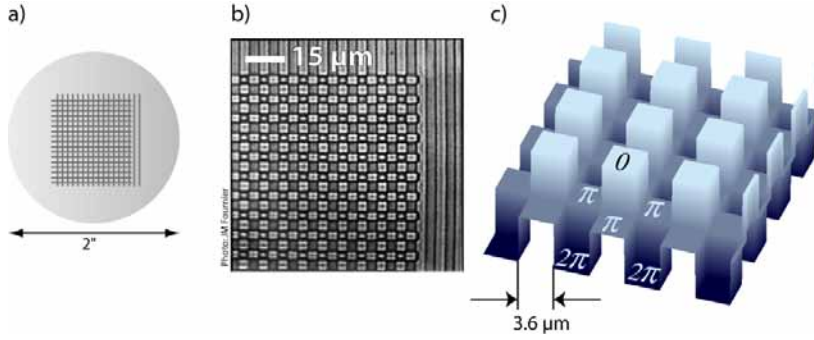


**Figure 3.11:** Talbot plate: 2D phase Ronchi ruling used as DOE for generation of Talbot and Lohmann images. a) Schematic of the engraved surface on a 2" quartz wafer. b) SEM images of the Phase Ronchi ruling; the ridges are  $3.6 \mu\text{m}$  wide. c) Representation of the 3-level profile with  $\pi$  induced phase shift for illumination at 514.5 nm in air.

Simulations for  $\lambda = 514 \text{ nm}$  give the intensity in Talbot sub-images with very sharp gradients and the Talbot effect also creates a local field enhancement. Figure 3.12 presents the simulated intensity pattern at different  $z$  levels (a) and c)), as well as a profile through the  $xy$  plane located  $50 \mu\text{m}$  after the plate ( $\frac{z_T}{4}$ ) (b)) simulated at 532 nm in water. The initial intensity is uniform and set to 1 (arbitrary units).

The trapping laser at our disposal for the present study is a doubled Nd:Vanadate emitting at 532 nm and the ruling had to be used in water for generating the Talbot planes inside the cell. The performance of the plate was then calculated for a wavelength of 532 nm illuminating the DOE immersed in water, even though the plate was designed for another use (514 nm in air). The simulation showed that the discrepancy in the wavelength was not so critical. The wavelengths ratio is  $514.5/532 = 0.96$  which leads to a small contrast diminution in the interesting sub-Talbot planes. On the other hand, the use of water instead of air considerably affects the phase difference since the phase shift  $\Delta\phi$ , given by  $\frac{2\pi}{\lambda}(n_1 - n_2)h$ , is only  $0.56\pi$  in water instead of  $\pi$  in air.

Although this phase plate already gives interesting light intensity patterns, it seemed important to find the optimal characteristics for designing new diffractive elements for optical trapping. The next part presents the study of the influence of the parameters of the diffractive plate on the Talbot images.

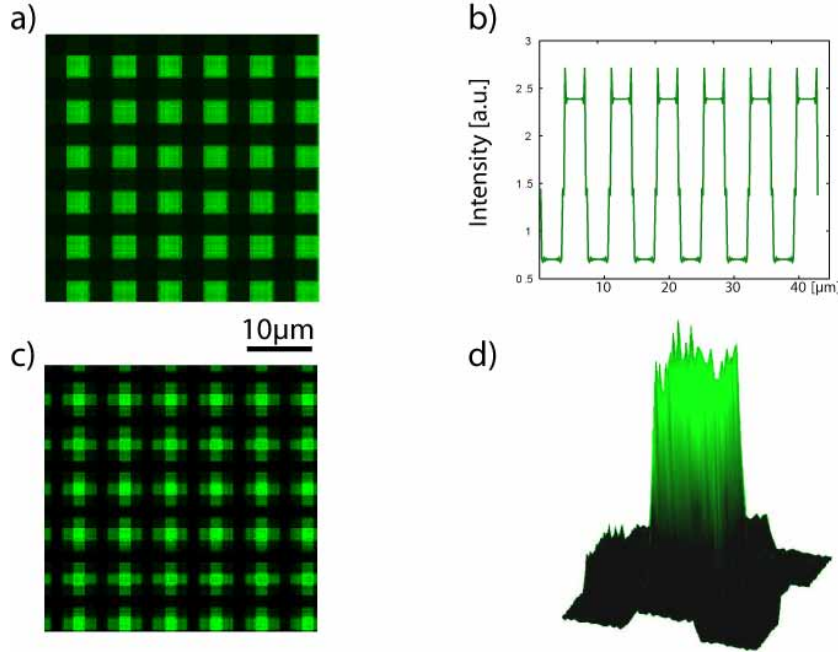


**Figure 3.12:** Numerical simulation of intensity at different levels behind a three level phase plate illuminated by a plane wave whose wavelength is 532 nm. The Fresnel propagation has been simulated in water. a) 50  $\mu\text{m}$  and c) 60  $\mu\text{m}$  behind the plate. b) Intensity profile in the plane displayed in a). d) 3D representation of the intensity of one element in the plane displayed in c).

### Phase mapping in Talbot images

The Talbot images, and more particularly the sub-images in the case of Lohmann images, depend directly on the structure of the periodic object. If the first Talbot plane is always located at the Talbot distance  $Z_T$ , the sub-images positions vary as a function of the parameters of the ruling, in particular the induced phase shift and the duty cycle  $\frac{w}{d}$ , where  $w$  is the width of the phase shifted area and  $d$  the pitch of the grating (see figure 3.6). The study is restricted to a two level diffractive plate of infinite dimensions with rectangular grooves in one and two dimensions. The duty cycles studied are  $\frac{1}{2}$ ,  $\frac{1}{3}$  and  $\frac{1}{4}$ . The illumination is an infinite plane wave with constant intensity whose value is set to 1.

In the case of a uniform illumination, the intensity pattern in Talbot images (i.e. at a distance  $Z_T$  from the grating) is also uniform since self-images are similar to the original intensity distribution at the ruling level. The same consideration is valid at half the Talbot distance. This can be easily

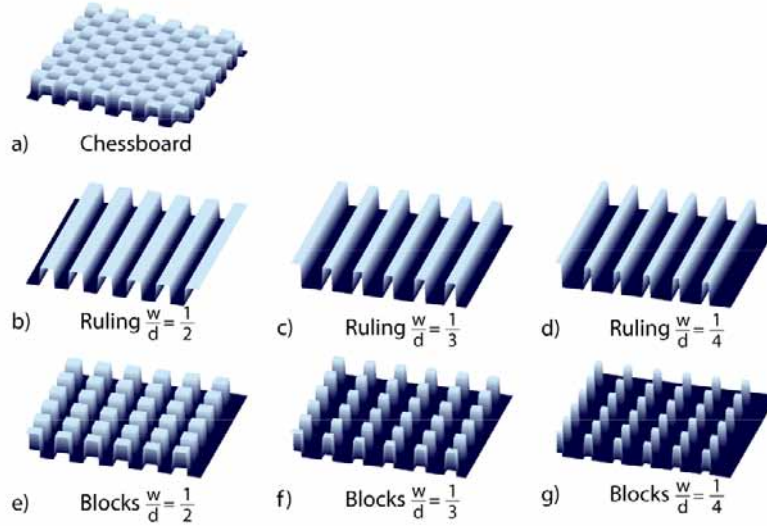


**Figure 3.13:** Representation of simulated phase plate patterns for generation of Lohmann images. The phase shift is induced by the steps.

understood when having in mind what happens in the case of the Talbot effect with an amplitude ruling as presented on page 60 and following. At  $\frac{Z_T}{2}$ , the amplitude image of the grating is inverted. With a uniform amplitude distribution, no difference is visible between the two planes ( $Z_T$  and  $\frac{Z_T}{2}$ ). On the other hand, in between these particular planes, sharp intensity patterns appear; their contrast strongly depending on the phase shift induced by the diffractive element.

We observe two main cases, particularly interesting to us, providing different structures in the  $z$  direction for two phase shifts  $\Delta\phi$ , namely  $\frac{\pi}{2}$  and  $\pi$ . For other values of  $\Delta\phi$  between  $\frac{\pi}{2}$  and  $\pi$  we observe a fading superposition of the two intensity patterns generated by the phase shifts of  $\frac{\pi}{2}$  and  $\pi$ . For simplicity and for generalization, the following simulations are performed for a wavelength of  $\lambda = 1000$  nm and a ruling pitch  $d = 20$   $\mu\text{m}$ . The observed area extends between  $z = 0$  and  $z = Z_T$ . Obviously, the same pattern is repeated every  $Z_T$ . The algorithm makes no discrimination between near and far Talbot planes; in reality, if the illuminated area is limited, border effects arise and are non negligible for Talbot planes located far away from the diffractive plate.

Let us first consider a one dimensional phase Ronchi ruling whose profile is presented in figure 3.13 b). The fresnel propagation simulations for this phase grating are represented in figure 3.14 (a)-f) are xy sections whereas g)

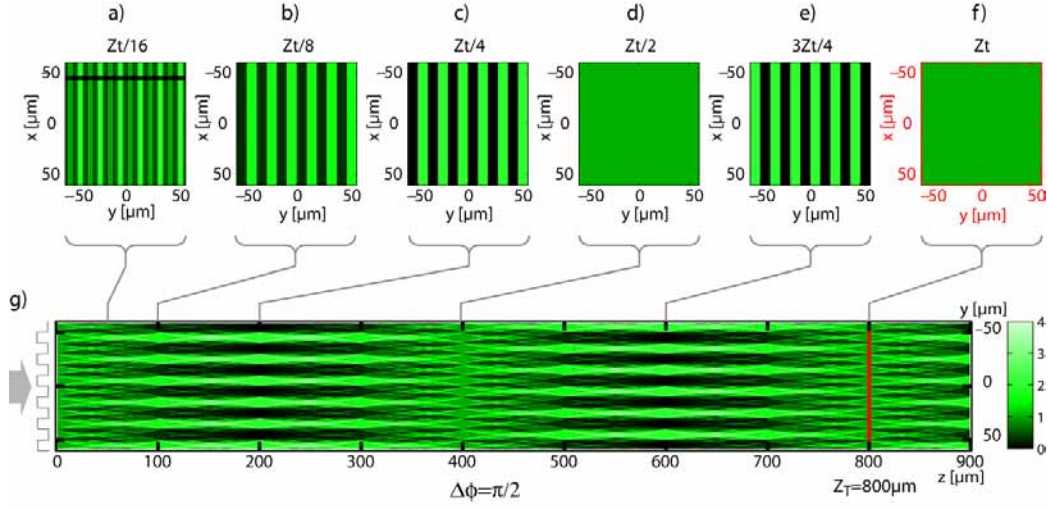


**Figure 3.14:** Simulation of the Fresnel diffraction over the Talbot distance ( $800 \mu\text{m}$ ) behind a 1D phase Ronchi ruling with  $\Delta\phi = \frac{\pi}{2}$  for  $\lambda = 1000 \text{ nm}$  and  $d = 20 \mu\text{m}$ . a)-f) intensity distribution in the  $xy$ -plane at different distances  $z$ . g) intensity distribution over the  $yz$ -plane along the black line in a); the Talbot distance is showed by the red stroke.

is a  $yz$  section). When the height of the groove is such as to generate a  $\frac{\pi}{2}$ -phase shift for the used wavelength, a sharp intensity profile appears at  $z = \frac{Z_T}{4}$  and  $z = \frac{3Z_T}{4}$  (figure 3.14 c) and e)). The intensity pattern is inverted between the two sub-images as given in figure 3.14 c) and e)). At multiple of  $\frac{Z_T}{8}$  the same pattern appears but presents a weaker intensity contrast (figure 3.14 b)). All bright areas are centered at the same lateral positions over the first half of the Talbot distance (between  $z = 0$  and  $\frac{Z_T}{2}$ ) whereas over the second half (from  $\frac{Z_T}{2}$  to  $Z_T$ ) they are inverted. This forms several "cages" of light over  $Z_T$ . At  $\frac{Z_T}{16}$ , the intensity pattern is still a Ronchi ruling but with a pitch being half of the one of the original ruling [152]. Figure 3.15 displays a "zoom" on the first quarter of the Talbot distance ( $200 \mu\text{m}$ ). The plots along the  $z$ -axis (figure 3.15 b)) and along the  $y$ -axis (figure 3.15 c)) show the intensity profiles. Peaks show how the field is locally enhanced. Compared to the initial intensity value set equal to one, at fractional Talbot planes, the intensity is doubled over every other square; in between, the intensity can reach over 4 times the initial value. The Talbot effect creates a high gradient in both  $y$ - and  $z$ - directions and the field enhancement is a key for optical trapping. The frequency doubling is obviously another very interesting characteristic that can be taken advantage of in trapping schemes.

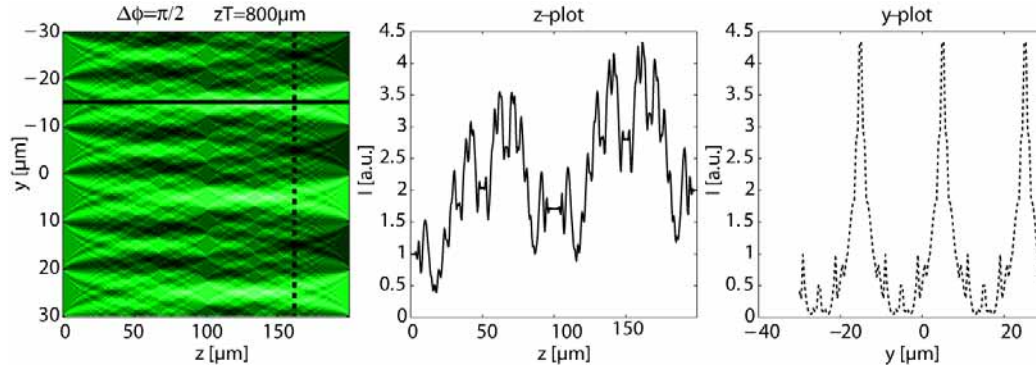


**Figure 3.15:** Detailed view and intensity profile of the Fresnel diffraction of a 1D phase Ronchi Ruling with phase shift  $\Delta\phi = \frac{\pi}{2}$ .

In the case of a phase shift  $\Delta\phi = \pi$ , the phase plate generates eight times the same intensity pattern inside  $Z_T$ , instead of two for  $\Delta\phi = \frac{\pi}{2}$  and the eight patterns are placed one after the other without contrast inversion. The lateral shift observed between two sub-Talbot planes observed in the  $\frac{\pi}{2}$  case does not take place with a  $\pi$  phase shift (figure 3.16). Nevertheless the intensity maximum is the same as for  $\Delta\phi = \frac{\pi}{2}$  and reaches about four times the value of the illumination intensity. Detailed plots can be found in appendix B.

The gain in intensity can be still increased by using a two-dimensional array like the one presented in figure 3.13 a). The diffractive plate resembles a chessboard with engraved squares. For a  $\frac{\pi}{2}$  phase shift a doubling of the number of sub-Talbot planes is observed. The same intensity pattern is repeated four times along one Talbot distance (figure 3.17 c)). This doubling can be explained by the effect of the periodicity in both directions. However, the doubling of the number of sub-Talbot planes does not occur with a  $\pi$  phase shift (figure 3.17 d)). On the other hand, for this latter phase shift, the intensity maxima reaches over 16 times the value of the uniform illumination (figure 3.17 g) and h)). This intensity increase makes the chessboard pattern a good candidate for optical trapping. Moreover, it presents a second advantage in the  $\frac{\pi}{2}$  case. In comparison with the field diffracted by a 1D ruling (figure 3.14 g)) where the high intensity areas have a very elongated shape (aspect ratio  $\sim 1/10$ ), the potential wells created with the  $\frac{\pi}{2}$  2D chessboard are more confined (figure 3.17 c)) and the intensity gradient along the  $z$  axis is stronger. The aspect ratio depends on the pitch of the ruling since

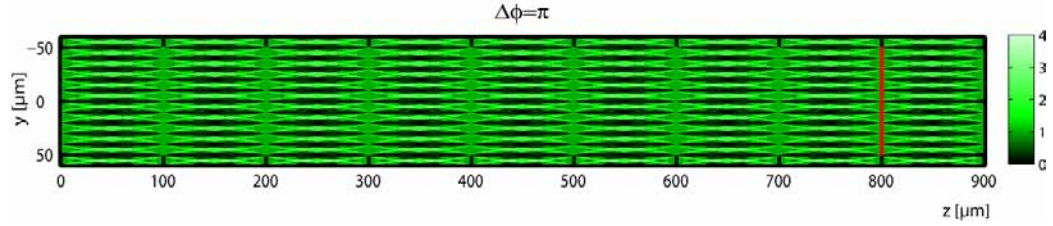


**Figure 3.16:** Simulation of the Fresnel diffraction over the Talbot distance (800  $\mu\text{m}$ ) behind a 1D phase Ronchi ruling with  $\Delta\phi = \pi$ .

the periodicity in  $z$  varies quadratically with  $d$ . The longitudinal confinement is the strongest in the 2D chessboard  $\pi$  phase shift case (figure 3.17 g).

The simulation of the diffraction generated by patterns with duty cycles different from  $\frac{1}{2}$ , which seemed to be good candidates for optical trap arrays, did not show interesting intensity schemes. Figure 3.18 displays the intensity distribution along the  $z$  axis behind a plate with duty cycles of  $\frac{1}{4}$  and a phase shift of  $\pi/2$ . Unfortunately, the sub-Talbot planes are not well defined and the gradients in the  $z$  direction are not sufficient for generating trapping planes and the local intensity enhancements are much lower than in the chessboard case. Other results concerning various duty cycles can be found in appendix B.

### Discussion on numerical simulation

The Fresnel formula used for the calculation of diffraction in the vicinity of the phase plate is an approximation and some assumptions have been made. The calculation is performed with all mathematically possible spatial frequencies but this model does not take into account the optical limits imposing a cut-off frequency of  $\frac{1}{\lambda}$ . These simplifications led to very sharp profiles in intensity planes with spatial variations that are smaller than  $\lambda$ , which is physically not possible. Even though the sharpness of the results is too high, the Fresnel algorithm gives pertinent results for the positions of Talbot sub-images with a good approximation of the patterns.

Figure 3.19, kindly provided by E. Maréchal, presents a comparison of two simulations of the diffraction by a phase Ronchi ruling with a  $\pi$  phase shift and a pitch of 10  $\mu\text{m}$ , performed in the same conditions (sampling steps, etc.). A width of 40 microns is illuminated and light propagation is represented over 30 microns only. Figure a) is calculated with the Fresnel



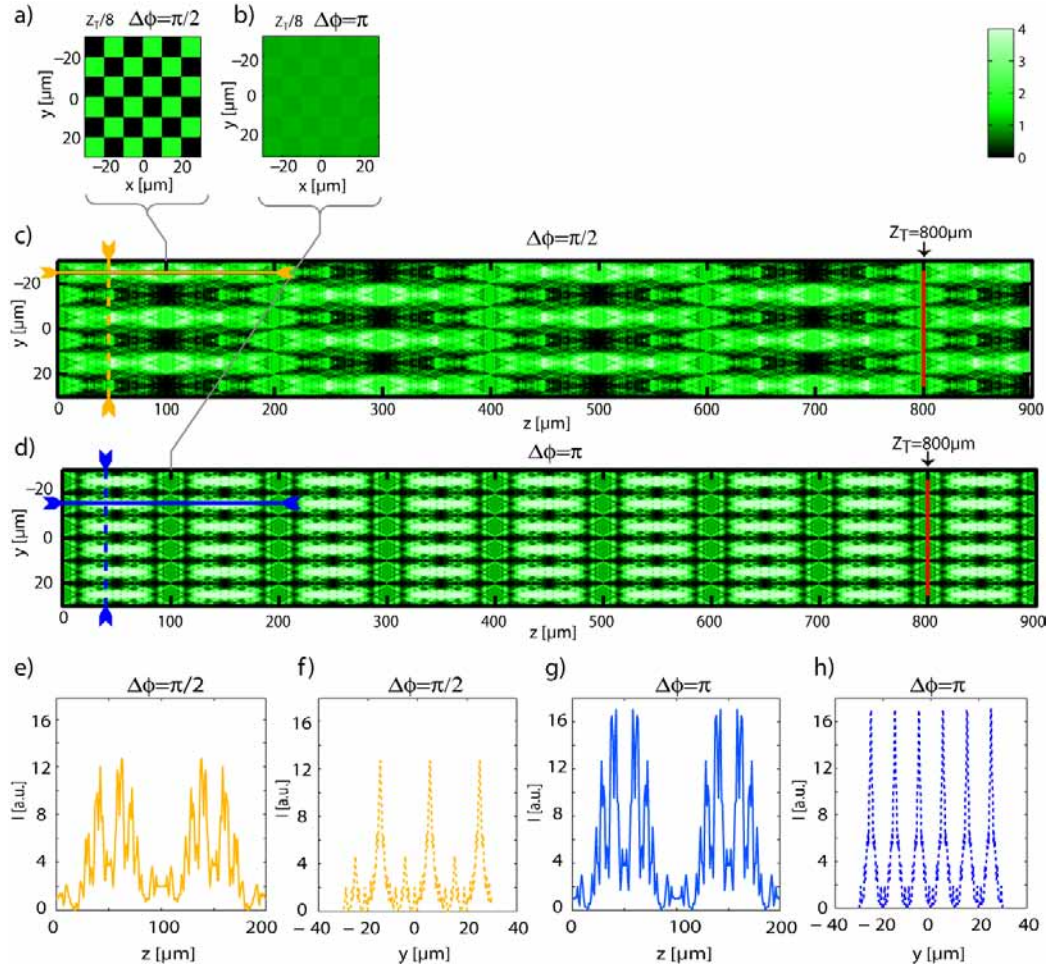


**Figure 3.17:** Simulation of the Fresnel diffraction over the Talbot distance ( $800 \mu\text{m}$ ) behind a chessboard-like phase grating with phase shift of  $\frac{\pi}{2}$  (a), (c), (e), (f)) and  $\pi$  (b), (d), (g), (h))

kernel and figure b) by the more rigorous Rayleigh-Sommerfeld formula. The latter gives a smoother results, closer to the real intensity pattern.

Regardless of its small variations to Rayleigh-Sommerfeld kernel, the Fresnel calculation provides an easy and useful tool for the conception of optical traps. In addition to Talbot planes localization, intensity maxima positions and gradient strengths, the simulations give relevant predictions on the influence of various parameters of the systems like the phase shift variation, the influence of the wavelength, the pitch of the pattern or also the impact of the size of the illuminated area. It has been shown on page 68 that replacing a 514.5 nm laser line with a 532 nm one is not so critical for trapping

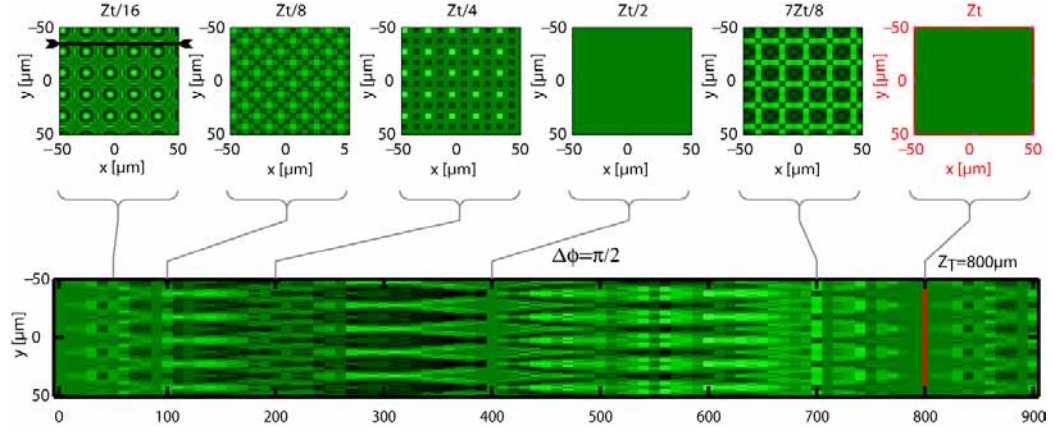


**Figure 3.18:** Intensity distribution along the  $z$ -axis behind a plate with duty cycles of  $\frac{1}{4}$  and a phase shift of  $\pi/2$  as illustrated in figure 3.13 g).

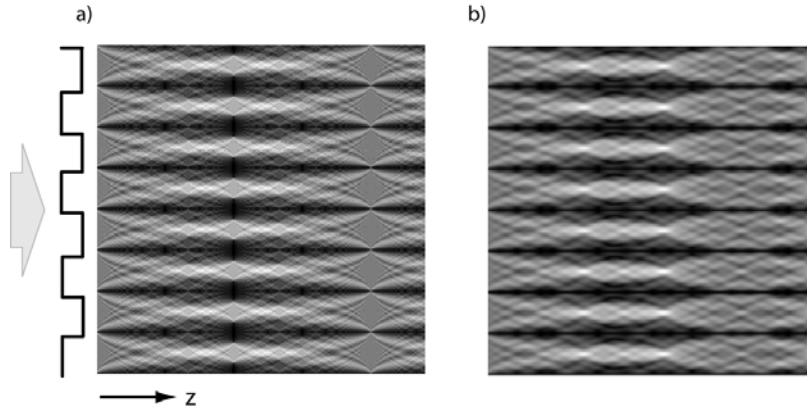


**Figure 3.19:** Comparison between Fresnel (a) and Rayleigh-Sommerfeld (b) propagation kernel on the diffraction of a phase Ronchi ruling with  $\pi$  shift and  $5 \mu\text{m}$  grooves.

experiments. In the same line of tolerance an error as high as 10% on the height of the engraved area of the plate is acceptable. This precision is easily achievable by the technologies at our disposal (see appendix C).

### 3.3.4 Three dimensional trapping in Talbot lattices

#### Experimental optical templates

The Talbot simulations are in good agreement with images recorded in the experimental setup, as demonstrated by figure 3.20 comparing simulated and experimentally recorded intensities at different levels of the diffracted field.



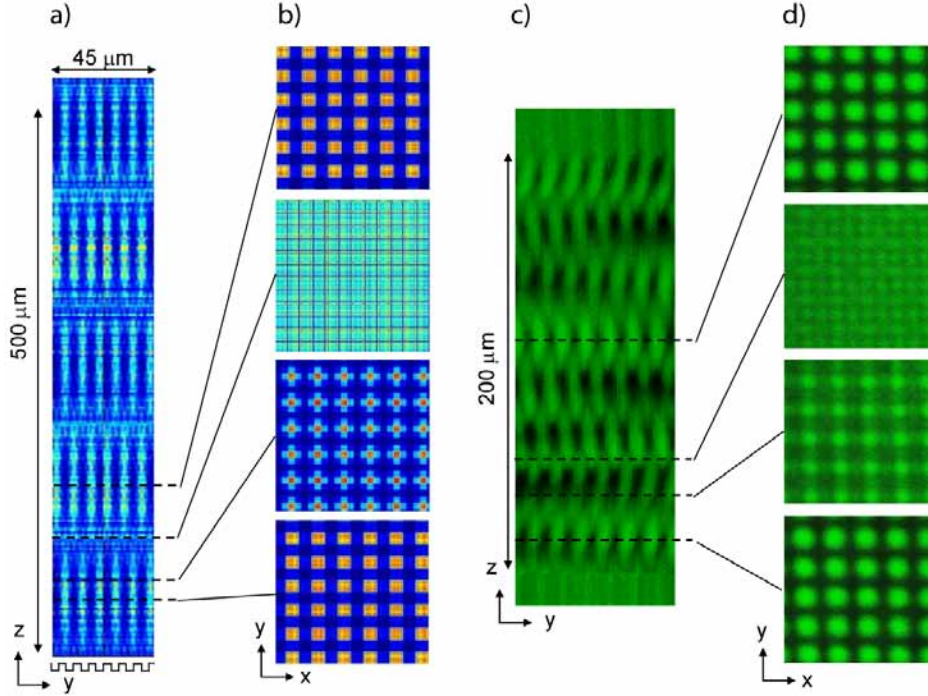


**Figure 3.20:** Comparison of fields diffracted by the three level phase plate illuminated with a 532 nm laser: a), b) simulations and c), d) experimental.

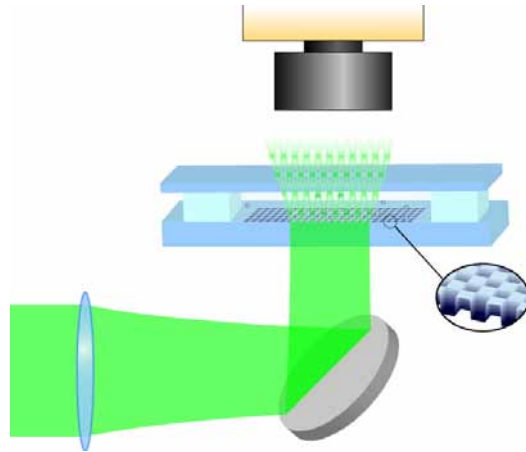


**Figure 3.21:** Setup for trapping particles in Talbot lattices. The diffractive element is illuminated from below and the fractional effect creates several traps arrays at different heights inside a chamber. A long working distance MO allows observation from above.

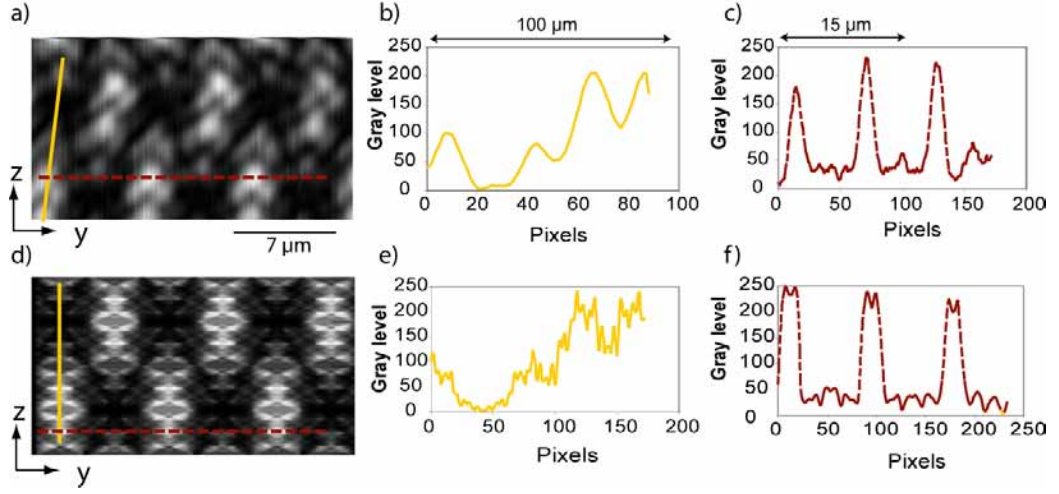


**Figure 3.22:** Fresnel propagation in the  $z$ -direction behind a diffractive plate. a)-c) experimental data recorded over half of the Talbot distance (about  $100\ \mu\text{m}$ ) behind a phase chessboard with a pitch of  $7.2\ \mu\text{m}$ . d)-f) simulated intensity profile in  $z$ -direction.

The diffractive element tested here is the three level plate presented in figure 3.11 with a pitch of  $7.2\ \mu\text{m}$ . A stack of images of the  $x$ - $y$  planes are recorded by moving the microscope objective mounted on a motorized stage in the  $z$ -direction as schemed in figure 3.21. The stack is then numerically sliced to get the  $x$ - $z$  (or  $y$ - $z$ ) intensity propagation. The greater number of contrast inversions present in the experimental image of figure 3.20 is due to an unwanted lateral shift caused by creeping when moving along the  $z$  axis.

Figure 3.22 compares the simulation by the Fresnel kernel propagator with the recorded intensity profile. The experimental data (figure 3.22 a)-c)) are taken with a diffractive plate designed and manufactured at EPFL (see appendix C). The structure is a 2D chessboard (figure 3.13 a)) immersed in water with a pitch of  $7.2\ \mu\text{m}$  and a phase shift of  $\frac{\pi}{2}$  at  $532\ \text{nm}$ . The images were recorded by a 1 Megapixel CMOS camera (MV-D1024E, Photonfocus, Switzerland). Images reconstruction was performed as described above. One can notice a very good agreement with the theoretical case. The small variations between the simulated and experimentally measured intensity curves are due to artifacts in the Fresnel calculations, as discussed previously. The observed dynamic is very comparable to the theoretical one, showing that the desired intensity gradient have been achieved.

### Optical trapping results

Trapping in Talbot planes, or more precisely in Talbot sub-images, is achieved by placing the sample on the diffractive area and by illuminating the phase plate with a smoothly focused beam. The solution of suspended particles is deposited directly on the structure inside a chamber made by a PDMS spacer and closed by a microscope coverslip as sketched in figure 3.21. Several traps planes are created inside the chamber, their number depends on the distance between Talbot sub-images. Particles in the diffracted field are extremely easily trapped laterally in the lattice. An intensity as small as a few nanowatts per trap is sufficient for the confinement in x and y directions. At such low power, the weight of polystyrene spheres is sufficient to counterbalance the radiation pressure, then the particles remain near the bottom of the cell where they get trapped in arrays. However as soon as the power increases, the gradient force in the z direction is weaker than the scattering force. For a stable 3D trapping, a compensation of the radiation pressure is thus necessary. A reflective surface at the top of the cell has been used for this purpose leading to an equilibrium at several fractional planes. Images of particles trapped simultaneously at different levels are presented in figure 3.23 a)-c). The beads remain trapped in their respective planes while the imaging system is focusing at the three different depths in the cell. The white arrow points to a bead trapped in the middle level (b)) whereas a) is a level above it and c) under. On d) a superimposition of the grating structure and an image of a trapped plane shows the lateral confinement in the pattern. Most experiments have been performed with the M.I.T. Lincoln lab's three level diffractive plate, simply because this was the sole diffractive element at our disposal for a long time during the course of this thesis.

### Discussion on Talbot trapping

With weak concentrations of objects in the solution, the Talbot effect is well suited to create multi layers of traps. It has the capability of creating stacks of trap arrays even if some of the lower traps are occupied, the effect being self-healing. However, the density of particles in the solution must not be too high. Indeed, when too many particles are trapped in one of the trapping planes, they considerably disturb the wave front, thus preventing a good reconstruction of the Talbot images at upper levels.

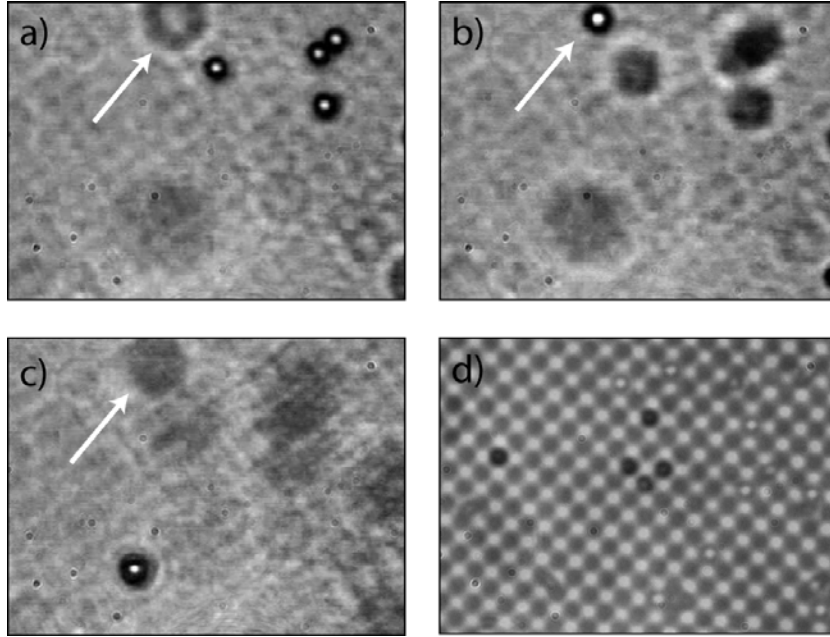


**Figure 3.23:** Polystyrene beads (3.5 microns in diameter) trapped at three different fractional Talbot planes. a) upper level, b) middle level and c) lower level. The arrow points to the same bead in each image. d) superimposition of the image of trapped particles with an image of the grating's pattern. The lateral alignment over the pattern is visible.

The manufacturing of diffracting plates with different pitches allows generating traps of various lateral sizes, selected according to the dimensions of the particles to be trapped. Meanwhile, the size of the trap in the  $z$  direction do not vary linearly since it is proportional to the square of the pitch. The traps are then very asymmetrical, particularly for sizes much bigger than the wavelength. Nevertheless, with the help of radiation pressure compensation, the  $z$ -gradient is sufficient to stabilize particles in Talbot planes.

### 3.4 Conclusion

Compared to an imaging system, the Fresnel diffraction regime exploited in this chapter presents the advantage to avoid filtering of any spatial frequencies. As expected, this feature is very interesting for optical trapping since it allows the construction of high intensity gradients.

We first exposed the modulation of the field created by a single sphere. This simple structuring of light was sufficient to trap and arrange a large

number of particles in the Fresnel domain. This principle has been exploited in a two-level chamber, using the diffraction pattern of an ensemble of beads to create optical traps. The diffracted field of a self-assembly of polystyrene particles has been studied. We have described the clear manifestation of a Talbot effect generated by the scattering of the ensemble of trapped beads. To take advantage of the self-imaging effect, the Fresnel diffraction of various periodic structures has been numerically simulated. The structuring of light due to a periodic phase distribution is much more interesting for optical trapping than the one produced by an amplitude distribution, since it avoids intensity losses. Moreover, it has been theoretically shown that an intensity increase of a factor 16 could be achieved. The design of periodic phase diffractive elements has been optimized. A chessboard like pattern is the more appropriate scheme among the ones we studied to create local field enhancement. Square posts in 1D and 2D separated by a distance greater than their width (duty cycle  $\neq \frac{1}{2}$ ) did not provide any pattern with well defined traps.

The periodization of the electromagnetic field generated by the Talbot effect allows creating three dimensional optical wells. The optical trapping of micron-sized polystyrene particles at different heights has been demonstrated. Such a stable 3D trapping has been obtained by adding counter-propagating light. Further experiments with unstructured counter-propagating light would be interesting for the continuation of this study.



---

# Optical binding

## 4.1 Introduction

In chapter 1 we have mentioned three types of optical forces. The gradient force and the scattering force are well known and commonly used to describe trapping phenomena by the communities manipulating atoms and mesoscopic particles. The third one, referred to as the optical binding force, is not so widely discussed in the literature but can be very important in many body systems and has to be taken into account as soon as several particles are simultaneously immersed in an electromagnetic field. These interactions and their consequences on stable multiple optical trapping are studied in this chapter.

## 4.2 Optical binding forces and optical matter

First reported in 1989 by Fournier et al. [58, 23], optical binding forces are today studied by several groups but they probably remain not taken into account in numerous studies of multiple trapping. Binding forces arise when several particles are in presence of an intense optical field. In section 3.2 we have seen how one particle can influence the trapping of other particles situated in its vicinity due to the interference of its own scattering with the impinging wave. Indeed, the optical interaction between particles is always mutual and manifests itself through self consistency. The explanation can be formulated in the Rayleigh regime considering two or more particles as oscillating dipoles [58, 153, 154].

$$F_{binding} = \alpha^2 k^2 I^2 \frac{\sin(kr)}{r} \quad (4.1)$$

$\alpha$  is the polarizability given by equation (1.4),  $r$  is the distance between the two oscillators,  $I$  the intensity of the field and  $k$  the wave number.

Optical binding has been observed in line traps created by cylindrical lenses [58, 155], by counter-propagating beams [156], by interference fringes [34, 157], or between facing optical fibers [158, 159, 160, 161] and also in two dimensions within the evanescent field [31, 70].

Theoretical work on optical binding has been performed by many researchers and it is still a popular subject of investigation. Particle behavior and binding forces have been simulated in one dimension [153, 162] or in two dimensions either in a uniform field [163, 164] or in a large interference



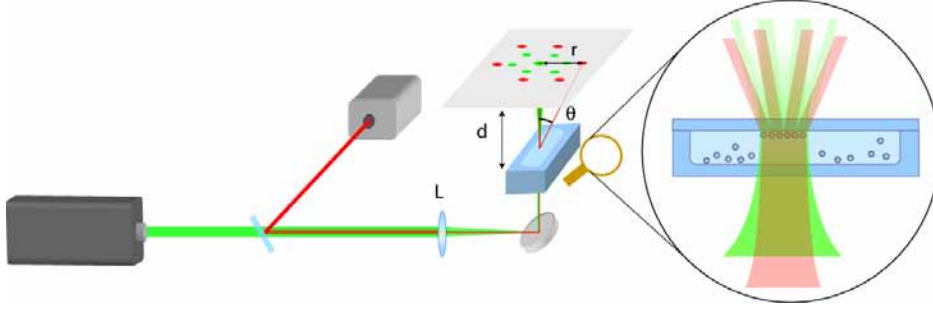


**Figure 4.1:** Setup for study optical binding. A beam is focused inside a cell containing dielectric particles in solution. A secondary laser is used to probe the crystal at another wavelength.

field [93, 94, 165, 166]. The influence on optical binding of a dielectric surface [154] or of a near-field scanning microscope probe [167] has also been theoretically analyzed. However, today's computer calculation power is not sufficient to simulate the most common experimental cases with a rigorous model. The simulations are restricted to small particles or to a very few number of particles in the micrometer range.

## 4.3 Study of self assembly

### 4.3.1 Experimental setup

Optical binding forces may arise in any light intensity distribution. Experimentally, the simplest one is a gaussian beam. We propose a setup with a single beam slightly focused in a cell containing polystyrene particles suspended in water. In order to use the cell in an horizontal position, the beam coming out of the Verdi laser presented in page 21 is folded by a mirror as represented in figure 4.1. The focusing lens ( $f=150$  mm) is mounted on a translation stage to adjust the position of the focal area thus varying the size of the beam at the top level of the cell where beads are trapped. The focusing lens also controls the intensity of the electromagnetic field in the cell. The low intensity probe He-Ne laser allows non perturbing illumination and investigation of the behavior of beads. The beads plane can be observed through the imaging system described in figure 2.10; investigation on the beads behavior in that plane can also be performed by taking advantage of the diffraction in the far field, e.g. by looking at a diffuser placed as represented in figure 4.1.

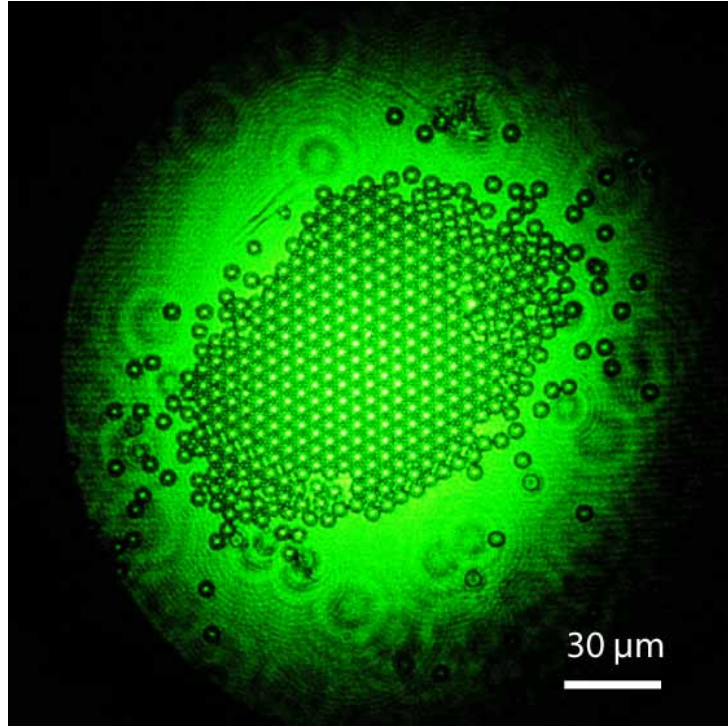


**Figure 4.2:** Self arrangement of 5  $\mu\text{m}$  polystyrene beads at the center of a Gaussian beam

### 4.3.2 Creation of optical crystals

When the Gaussian beam illuminates the cell containing a solution of polystyrene spheres, the beads that "perceive" the gradient of intensity are trapped in the beam and agglomerate at the center. Due to trapping and binding forces, they self arrange close-packing to form 2D-optical crystals characterized by an hexagonal pattern. Figure 4.2 presents the formation of a crystal made of 5  $\mu\text{m}$  beads. The observation plane is located at the top of the cell where beads are pushed due to the scattering force. Particles experience differently the radiation pressure depending on their distance to the beam axis. This phenomena is evidenced in figure 4.2 where rings of unfocused beads at the border of the Gaussian light distribution correspond to particles rising more slowly to the top due to lower intensity. When this picture was taken, the crystal was still growing.

The diffracted light field by particles immersed in the impinging field interferes with this one. Due to the periodicity of the alignment, the resulting diffraction pattern creates fringes in six directions corresponding to the three

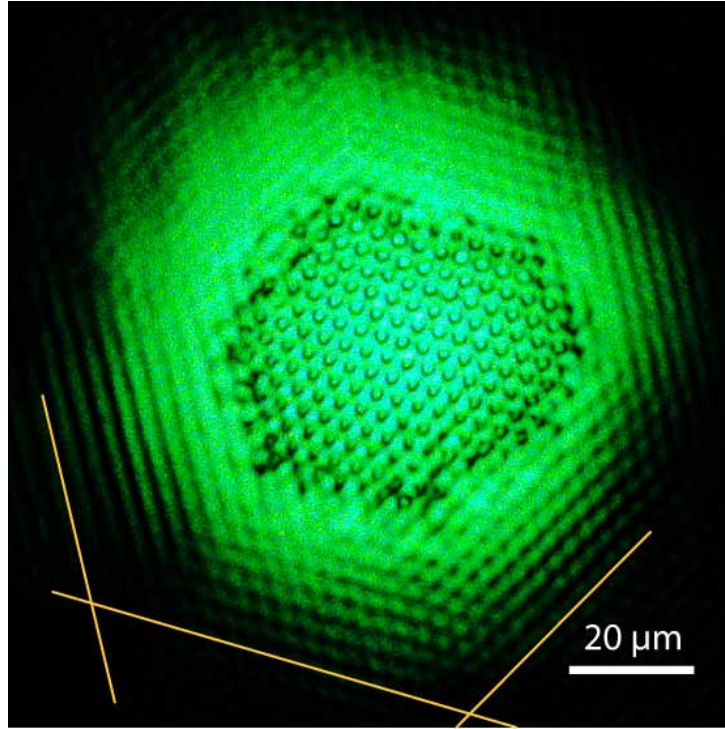


**Figure 4.3:** Fringes created by the interference between the impinging plane wave and the field diffracted by the crystal of  $3.5\ \mu\text{m}$  polystyrene beads

axis of the crystal. Those fringes are visible at the border of the beads array in figure 4.3. They are more easily distinguishable when the image is slightly defocused. Particles surrounding the crystal are sensitive to these field variations and can be momentarily trapped in the fringes.

Since the Gaussian distribution extends to infinity (even though, in the practical case, it is clipped by the optical system), beads located far away from the optical axis are also attracted to the beam center. This slow process brings continuously particles to the system. Each new particle arriving in the crystal imposes a whole reorganization of this one and leads to a new configuration. Due to Brownian motion, the crystal is perpetually stirred (rotating, expanding or contracting). Figure 4.4 presents the evolution of the movement of a crystal of  $3.5\ \mu\text{m}$  beads. The dotted line indicates the fringes' orientation and the solid line, the orientation of the crystal.

As in solid crystals, dislocations may arise, particularly when the array reaches a critical size. Depending on the crystal size, sub-crystals are formed with similar or with different pattern orientations (figure 4.5 b) and a) respec-

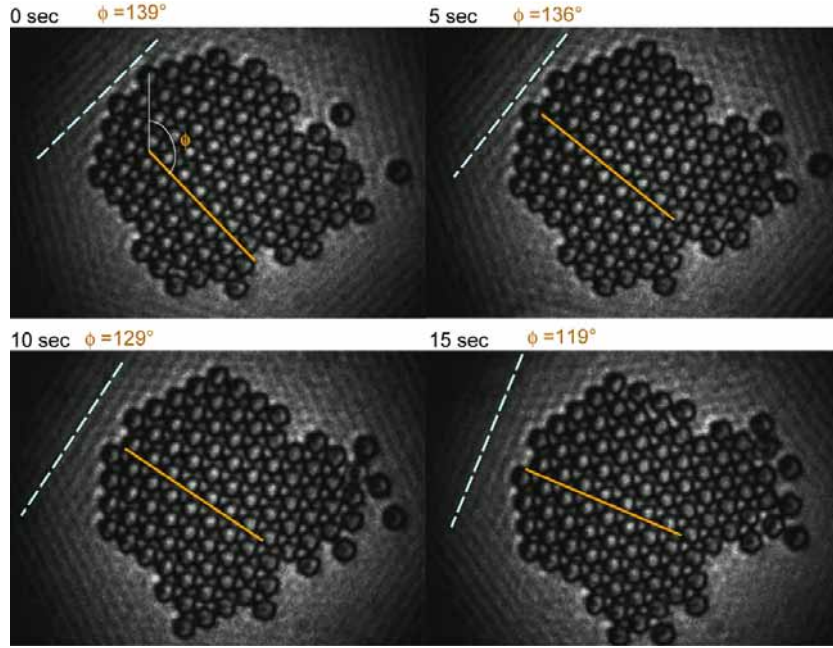


**Figure 4.4:** Rotation of an optical crystal of  $3.5 \mu\text{m}$  beads in a single Gaussian beam. Images are recorded at five second intervals.

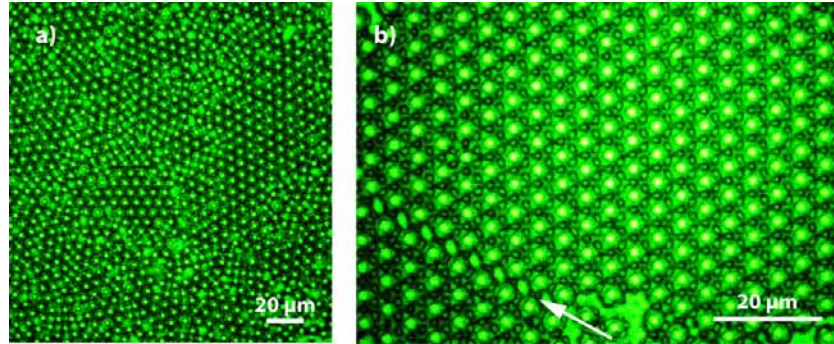


**Figure 4.5:** Dislocations in optical crystals made of a)  $6 \mu\text{m}$  beads and b)  $5 \mu\text{m}$  beads.

tively). "Melting" of the crystal can be observed when the power is turned down, as soon as cohesion forces vanish. As of today, the physics causing such dislocation has not been elucidated. Phase transitions have been suggested as a possible explanation [168, 169].

Intrinsic characteristics of the crystal and binding formation can be observed in its diffraction pattern. The k-space image gives statistical information on the pitch of the pattern (i.e. the distance between particles), the stability of the crystal, the presence of dislocations, etc. Compared to the



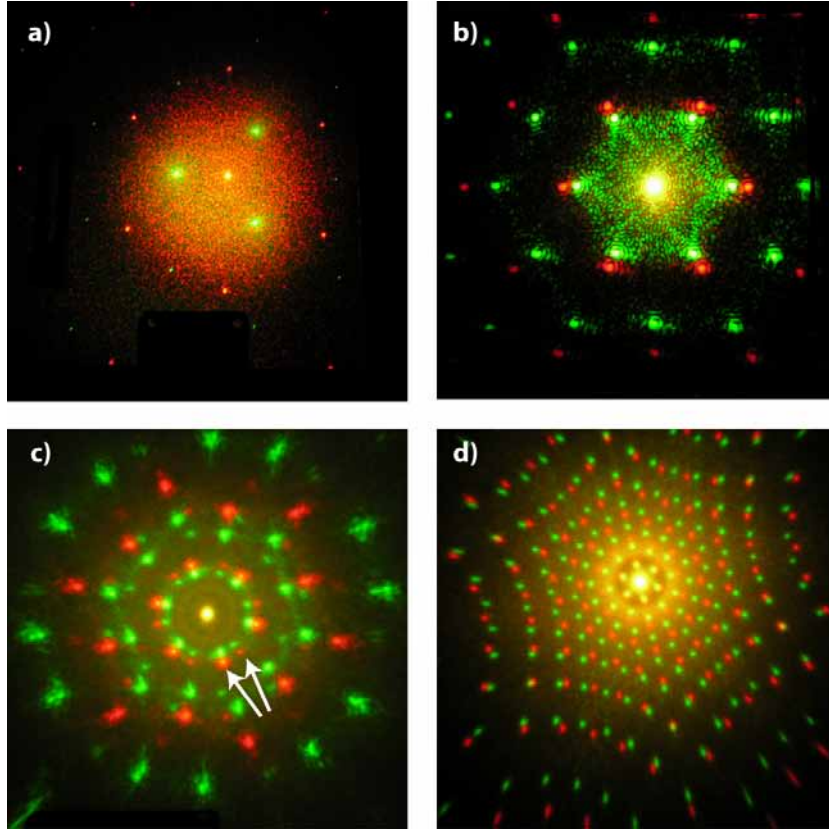


**Figure 4.6:** Diffraction pattern of beads arrays: trapped in a) hexagonal optical pattern , self arrangement in close-packing of b)  $3.5 \mu\text{m}$  beads and d)  $5 \mu\text{m}$  beads; c) dry close-packing array of  $2.06 \mu\text{m}$  beads with dislocations (manifested through the the presence of double spots indicated by the arrows). This latter is not created optically.

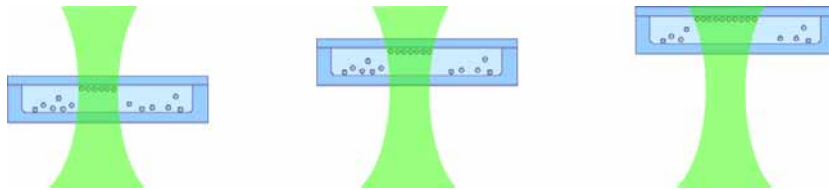


**Figure 4.7:** Variation of beam size for optical binding experiments. The cell is moved along the z-axis to work at different beam sizes. The focal length of the system is 150 mm.

diffraction of an array of beads trapped in an hexagonal interference pattern (figure 4.6 a)) the diffraction spots of a self array are fuzzier due to the inhomogeneous movement of the crystal (figure 4.6 b)). Dislocations are revealed by the presence of double diffraction spots in the k-space (figure 4.6 c)).

Power	At waist $2w_0 \approx 24\mu\text{m}$	750 $\mu\text{m}$ above the waist $2w_z \approx 32\mu\text{m}$	1250 $\mu\text{m}$ above the waist $2w_z \approx 43\mu\text{m}$
0.5W	44 Beads	-	-
1W	64 Beads	113 Beads	142 Beads
3W	68 Beads	199 Beads	198 Beads

**Table 4.1:** Maximal crystals sizes of 3.5  $\mu\text{m}$  polystyrene beads as a function of the input power

### 4.3.3 Generation of various sizes of crystals

Optically bounded crystals arise easily in a Gaussian trap. Since the Gaussian beam can be endlessly extended, it seems that the crystal could grow endlessly. However, the intensity required for forming and stabilizing the crystal is high and the optical binding between particles could also have a limited acting range [168, 169]. The following experiments show some of the limitations of such systems to create large assemblies of microscopic particles. Table 4.1 gives the characteristics of the largest crystals of 3.5  $\mu\text{m}$  polystyrene beads ( $n=1.6$ ) achieved depending on the input power and on the beam size. The crystals were formed according to the scheme of figure 4.1 with a slightly more complex focusing system. A  $\sim 10$  mm diameter collimated beam coming out of a telescope impinges on the focusing device which is composed of two plano-convex lenses (1000 mm and 200 mm focal length). The resulting effective focal length is about 150 mm. In order to change the beam width at the level of the crystal formation, the distance along the z-axis between the cell's top and the beam waist is varied between 0 and 1.250 mm as illustrated in figure 4.7.

The results presented in table 4.1 reveal the maximal crystal sizes that have been obtained by varying the width and the intensity of the beam. They show that the formation of stable self-arrangement requires both high intensity and high gradient. A half-watt extended over an area of about 40 micrometers in diameter does not provide a sufficient power for forming a compact crystal in water. At this power level, beads tend to slightly move away from each other in a disorganized manner. The loss of intensity gradient and the diminution of local fluence on each particle taking part in the binding reduce the possibility to expand the crystal. Figure 4.8 presents the Gaussian intensity profiles of for each trap's size at different power levels. Increasing

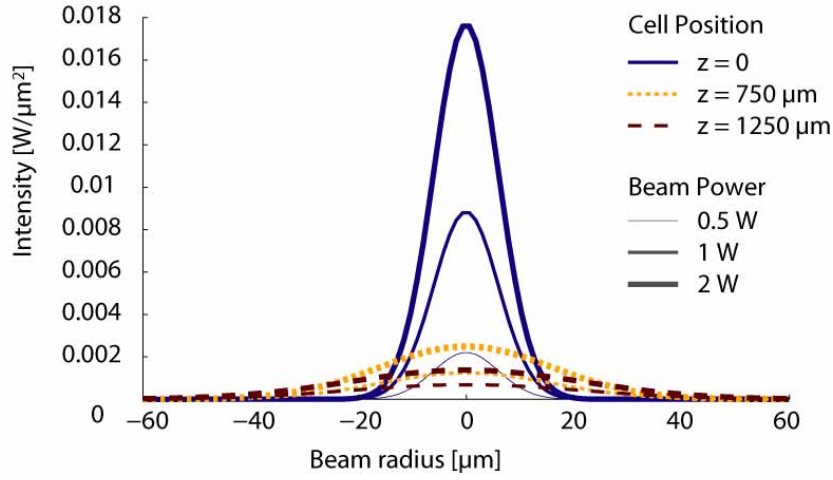


**Figure 4.8:** Intensity of the beams of table 4.1 depending on  $z$  and on three beam power (relative size).

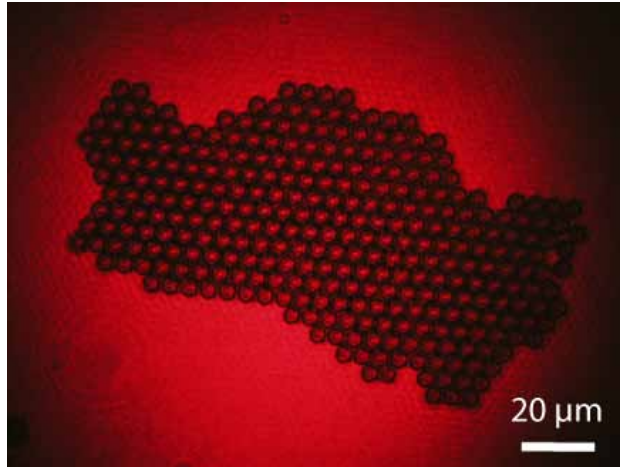


**Figure 4.9:** Dry 2D crystal of five  $\mu\text{m}$  polystyrene spheres obtained after evaporation and illuminated by He-Ne laser light. Particles are in contact with each others.

the beam size implies a loss of fluence: the intensity over each single bead is reduced and the gradient decreases. It has also been theoretically shown, in the dipolar approximation, that the binding force collapses for a large number of particles [168].

#### 4.3.4 Beads spacing in self assembly

The close-packing form of the crystal is partially due to the gradient of the gaussian trap. Microscopic particles arrange in the potential well as macro-

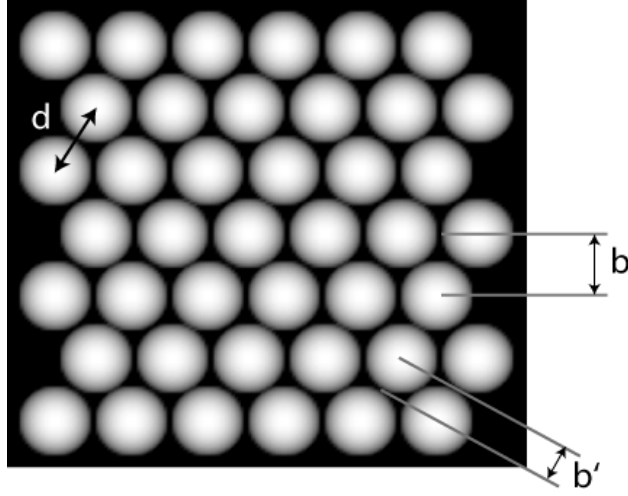


**Figure 4.10:** Close-packing array of spherical particles and associated spatial frequencies ( $\frac{1}{b}$  and  $\frac{1}{b'}$ ).

scopic beads would do in a bowl, minimizing the space between them to minimize the energy of the system. However, due to multiple scattering of the particles and to the periodicity of the beads array, optical binding occurs and counteracts the gradient force. This implies that beads will not necessarily sit in contact with each other. The demonstration of the influence of the optical binding is made by comparing the distance between particles in an hexagonal array in a laser trap with the distance between particles in a dry close-packing array. This latter is obtained by evaporating a droplet of beads diluted in a solution of water and isopropanol deposited on a glass microscope slide. In order to obtain a monolayer of beads in contact with each other, the evaporation process has been adjusted by heating the substrate and by varying the concentration of isopropanol and water. A dry 2D crystal of  $5\ \mu\text{m}$  polystyrene spheres is visible in figure 4.9. The inter-particle distance was evaluated by measuring the diffraction angles in the reciprocal lattice. The setup sketched in figure 4.1 shows the principle of measurement of the diffraction on a diffuser placed at a known distance of the diffracting array. The beads spacing is calculated using the diffraction of the trapping laser at 532 nm and the one of the additional red He-Ne laser at 632.8 nm. The pitch of the array  $b$  is given by:

$$b = \frac{m\lambda}{\sin(\theta_m)} = m\lambda\sqrt{1 + \frac{d^2}{r^2}} \quad (4.2)$$



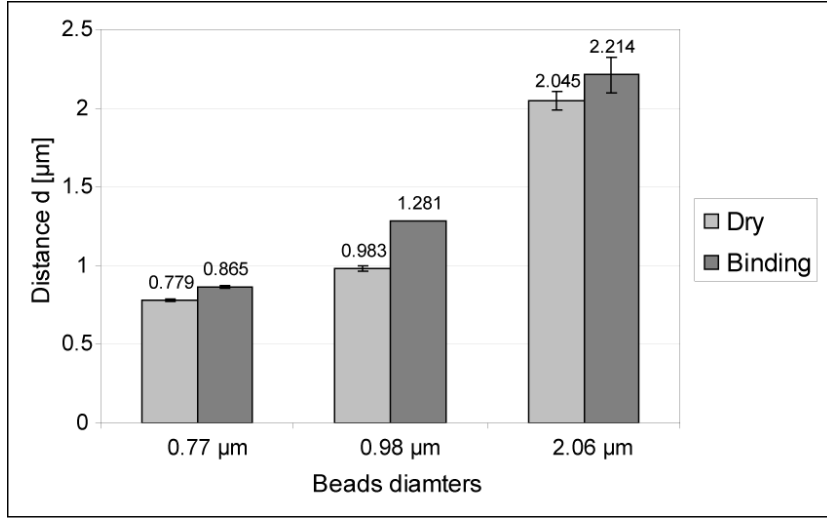


**Figure 4.11:** Comparison of inter-beads distance in dry close-packing arrays and optically bound crystals for different polystyrene bead sizes.

where  $m$  is the order of diffraction,  $d$  the distance between the array and the diffuser, and  $r$  the measured distance of diffraction spots from the optical axis (see figure 4.1).

It does not matter if we measure the distance of beads immersed in water or in air. Taking refraction into account, the directions of diffraction in air of a set of beads immersed in water are identical to the ones of the same set immersed in air. Indeed, with  $\sin \theta_{water} = \frac{\sin \theta_{air}}{n_{water}}$  and  $\lambda_{water} = \frac{\lambda_{air}}{n_{water}}$  we get:

$$b_{water} = \frac{\lambda_{air}/n_{water}}{\sin(\theta_{air})/n_{water}} = \frac{\lambda_{air}}{\sin(\theta_{air})} = b_{air} \quad (4.3)$$

Since the beads are arranged in hexagonal arrays due to close packing in a single Gaussian beam, we get two distinct diffraction directions (modulo  $\pi/3$ ): the first diffraction order gives the distance  $b$  represented in figure 4.10 which corresponds to the distance between two lines of beads; the order tilted by  $\frac{\pi}{6}$  gives the distance  $b'$  in figure 4.10 which would correspond to the radius of the beads, in the special case when spheres touch each others. The additional spacing between beads in optical crystals is obtained by calculating the difference between the measured distance  $d$  and the theoretical distance corresponding to spheres being in contact  $d_0 = 2a$ ,  $a$  being the radius of the

Beads $\varnothing$ [ $\mu\text{m}$ ]	B/D	Measured distance $d$ [ $\mu\text{m}$ ]	Error [ $\mu\text{m}$ ]	Difference with $\varnothing$ [ $\mu\text{m}$ ]	Difference in $\lambda_{\text{water}}$
0.77	D	0.779	$\pm 0.012$	0.009	0.024
0.77	B	0.865	$\pm 0.010$	0.095	0.238
0.98	D	0.983	$\pm 0.018$	0.002	0.006
0.98	B	1.281	$\pm 0.001$	0.301	0.753
2.06	D	2.045	$\pm 0.058$	-0.015	-0.038
2.06	B	2.214	$\pm 0.114$	0.154	0.382
3.5	D	3.542	$\pm 0.044$	0.042	0.104
3.5	B	3.500	$\pm 0.137$	0.000	0.000
5	D	5.281	$\pm 0.099$	0.281	0.703
5	B	5.096	$\pm 0.219$	0.096	0.240

**Table 4.2:** Measurement of the pitch of close-packing arrays of polystyrene beads. Comparison is made between self-organized beads in intense optical field (B) and in dry close-packed monolayer array (D). Measurement have been done on the first order of diffraction at two different wavelengths (532 nm and 632.8 nm) and averaged.

particles.

$$d = \frac{2b}{\sqrt{3}} \quad (4.4)$$

The results measured with the first order of diffraction, recorded at two different wavelengths, are presented in table 4.2 and on the graph of figure 4.11. In the case of dry close-packing arrays, no spacing between the beads are noticed, while for beads assembled in an intense optical field, additional gaps are perceived. For 2.06  $\mu\text{m}$  beads, the difference corresponds to 154 nm; for 0.98  $\mu\text{m}$  beads it corresponds to 301 nm; and for 0.77  $\mu\text{m}$  beads it corresponds to 95 nm. The presence of a gap between particles is clearly a manifestation of optical binding. In the present case, the binding forces act against the gradient force and tend to separate the beads while the gaussian potential well try to get them in contact. A variation of the crystal pitch due to size distribution and size discrimination during the two different processes (binding and drying) can be excluded. Indeed, the beads diameter variation in the sample is smaller than the value of the gap found in the experiment (according to the manufacturer, standard deviation are 0.025, 0.029 and 0.024  $\mu\text{m}$  for 0.77, 0.98 and 2.06  $\mu\text{m}$  beads diameter respectively). For large beads, measurement errors are bigger due to smaller distance between diffraction spot. This explains the variation between B/D cases. For particles with a diameter greater than 2-microns ( $\varnothing=3.5 \mu\text{m}$  and  $\varnothing=5 \mu\text{m}$ ) no spacing was observed in optically bound crystals. This fact was

also reported by Singer et al.[159] in a one-dimensional case, although their work relates to a very different configuration. Obviously, lateral scattering in our case is much weaker than the forward scattering used for binding in an inline trap between two fibers. On the other hand, the large number of objects taking part in the process enhances the binding effect. The numerical values of the gap should be compared with theoretical simulations; this was unfortunately not feasible in the frame of this study.

## 4.4 Conclusion

The influence of optical binding on two-dimensional arrangement of particles has been presented through different experiments. The manufacturing of large crystals of particles is limited in size and leads to formation of dislocations in the optical arrangement. Observations and measurements performed in the k-space gave information on the crystal properties. By this mean, the inter-particle spacing has been studied and gaps between spheres depending on their size has been observed for particles up to two microns in diameter.



---

## Conclusion and Perspectives

## 5.1 Summary and Conclusions

In this thesis, we presented new schemes to sculpt light intensity distribution in order to create new templates adapted to multiple optical trapping. In particular we proposed and studied solutions to address simultaneously extremely large number of traps. This work relies essentially on the phenomenon of interference, particularly on its endless possibilities to shape the whole electromagnetic field. This is achieved by superposition of waves coming either from several laser beams, from dedicated phase structures or from the trapped objects themselves. By unconventional uses of diffraction, we built novel intensity landscapes to confine particles in two and three dimensions. The originality of this work relies on the unusual method employed for optical trapping.

In chapter 2 we studied different configurations for amplitude division and beams superposition. For linear and hexagonal traps, no a priori knowledge could serve as a guide for adapting trap's size to particle's dimension. The influence of the interferometric trap's size has been investigated for the first time and we reported that, in the studied cases, a fringes'size slightly bigger than the particle diameter was the most suited for an efficient trapping. It is well known that the intensity gradient is a key parameter for trapping particles in the Rayleigh and ray optics regimes. We showed experimentally how the gradient of intensity influences the trapping strength also in the Mie regime. In order to generate very sharp gradients, a novel approach using multiple beam interference has been proposed and tested to trap micron-sized particles.

Interferometric traps have been successfully implemented in a microfluidic environment giving promising solutions for lab-on-a-chip applications.

More complex interference schemes making use of a diffractive element have been realized in the Fresnel diffraction domain. The utilization of the diffraction of trapped particles has been exploited in an atypical way to create optical potential for trapping other particles. Another interesting feature of the Fresnel diffraction is the "self imaging" properties known as Talbot effect. It has been observed from a periodic array of trapped spheres. This phenomenon has been studied and revealed remarkable properties for optical trapping; the three dimensional landscaping, the high lateral intensity

gradients, the simplicity of the setup and the huge number of traps produced at once are among the assets of the system. The investigation through numerical simulations of Fresnel diffraction of periodic structures and the analysis of Talbot sub-images led to the optimization of structures for optical trapping. Diffractive plates with a chessboard like phase pattern show to be the most suited for trapping and offer up to a 16 times theoretical localized intensity enhancement.

Inevitably as soon as several particles are immersed in the same electromagnetic field, interaction effects due to optical binding have also been studied. Creation of large 2D arrays of spheres by self arrangement has been described and their limitations have been highlighted. Optical binding has been observed in 2D crystals for particles with diameter as big as two microns.

Trapping schemes presented in this work provide solutions for creating very large numbers of trapped objects, settling the possibility for rapid and massively parallel screening as often required in biotechnology. Up to 24,000 traps have been realized to trap 1-micron spheres simultaneously. All solutions proposed in this work to create traps avoid the need of high numerical aperture microscope objectives, this renders them easily implementable in microfluidics environment.

## 5.2 Perspectives

Our experimental results have shown the potential of various systems susceptible to perform massively parallel trapping. Combining optical manipulation and microfluidics was a constant concern over the entire work. Some further experiments are suggested hereunder to move forward a deeper understanding of optical mechanisms and to implement them in dedicated systems.

As explained earlier, a compensation of radiation pressure is necessary in several cases for trapping in the  $z$  direction. The reflecting interface used in some experiments could be advantageously replaced by an independent counter-propagating beam allowing a better control of the equilibrium in the optical axis, at the price of not recycling light. In the same idea, a four wave mixing setup, using photo-refractive crystals, could be used for a precise compensation of scattering force.

Talbot trapping has not yet been tested in microfluidics; insertion of Talbot structures in a microfluidic chip would allow further measurements of the trapping forces.

Finally, optical binding in two dimensions still lets a lot of room for research. The study of optical crystals with smaller particles, particularly with diameter smaller than the wavelength, would add to the comprehension of optical interactions. The suppression of the Gaussian intensity profile, for example by the use of "top-hat" beam shaper, could dissociate the effect of the gradient force of the one of the binding force and lead to a better understanding of this latter. The analysis of optical binding in interference fringes would be interesting to compare with the one dimensional case studied in other theoretical works.

Very large arrays of particles have been proposed and studied for the purpose of making extremely large mirrors for space telescopes. So-called "Laser Trap Mirrors" should be build in space. The concept still needs ample investigation.

The potential of coherent light to create interference still offers a wealth of promising opportunities to manipulate small objects.



---

# Acknowledgements

This work would have been impossible without the contribution of many persons, their scientific knowledge, their technical skills or their human qualities. All the conditions were met to achieve this PhD work within an pleasant framework. I want to express especially my grateful thanks to:

- René Salathé who was my thesis advisor and gave me the opportunity to make my PhD work in a dynamic environment at the Advanced Photonics Laboratory.
- Jean-Marc Fournier for having taught me the mysteries and subtleties of optics, for his patience, his competence, his confidence and his friendship. A special thanks for all the time he spent for the correction of the manuscript and for all the ideas he gave me.
- Kishan Dholakia (University of St. Andrews) and Tomasz Grzegorzczak (Massachusetts Institute of Technology) for having accepted to be members of the jury and for stimulating discussions.
- Pierre Jacquot for having accepted to be examiner of the thesis, to have let his lab and equipment at our disposal and for his useful advises and comments
- Olivier Martin for being president of the Jury
- Fabrice Merenda who was an excellent colleague not only for sharing his knowledge in general physics, quantum physics, Matlab, L<sup>A</sup>T<sub>E</sub>X,... but also for all the leisure time we spent together
- Guy Delacrétaz who created an enjoyable atmosphere in the group
- Gerben Boer for his great teaching qualities and the humour he spread
- Claude Amendola for all the mechanical pieces he made, for his availability and for all the tricks and tips he shared with me
- Alejandro Salamanca on who I could rely for all computer problems
- Ronald Gianotti for his help with electronic devices
- Alexandre Perentes for the nice ambiance in the office and for his coffee machine which was not useless to bring this thesis to an end
- Francois Aguet for helping me with image processing and for his technical support of ImageJ
- Jean Berney for interesting discussions and his help for L<sup>A</sup>T<sub>E</sub>X
- Thomas Sidler and his perpetual stimulating comments
- Thierry Blu for his support with Fresnel propagation
- Olivier Moine for his theoretical calculations of our experimental data
- Etienne Maréchal for interesting discussions on light propagation

- Lina Huang who continues working on our interference trapping setup
- Robert Johann and Ronit Marabi for their help with microfluidic devices
- Georges-André Racine who realized the Talbot diffractive plate at CMI
- Manuelle Borruat and Yvette Bernhard, our secretaries, for all the help they gave in many situations and for their kindness.

I also want to thanks all the students who worked on the optical trapping experiments: Xavier Tardy, Elodie Lamothe, Olivier Blanc, Jonathan Cretegy, Matthieu Grossenbacher, Yari Luchessa, Yoan Michaud, Schomiron Neogy, and Jolyon Roth. I am also grateful to all colleagues of the Institute of Applied Optics, who contributed to the smooth progress of this work. A special thanks to my family who always supported and encouraged me and particularly to Sophie for her understanding, her attention, and for all she did to prevent me from being totally caught by my optical traps.

This work was supported by CTI and CMMX.



---

# Appendix

## A Lab-on-a-chip

### A.1 State of the art

In the late 80's, thanks to the huge development of microtechnologies, many groups have started integrating several functions into a single chip. The idea to perform pre-treatment, analysis, cleaning and sorting of biological objects at a small scale has rapidly spread out giving birth to the concept of micro total analysis system ( $\mu$ TAS) or lab-on-a-chip (LOC). The first lab-on-a-chip was a chromatograph realized by Terry in 1975 [170]. Since then multiple functionalities have been integrated on LOC such as micropumps, microvalves and chemical sensors ([105, 106]). Very large scale of integration of microfluidics in a chip have been realized by Quake's group [171, 172, 173]. The addition of an integrated manipulation tool, thanks to optical tweezers, [11, 108] allows a increasingly more precise control, up to the single element level. Optical manipulation of passive elements can add features to a simple chip, for example optically driven micropumps or microvalves [109, 174, 175]. But the main advantage of the use of optical tweezers is the immobilization and transportation of biological objects in a non invasive way [176, 110, 107, 112, 177, 178]. Light template created through interference have been used for particles and cells sorting in microfluidics [13]. Microfluidic chips are generally molded in silicone elastomer by soft lithography. Figure A.1 shows a picture of a three-ways chip.

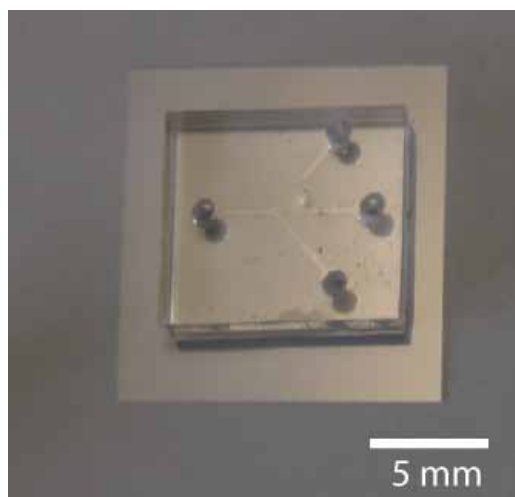


**Figure A.1:** Silicone microfluidic chip with three inlets and one outlet. Holes are punched for the connection to fluidic control tubes.

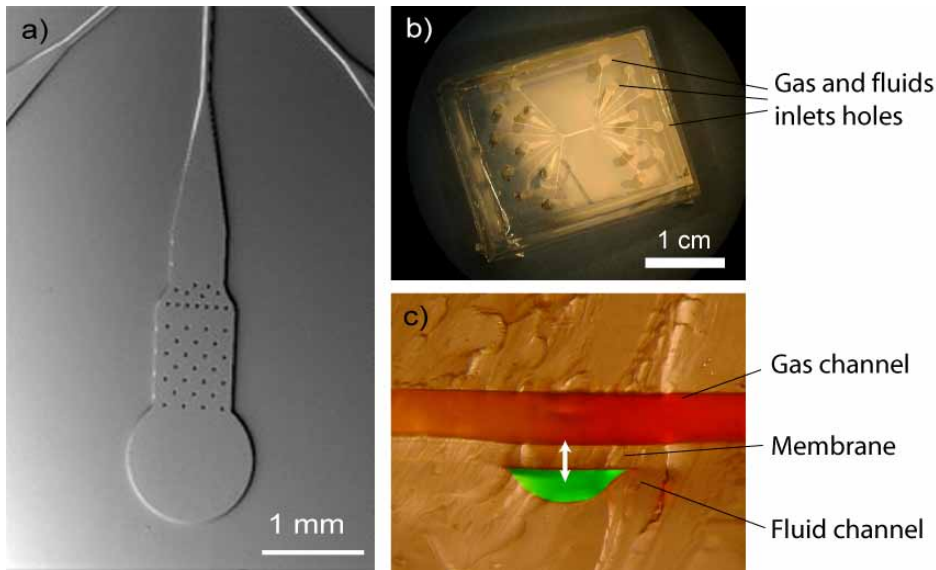


**Figure A.2:** Additional features on microfluidic chips. a) Filtering posts at the entrance of a channel. b) Three layer PDMS chip with pressure driven on-chip valves. c) Cross section of a valve.

## A.2 Microfluidic chip fabrication

Soft photolithography used to build microfluidic chips could be made through the facilities provided by the *Centre de Microtechnologies* (CMI) at EPFL. Standard process is summarized in this paragraph. A polydimethylsiloxane (PDMS) elastomer (Sylgard 184, Dow Corning, USA) is molded on a positive master of the channels made in SU-8 photoresist on silicon wafer by standard photolithography. The detailed technique of fabrication can be found in [179]. The 3 mm PDMS layer is cut in pieces after having been heated in oven for 2 hours at 70°C. Inlet entrances are punched by small tubes of 1 mm diameter. The cut piece of PDMS is bounded by surface activation in an oxygen plasma chamber to a standard thin microscope coverslip (ca. 170  $\mu\text{m}$  thick) which constitute the bottom of the chip. A schematic cut of a PDMS chip is presented in figure 2.17 a).

Simple microfluidic chips can be improved by adding other features. The addition of filters, at the inlets, consisting of PDMS posts prevents contamination and blocking of the channels (figure A.2 a)). A three-layer technique has been developed at the *Laboratory of Microsystems* to build on-chip valves for the independent control of each inlet's channel and is presented in figure A.2 b) and c).

### A.3 Lab-on-a-chip concept

The combination of microfluidic chips with micromanipulation tools and diagnosis systems such as fluorescence techniques (labelling with fluorescent marker, fluorescence lifetime imaging (FLIM), fluorescence resonant energy transfer (FRET), fluorescence recovery after photobleaching (FRAP)) or Raman spectroscopy provides a miniaturized analysis factory often combined in a standard inverted microscope used by biologists. Figure A.3 presents a setup combining various features of the lab-on-a-chip mounted on an inverted microscope. We built and used this system for online monitoring of hybridization of DNA immobilized on trapped beads. It was a simple multiple optical trapping systems, composed of independent laser diodes, associated with micro-biochemistry tools. This section of the thesis work is not reported in the present dissertation.



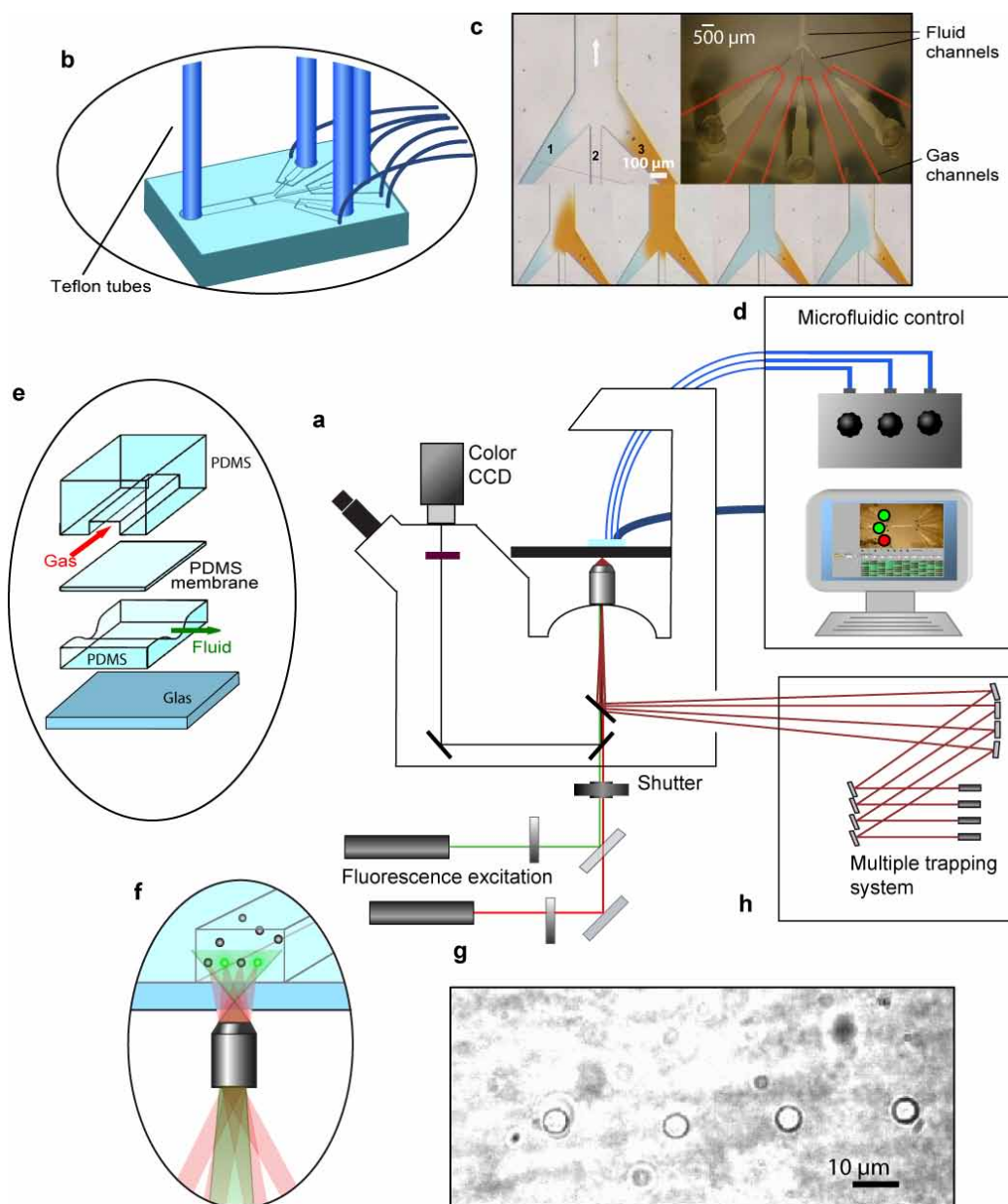
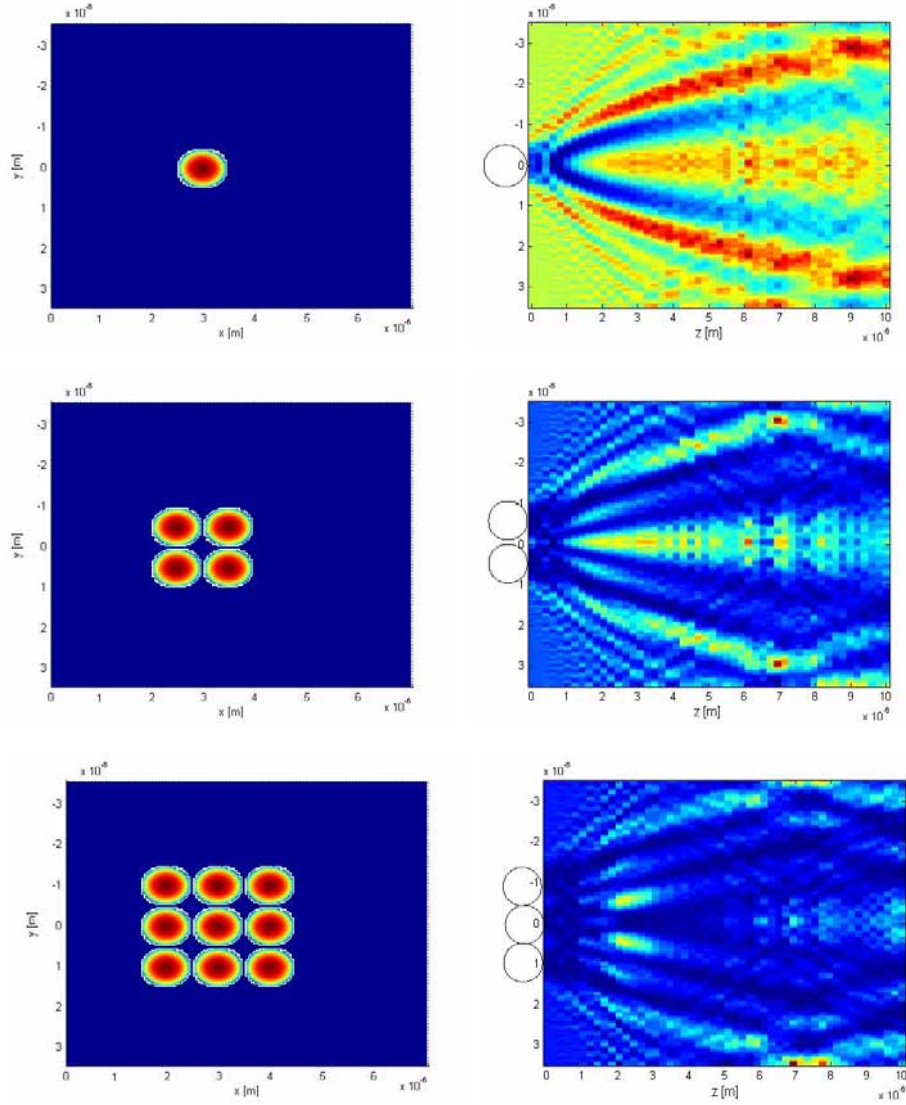


**Figure A.3:** a) Inverted microscope b) microfluidic chip connections: reactants reservoirs (larger tubes) and gas pressure (smaller tubes) c) Microfluidic chip with on-chip valves and flow sequence illustrated with colored solutions d) Microfluidic control (computer driven valves actuation and manual flow pressure regulation) and on-chip valve construction e) Construction of 3-layers valves f) Optical traps and fluorescence excitation g) Four 5- $\mu\text{m}$  polystyrene beads trapped in the central channel and observed in transmission h) Multiple optical traps generation (4 independent laser sources).

## B Fresnel calculations

The following figures present the results of numerical simulations of the Fresnel diffraction behind various structures calculated according to the method described in paragraph 3.3.3.

Phase shift in xy plane	Fresnel diffraction along yz axis
-------------------------	-----------------------------------



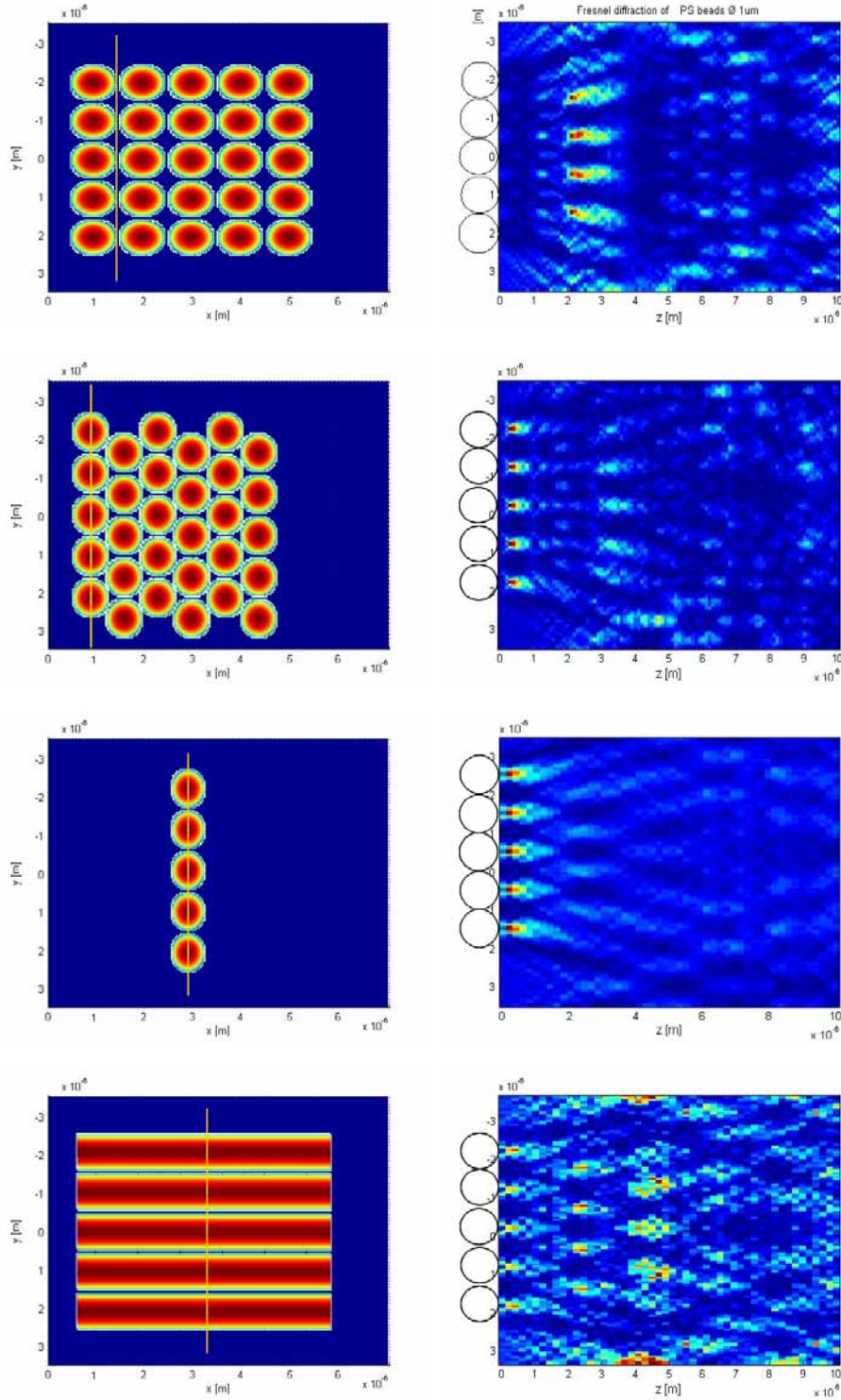


**Figure B.1:** Fresnel diffraction of beads or infinite cylinders. Left column: representation of the phase shift due to the beads or cylinders ( $n=1.6$ ). Right column: Fresnel diffraction calculated over 100 microns

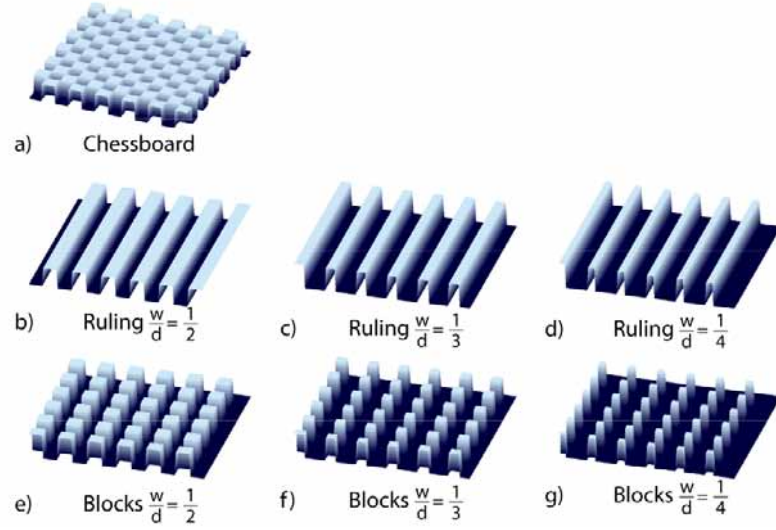


**Figure B.2:** Representation of simulated phase plate patterns for generation of Lohmann images.

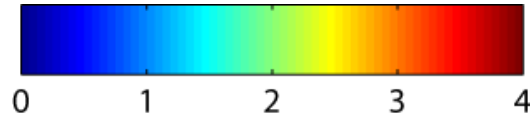


**Figure B.3:** Scale bar of intensity level [arbitrary units]- (illumination level is 1) for following simulation (except for figure B.5 and B.7 where maxima is 16)



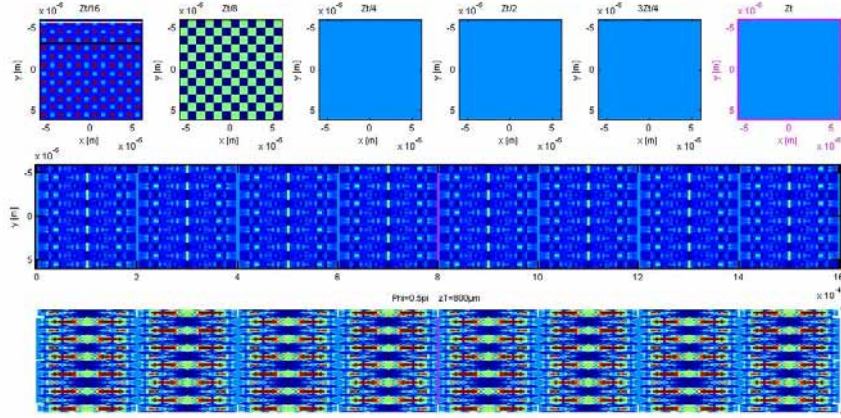


Figure B.4: Phase plate of figure B.2 a),  $\Delta\phi = \pi/2$ ,  $d = 20\mu\text{m}$

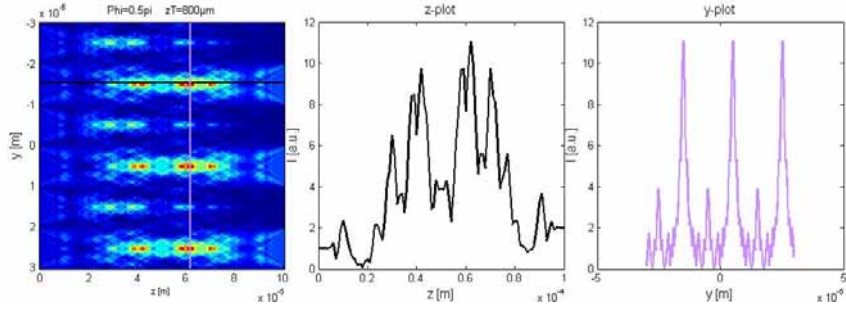


Figure B.5: Phase plate of figure B.2 a),  $\Delta\phi = \pi/2$ ,  $d = 20\mu\text{m}$

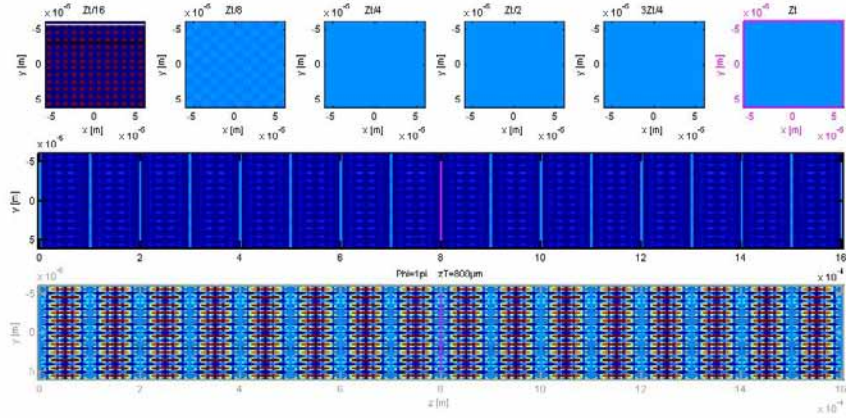


Figure B.6: Phase plate of figure B.2 a),  $\Delta\phi = \pi$ ,  $d = 20\mu\text{m}$

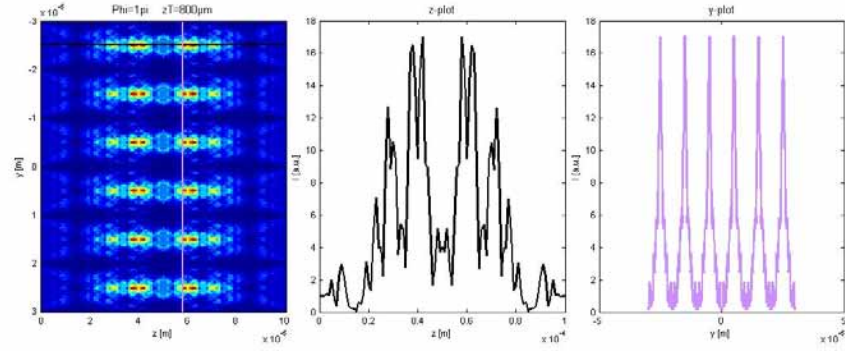


Figure B.7: Phase plate of figure B.2 a),  $\Delta\phi = \pi$ ,  $d = 20\mu\text{m}$

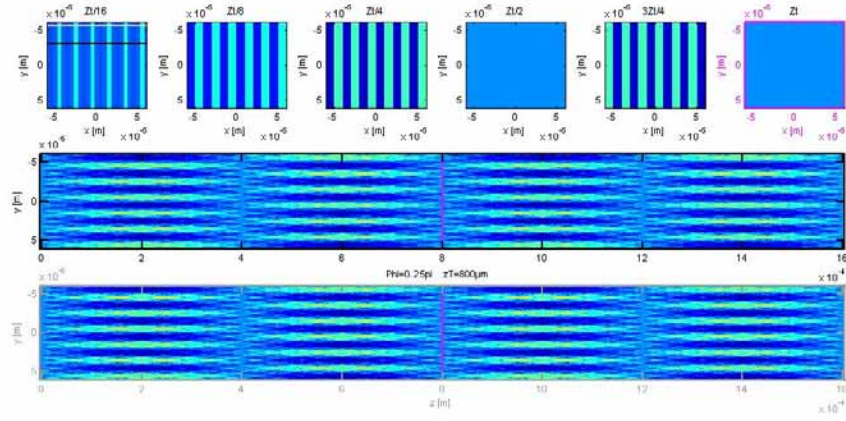


Figure B.8: Phase plate of figure B.2 b),  $\Delta\phi = \pi/4$ ,  $d = 20\mu\text{m}$

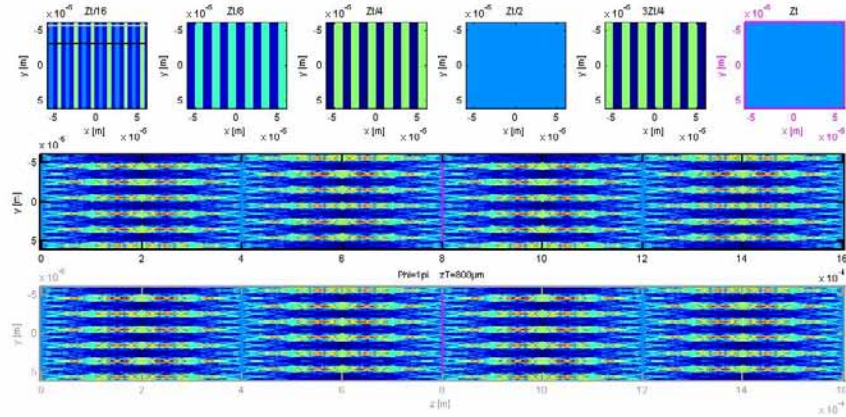
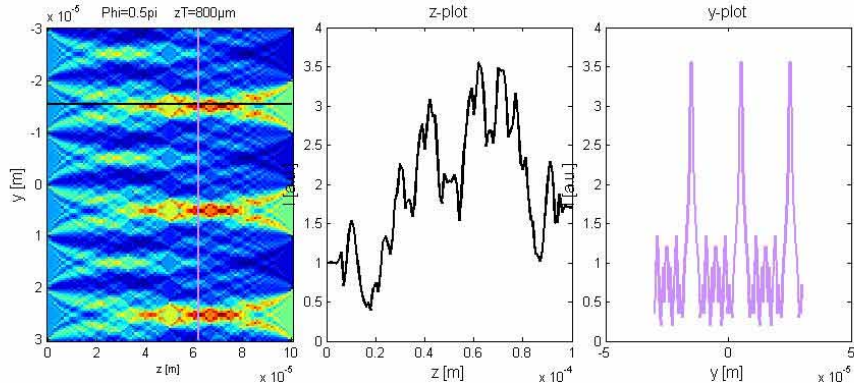
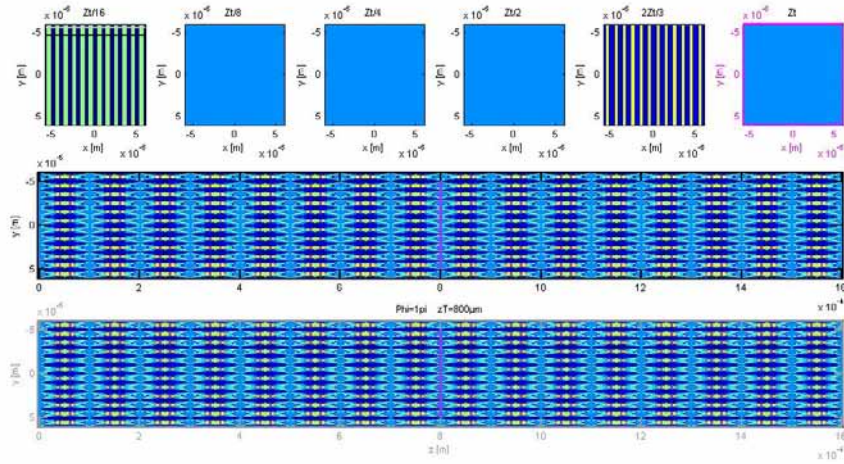


Figure B.9: Phase plate of figure B.2 b),  $\Delta\phi = \pi/2$ ,  $d = 20\mu\text{m}$



**Figure B.10:** Phase plate of figure B.2 b),  $\Delta\phi = \pi/2$ ,  $d = 20\mu\text{m}$



**Figure B.11:** Phase plate of figure B.2 b),  $\Delta\phi = \pi$ ,  $d = 20\mu\text{m}$

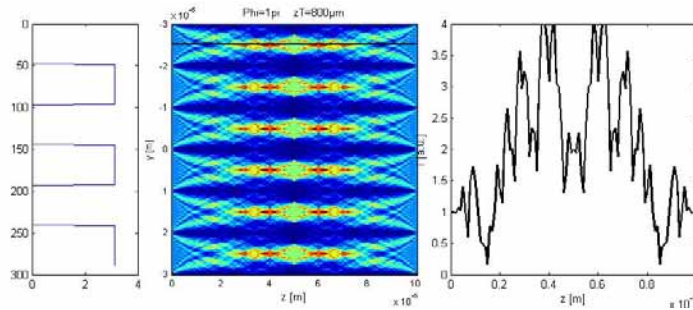


**Figure B.12:** Phase plate of figure B.2 b),  $\Delta\phi = \pi$ ,  $d = 20\mu\text{m}$



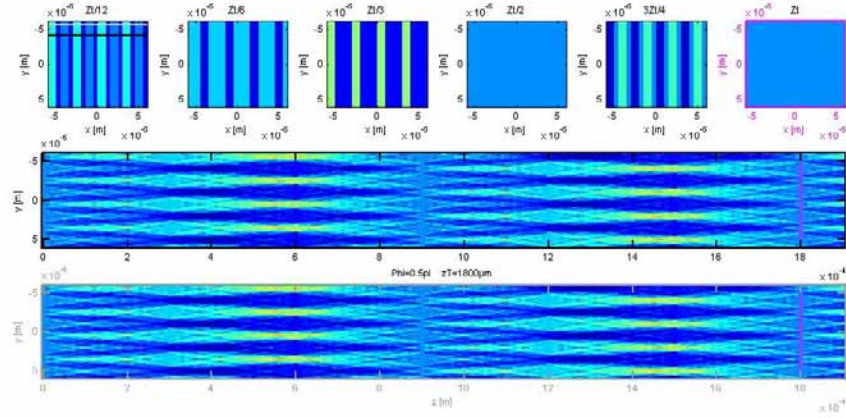


Figure B.13: Phase plate of figure B.2 c),  $\Delta\phi = \pi/2$ ,  $d = 30\mu\text{m}$

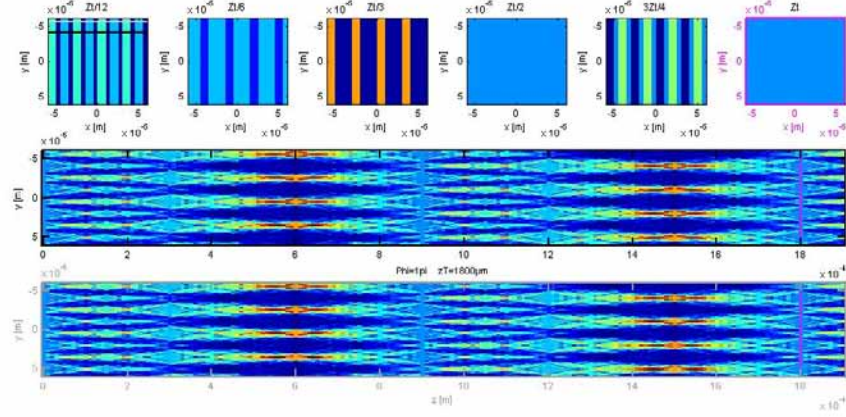


Figure B.14: Phase plate of figure B.2 c),  $\Delta\phi = \pi$ ,  $d = 30\mu\text{m}$

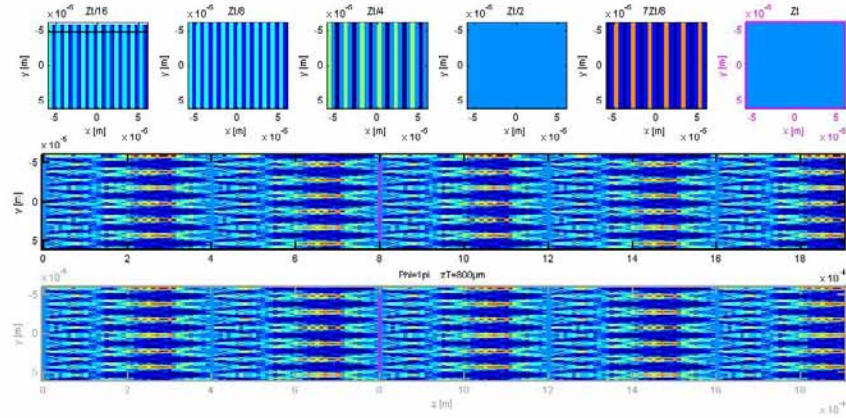


Figure B.15: Phase plate of figure B.2 d),  $\Delta\phi = \pi$ ,  $d = 20\mu\text{m}$



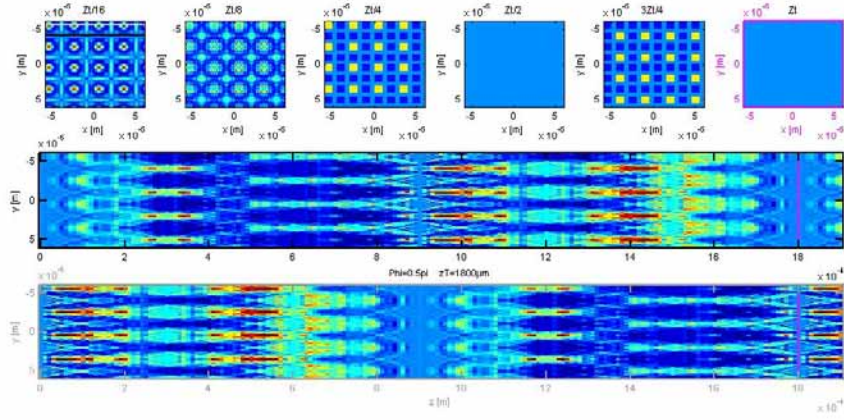


Figure B.16: Phase plate of figure B.2 f),  $\Delta\phi = \pi/2$ ,  $d = 30\mu\text{m}$

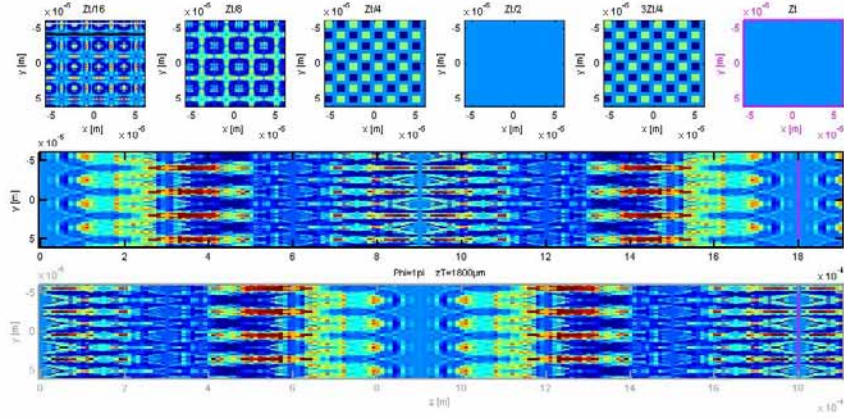


Figure B.17: Phase plate of figure B.2 f),  $\Delta\phi = \pi$ ,  $d = 30\mu\text{m}$

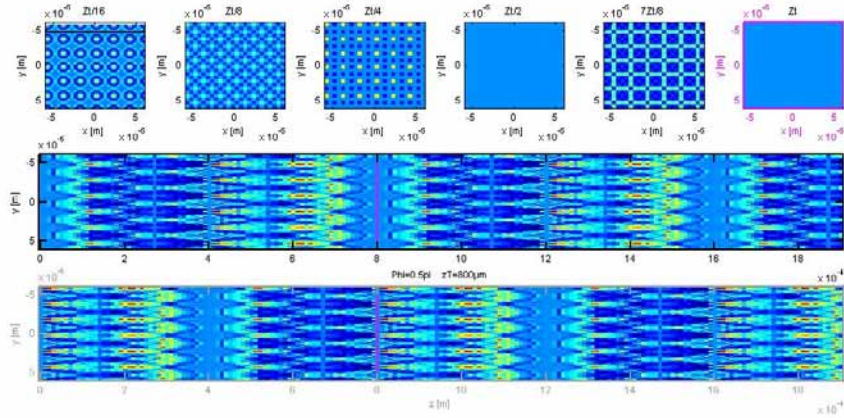
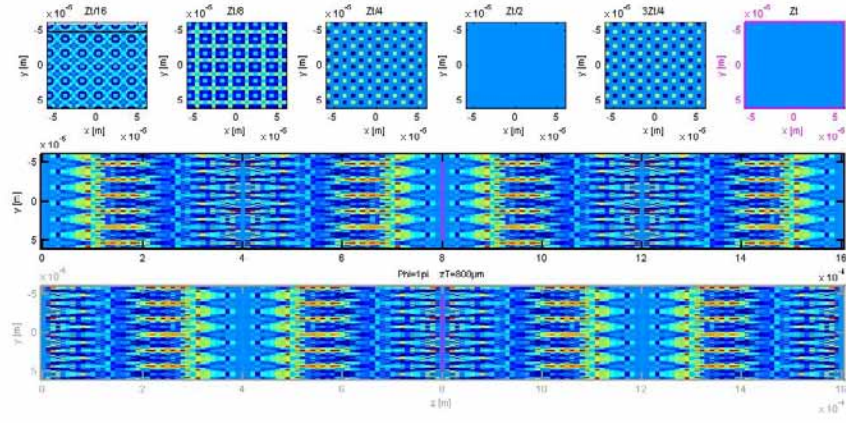


Figure B.18: Phase plate of figure B.2 g),  $\Delta\phi = \pi/2$ ,  $d = 20\mu\text{m}$



**Figure B.19:** Phase plate of figure B.2 g),  $\Delta\phi = \pi$ ,  $d = 20\mu\text{m}$

## C Diffractive plate fabrication

Diffractive plates have been realized through facilities at the *Centre de Microtechnologies* (CMI) at EPFL following our design. Chess-board-like patterns with next pitches have been etched in silica wafer: 1, 1.6, 2, 3, 3.6, 4, 5, 6, 7.6 and 10  $\mu\text{m}$ . For each pitch, two plates have been created on the wafer at different positions. This ensures that at least one of them has the desired depth, despite the concentric anisotropy in the etching depth uniformity. The patterns have been transferred on photoresist through direct laser writing. Since the scanning laser beam has a width of 200  $\mu\text{m}$ , the half of each graved pattern has been etched only on 180x180  $\mu\text{m}$  squares to prevent misalignment. The steps of the process are summarized hereunder. Figure C.1 shows the detailed layout and figure C.2 an optical and a SEM image of 3.5  $\mu\text{m}$  and 2.5  $\mu\text{m}$  structure respectively. Two wafers have been prepared with phase shift in water of  $\pi$  and  $\pi/2$  for a 532 nm wavelength according to following parameters:

Substrate:  $\text{SiO}_2$

Lambda  $\lambda$ : 532 nm

n Substrate:  $n_s = 1.46077$

n Water:  $n_w = 1.33585$  (25°C)

Ridges' Pitch : 1-10  $\mu\text{m}$

Ridges' Depth:

$$\Delta\phi = \frac{2\pi}{\lambda} \Delta\delta$$

$$\Delta\delta = (n_{\text{substrate}} - n_{\text{water}}) h$$

For  $\Delta\phi = \pi$ ,

$$h = \frac{0.532}{2(1.46077 - 1.33585)} = 2.129 \mu\text{m}$$

### Process

- Processing on fused silica 100mm wafer
- Desorption by plasma O<sub>2</sub> activation
- Coat and soft-bake AZ1512 photoresist (1.5  $\mu\text{m}$ )
- Direct laser writing of dense 2D draughtboard pattern
- Pattern transfer using AMS200 dry etcher
- Resist to silica selectivity PR:SiO<sub>2</sub> 1:7
- Etching depth uniformity 1.1% (structures inside 40mm radius circle)
- Final dicing of individuals chip

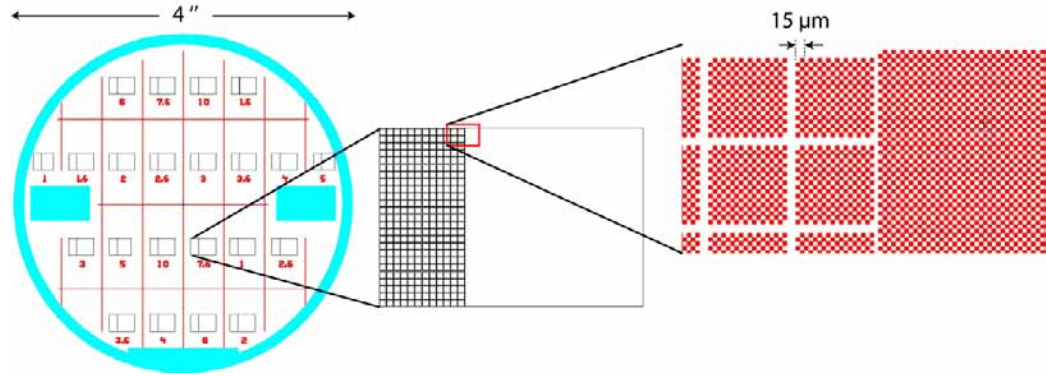


**Figure C.1:** Layout of a 4 inch  $\text{SiO}_2$  wafer with position of the diffractive structures. Numbers correspond to the half of the pitch of each pattern.

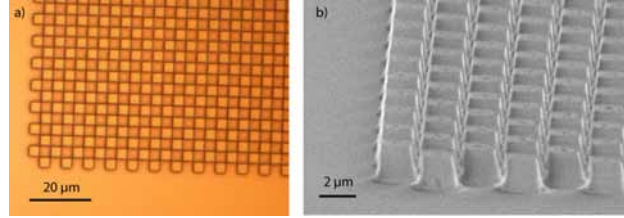


**Figure C.2:** a) Optical image of the top view of a  $3.6 \mu\text{m}$  chessboard structure. b) SEM image tilted by  $83^\circ$  of a  $2 \mu\text{m}$  structure.

The profile of the engraving was measured with an Alphastep 500 profiler on extension at the 4 angles of the pattern (the pattern itself being too fine to be measured) and is given in figure C.3. Table C.1 resumes measurements performed on two structures ( $1.6 \mu\text{m}$  and  $2 \mu\text{m}$ ) disposed at two different positions of the wafer. The etching depth corresponds to a  $\pi/2$  phase shift in water ( $1.0645 \mu\text{m}$  for  $\lambda = 532 \text{ nm}$ ).

Plate 2 microns Depth [ $\mu\text{m}$ ]	Plate 1.6 microns Depth [ $\mu\text{m}$ ]
1.066	0.995
1.053	0.99
1.069	1.005
1.068	0.995

**Table C.1:** Etching depth at the 4 corners of two structures (pitch =  $2 \mu\text{m}$  and  $1.6 \mu\text{m}$ , and  $\Delta\phi = \pi/2$ ) disposed at different positions on the wafer.

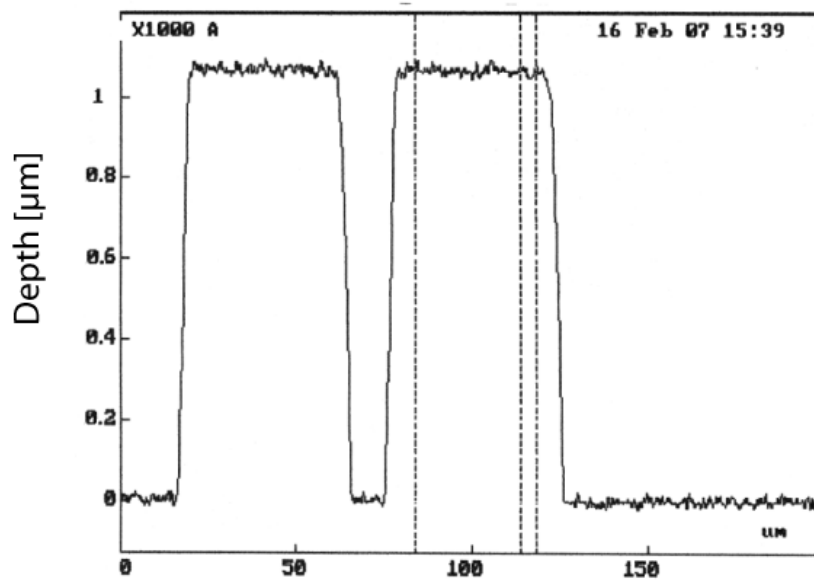


**Figure C.3:** Profile of the etching depth corresponding to a phase shift of  $\pi/2$  at 532 nm for the 2  $\mu\text{m}$  chessboard.



---

# Bibliography

- [1] E. F. Nichols and G. F. Hull, "The pressure due to radiation (second paper)," *Physical Review*, Vol. 17, No. 1, pp. 26–50, 1903. [2](#)
- [2] A. Ashkin, "Acceleration and trapping of particles by radiation pressure," *Physical Review Letters*, Vol. 24, No. 4, pp. 156–159, 1970. [2](#), [3](#)
- [3] A. Ashkin, J. M. Dziedzic, J. E. Bjorkholm, and S. Chu, "Observation of a single-beam gradient force optical trap for dielectric particles," *Optics Letters*, Vol. 11, No. 5, pp. 288–290, 1986. [2](#)
- [4] A. Ashkin, J. M. Dziedzic, and T. Yamane, "Optical trapping and manipulation of single cells using infrared-laser beams," *Nature*, Vol. 330, No. 6150, pp. 769–771, 1987. [3](#)
- [5] T. T. Perkins, S. R. Quake, D. E. Smith, and S. Chu, "Relaxation of a single DNA molecule observed by optical microscopy," *Science*, Vol. 264, No. 5160, pp. 822–826, 1994. [3](#)
- [6] M. Kurachi, M. Hoshi, and H. Tashiro, "Buckling of a single microtubule by optical trapping forces - direct measurement of microtubule rigidity," *Cell Motility and the Cytoskeleton*, Vol. 30, No. 3, pp. 221–228, 1995. [3](#)
- [7] M. D. Wang, H. Yin, R. Landick, J. Gelles, and S. M. Block, "Stretching DNA with optical tweezers," *Biophysical Journal*, Vol. 72, No. 3, pp. 1335–1346, 1997. [3](#)
- [8] Y. Tadir, W. H. Wright, O. Vafa, T. Ord, R. H. Asch, and M. W. Berns, "Micromanipulation of sperm by a laser generated optical trap," *Fertility and Sterility*, Vol. 52, No. 5, pp. 870–873, 1989. [3](#)
- [9] M. W. Berns, W. H. Wright, B. J. Tromberg, G. A. Profeta, J. J. Andrews, and R. J. Walter, "Use of a laser-induced optical force trap to study chromosome movement on the mitotic spindle," *Proceedings of the National Academy of Sciences of the United States of America*, Vol. 86, No. 12, pp. 4539–4543, 1989. [3](#)
- [10] J. Guck, R. Ananthakrishnan, T. J. Moon, C. C. Cunningham, and J. Kas, "Optical deformability of soft biological dielectrics," *Physical Review Letters*, Vol. 84, No. 23, pp. 5451–5454, 2000. [3](#), [4](#)
- [11] T. N. Buican, M. J. Smyth, H. A. Crissman, G. C. Salzman, C. C. Stewart, and J. C. Martin, "Automated single-cell manipulation and sorting by light trapping," *Applied Optics*, Vol. 26, No. 24, pp. 5311–5316, 1987. [3](#), [106](#)



- [12] M. M. Wang, E. Tu, D. E. Raymond, J. M. Yang, H. C. Zhang, N. Hagen, B. Dees, E. M. Mercer, A. H. Forster, I. Kariv, P. J. Marchand, and W. F. Butler, "Microfluidic sorting of mammalian cells by optical force switching," *Nature Biotechnology*, Vol. 23, No. 1, pp. 83–87, 2005. [3](#)
- [13] M. P. MacDonald, G. C. Spalding, and K. Dholakia, "Microfluidic sorting in an optical lattice," *Nature*, Vol. 426, No. 6965, pp. 421–424, 2003. [3](#), [32](#), [106](#)
- [14] Y. Liu, D. K. Cheng, G. J. Sonek, M. W. Berns, C. F. Chapman, and B. J. Tromberg, "Evidence for localized cell heating induced by infrared optical tweezers," *Biophysical Journal*, Vol. 68, No. 5, pp. 2137–2144, 1995. [3](#)
- [15] S. Ayano, Y. Wakamoto, S. Yamashita, and K. Yasuda, "Quantitative measurement of damage caused by 1064-nm wavelength optical trapping of escherichia coli cells using on-chip single cell cultivation system," *Biochemical and Biophysical Research Communications*, Vol. 350, No. 3, pp. 678–684, 2006. [3](#)
- [16] W. D. Phillips, "Laser cooling and trapping of neutral atoms," *Reviews of Modern Physics*, Vol. 70, No. 3, pp. 721–741, 1998. [3](#)
- [17] V. S. Letokhov, "Narrowing of doppler width in a standing light wave," *Jetp Letters-Ussr*, Vol. 7, No. 9, p. 272, 1968. [3](#)
- [18] T. W. Haensch and A. L. Schawlow, "Cooling of gases by laser radiation," *Optics Communications*, Vol. 13, No. 1, pp. 68–69, 1975. [3](#)
- [19] D. J. Wineland, R. E. Drullinger, and F. L. Walls, "Radiation-pressure cooling of bound resonant absorbers," *Physical Review Letters*, Vol. 40, No. 25, pp. 1639–1642, 1978. [3](#)
- [20] C. N. Cohentannoudji and W. D. Phillips, "New mechanisms for laser cooling," *Physics Today*, Vol. 43, No. 10, pp. 33–40, 1990. [3](#)
- [21] S. Chu, "Laser trapping of neutral particles," *Scientific American*, Vol. 266, No. 2, pp. 70–76, 1992. [3](#)
- [22] A. Chowdhury, B. J. Ackerson, and N. A. Clark, "Laser-induced freezing," *Physical Review Letters*, Vol. 55, No. 8, pp. 833–836, 1985. [3](#), [5](#), [13](#)
- [23] M. M. Burns, J. M. Fournier, and J. A. Golovchenko, "Optical matter - crystallization and binding in intense optical-fields," *Science*, Vol. 249, No. 4970, pp. 749–754, 1990. [3](#), [5](#), [13](#), [84](#)

- [24] A. Labeyrie, "Standing wave and pellicle - possible approach to very large space telescopes," *Astronomy and Astrophysics*, Vol. 77, No. 1-2, pp. L1-L2, 1979. [3](#)
- [25] K. Sasaki, M. Koshioka, H. Misawa, N. Kitamura, and H. Masuhara, "Pattern-formation and flow-control of fine particles by laser-scanning micromanipulation," *Optics Letters*, Vol. 16, No. 19, pp. 1463-1465, 1991. [3](#)
- [26] C. Mio, T. Gong, A. Terray, and D. W. M. Marr, "Design of a scanning laser optical trap for multiparticle manipulation," *Review of Scientific Instruments*, Vol. 71, No. 5, pp. 2196-2200, 2000. [3](#)
- [27] K. Visscher, S. P. Gross, and S. M. Block, "Construction of multiple-beam optical traps with nanometer-resolution position sensing," *Ieee Journal Of Selected Topics In Quantum Electronics*, Vol. 2, No. 4, pp. 1066-1076, 1996. [3](#)
- [28] A. Constable, J. Kim, J. Mervis, F. Zarinetchi, and M. Prentiss, "Demonstration of a fiberoptic light-force trap," *Optics Letters*, Vol. 18, No. 21, pp. 1867-1869, 1993. [4](#)
- [29] J. Kaes, J. Guck, and J. A. Chiang, "The optical stretcher - a novel tool to manipulate cells," *Biophysical Journal*, Vol. 76, No. 1, pp. A276-a276, 1999. [4](#)
- [30] S. Kawata and T. Tani, "Optically driven Mie particles in an evanescent field along a channeled waveguide," *Optics Letters*, Vol. 21, No. 21, pp. 1768-1770, 1996. [4](#)
- [31] C. D. Mellor, M. A. Sharp, C. D. Bain, and A. D. Ward, "Probing interactions between colloidal particles with oscillating optical tweezers," *Journal Of Applied Physics*, Vol. 97, No. 10, 2005. [4](#), [84](#)
- [32] M. Siler, T. Cizmar, M. Sery, and P. Zemanek, "Optical forces generated by evanescent standing waves and their usage for sub-micron particle delivery," *Applied Physics B-Lasers and Optics*, Vol. 84, No. 1-2, pp. 157-165, 2006. [4](#), [5](#), [35](#)
- [33] S. Gaugiran, S. Getin, J. M. Fedeli, G. Colas, A. Fuchs, F. Chatelain, and J. Derouard, "Optical manipulation of microparticles and cells on silicon nitride waveguides," *Optics Express*, Vol. 13, No. 18, pp. 6956-6963, 2005. [4](#)
- [34] J.-M. Fournier, M. M. Burns, and J. A. Golovchenko, "Writing diffractive structures by optical trapping," in *Practical Holography IX*, vol. 2406, pp. 101-111, SPIE Proc., 1995. [4](#), [5](#), [13](#), [63](#), [84](#)

- [35] M. Reichert, T. Haist, E. U. Wagemann, and H. J. Tiziani, "Optical particle trapping with computer-generated holograms written on a liquid-crystal display," *Optics Letters*, Vol. 24, No. 9, pp. 608–610, 1999. 4, 5
- [36] Y. Hayasaki, M. Itoh, T. Yatagai, and N. Nishida, "Nonmechanical optical manipulation of microparticle using spatial light modulator," *Optical Review*, Vol. 6, No. 1, pp. 24–27, 1999. 4, 5
- [37] E. R. Dufresne, G. C. Spalding, M. T. Dearing, S. A. Sheets, and D. G. Grier, "Computer-generated holographic optical tweezer arrays," *Review Of Scientific Instruments*, Vol. 72, No. 3, pp. 1810–1816, 2001. 4, 5
- [38] H. Melville, G. F. Milne, G. C. Spalding, W. Sibbett, K. Dholakia, and D. McGloin, "Optical trapping of three-dimensional structures using dynamic holograms," *Optics Express*, Vol. 11, No. 26, pp. 3562–3567, 2003. 4, 5
- [39] G. Sinclair, P. Jordan, J. Courtial, M. Padgett, J. Cooper, and Z. J. Laczik, "Assembly of 3-dimensional structures using programmable holographic optical tweezers," *Optics Express*, Vol. 12, No. 22, pp. 5475–5480, 2004. 4, 5
- [40] P. C. Mogenssen and J. Gluckstad, "Dynamic away generation and pattern formation for optical tweezers," *Optics Communications*, Vol. 175, No. 1-3, pp. 75–81, 2000. 4
- [41] J. Gluckstad, "Phase contrast image synthesis," *Optics Communications*, Vol. 130, No. 4-6, pp. 225–230, 1996. 4
- [42] C. Mennerat-Robilliard, D. Boiron, J. M. Fournier, A. Aradian, P. Horak, and G. Grynberg, "Cooling cesium atoms in a Talbot lattice," *Europhysics Letters*, Vol. 44, No. 4, pp. 442–448, 1998. 4, 63
- [43] Y. Ogura, K. Kagawa, and J. Tanida, "Optical manipulation of microscopic objects by means of vertical-cavity surface-emitting laser array sources," *Applied Optics*, Vol. 40, No. 30, pp. 5430–5435, 2001. 4
- [44] R. Dumke, M. Volk, T. Muther, F. B. J. Buchkremer, G. Birkl, and W. Ertmer, "Micro-optical realization of arrays of selectively addressable dipole traps: A scalable configuration for quantum computation with atomic qubits," *Physical Review Letters*, Vol. 89, No. 9, pp. –, 2002. 4
- [45] C. H. Sow, A. A. Bettiol, Y. Y. G. Lee, F. C. Cheong, C. T. Lim, and F. Watt, "Multiple-spot optical tweezers created with microlens arrays fabricated by

- proton beam writing,” *Applied Physics B-Lasers And Optics*, Vol. 78, No. 6, pp. 705–709, 2004. 4
- [46] F. Merenda, J. Rohner, P. Pascoal, J. M. Fournier, H. Vogel, and R. P. Salathe, “Refractive multiple optical tweezers for parallel biochemical analysis in micro-fluidics,” in *Complex Light and Optical Forces* (D. L. Andrews, ed.), vol. 6483, (San Jose), p. 08, SPIE Proc., 2007. 4
- [47] F. Merenda, J. Rohner, J. M. Fournier, and R. P. Salathe, “Miniaturized high-na focusing-mirror multiple optical tweezers,” *Optics Express*, Vol. 15, No. 10, pp. 6075–6086, 2007. 4
- [48] M. Ozkan, T. Pisanic, J. Scheel, C. Barlow, S. Esener, and S. N. Bhatia, “Electro-optical platform for the manipulation of live cells,” *Langmuir*, Vol. 19, No. 5, pp. 1532–1538, 2003. 4
- [49] P. Y. Chiou, A. T. Ohta, and M. C. Wu, “Massively parallel manipulation of single cells and microparticles using optical images,” *Nature*, Vol. 436, No. 7049, pp. 370–372, 2005. 4
- [50] M. P. Hughes, “Strategies for dielectrophoretic separation in laboratory-on-a-chip systems,” *Electrophoresis*, Vol. 23, No. 16, pp. 2569–2582, 2002. 4
- [51] U. Seger, S. Gawad, R. Johann, A. Bertsch, and P. Renaud, “Cell immersion and cell dipping in microfluidic devices,” *Lab On A Chip*, Vol. 4, No. 2, pp. 148–151, 2004. 4
- [52] C. R. Cabrera and P. Yager, “Continuous concentration of bacteria in a microfluidic flow cell using electrokinetic techniques,” *Electrophoresis*, Vol. 22, No. 2, pp. 355–362, 2001. 4
- [53] F. Assi, R. Jenks, J. Yang, C. Love, and M. Prentiss, “Massively parallel adhesion and reactivity measurements using simple and inexpensive magnetic tweezers,” *Journal Of Applied Physics*, Vol. 92, No. 9, pp. 5584–5586, 2002. 4
- [54] J. O. Kessler, “Hydrodynamic focusing of motile algal cells,” *Nature*, Vol. 313, No. 5999, pp. 218–220, 1985. 4
- [55] H. M. Hertz, “Standing-wave acoustic trap for nonintrusive positioning of microparticles,” *Journal of Applied Physics*, Vol. 78, No. 8, pp. 4845–4849, 1995. 4

- [56] V. A. Liu and S. N. Bhatia, "Three-dimensional photopatterning of hydrogels containing living cells," *Biomedical Microdevices*, Vol. 4, No. 4, pp. 257–266, 2002. 4
- [57] I. M. Peters, B. G. de Grooth, J. M. Schins, C. G. Figdor, and J. Greve, "Three dimensional single-particle tracking with nanometer resolution," *Review Of Scientific Instruments*, Vol. 69, No. 7, pp. 2762–2766, 1998. 4
- [58] M. M. Burns, J. M. Fournier, and J. A. Golovchenko, "Optical binding," *Physical Review Letters*, Vol. 63, No. 12, pp. 1233–1236, 1989. 4, 84
- [59] J. E. Curtis, B. A. Koss, and D. G. Grier, "Dynamic holographic optical tweezers," *Optics Communications*, Vol. 207, No. 1-6, pp. 169–175, 2002. 5
- [60] K. T. Gahagan and G. A. Swartzlander, "Optical vortex trapping of particles," *Optics Letters*, Vol. 21, No. 11, pp. 827–829, 1996. 5
- [61] P. A. Prentice, M. P. MacDonald, T. G. Frank, A. Cuschieri, G. C. Spalding, W. Sibbett, P. A. Campbell, and K. Dholakia, "Manipulation and filtration of low index particles with holographic laguerre-gaussian optical trap arrays," *Optics Express*, Vol. 12, No. 4, pp. 593–600, 2004. 5
- [62] W. M. Lee, X. C. Yuan, and W. C. Cheong, "Optical vortex beam shaping by use of highly efficient irregular spiral phase plates for optical micromanipulation," *Optics Letters*, Vol. 29, No. 15, pp. 1796–1798, 2004. 5
- [63] S. Parkin, G. Knoner, T. A. Nieminen, N. R. Heckenberg, and H. Rubinsztein-Dunlop, "Measurement of the total optical angular momentum transfer in optical tweezers," *Optics Express*, Vol. 14, No. 15, pp. 6963–6970, 2006. 5
- [64] V. Garces-Chavez, D. McGloin, H. Melville, W. Sibbett, and K. Dholakia, "Simultaneous micromanipulation in multiple planes using a self-reconstructing light beam," *Nature*, Vol. 419, No. 6903, pp. 145–147, 2002. 5
- [65] D. McGloin, G. C. Spalding, H. Melville, W. Sibbett, and K. Dholakia, "Three-dimensional arrays of optical bottle beams," *Optics Communications*, Vol. 225, No. 4-6, pp. 215–222, 2003. 5
- [66] K. Ladavac and D. G. Grier, "Microoptomechanical pumps assembled and driven by holographic optical vortex arrays," *Optics Express*, Vol. 12, No. 6, pp. 1144–1149, 2004. 5

- [67] A. Jesacher, S. Furhapter, S. Bernet, and M. Ritsch-Marte, “Diffractive optical tweezers in the fresnel regime,” *Optics Express*, Vol. 12, No. 10, pp. 2243–2250, 2004. 5
- [68] D. G. Grier, “A revolution in optical manipulation,” *Nature*, Vol. 424, No. 6950, pp. 810–816, 2003. 5
- [69] D. L. J. Vossen, A. van der Horst, M. Dogterom, and A. van Blaaderen, “Optical tweezers and confocal microscopy for simultaneous three-dimensional manipulation and imaging in concentrated colloidal dispersions,” *Review Of Scientific Instruments*, Vol. 75, No. 9, pp. 2960–2970, 2004. 5
- [70] C. D. Mellor and C. D. Bain, “Array formation in evanescent waves,” *Chemphyschem*, Vol. 7, No. 2, pp. 329–332, 2006. 5, 13, 84
- [71] A. E. Chiou, W. Wang, G. J. Sonek, J. Hong, and M. W. Berns, “Interferometric optical tweezers,” *Optics Communications*, Vol. 133, No. 1-6, pp. 7–10, 1997. 5, 13
- [72] M. P. MacDonald, L. Paterson, W. Sibbett, K. Dholakia, and P. E. Bryant, “Trapping and manipulation of low-index particles in a two-dimensional interferometric optical trap,” *Optics Letters*, Vol. 26, No. 12, pp. 863–865, 2001. 5
- [73] A. Casaburi, G. Pesce, P. Zemanek, and A. Sasso, “Two- and three-beam interferometric optical tweezers,” *Optics Communications*, Vol. 251, No. 4-6, pp. 393–404, 2005. 5, 13
- [74] W. Mu, G. Wang, L. Luan, G. C. Spalding, and J. B. Ketterson, “Dynamic control of defects in a two-dimensional optically assisted assembly,” *New Journal of Physics*, Vol. 8, 2006. 5, 13
- [75] J. M. Fournier, G. Boer, G. Delacretaz, P. Jacquot, J. Rohner, and R. P. Salathe, “Building optical matter with binding and trapping forces,” in *Optical Trapping and Optical Micromanipulation* (G. C. S. K. Dholakia, ed.), vol. 5514, (Denver), pp. 309–317, Proc. SPIE, 2004. 5
- [76] J. M. Fournier, J. Rohner, P. Jacquot, R. Johann, S. Mias, and R. P. Salathe, “Assembling mesoscopic particles by various optical schemes,” in *Optical Trapping and Optical Micromanipulation II* (G. C. S. K. Dholakia, ed.), vol. 5930, (San Diego), p. 32, SPIE Proc., 2005. 5, 63
- [77] G. Roosen, “La lévitation optique de sphères,” *Can. J. Phys.*, Vol. 57, pp. 1260–1279, 1979. 8

- [78] A. Ashkin, "Forces of a single-beam gradient laser trap on a dielectric sphere in the ray optics regime," *Biophysical Journal*, Vol. 61, No. 2, pp. 569–582, 1992. [8](#)
- [79] P. C. Ke and M. Gu, "Characterization of trapping force on metallic Mie particles," *Applied Optics*, Vol. 38, No. 1, pp. 160–167, 1999. [8](#)
- [80] F. Merenda, G. Boer, J. Rohner, G. Delacretaz, and R. P. Salathe, "Escape trajectories of single-beam optically trapped micro-particles in a transverse fluid flow," *Optics Express*, Vol. 14, No. 4, pp. 1685–1699, 2006. [8](#)
- [81] K. Visscher and G. J. Brakenhoff, "Theoretical-study of optically induced forces on spherical-particles in a single beam trap I Rayleigh scatterers," *Optik*, Vol. 89, No. 4, pp. 174–180, 1992. [9](#)
- [82] B. Richards and E. Wolf, "Electromagnetic diffraction in optical systems .2. structure of the image field in an aplanatic system," *Proceedings of the Royal Society of London Series a-Mathematical and Physical Sciences*, Vol. 253, No. 1274, pp. 358–379, 1959. [9](#)
- [83] Y. Harada and T. Asakura, "Radiation forces on a dielectric sphere in the Rayleigh scattering regime," *Optics Communications*, Vol. 124, No. 5-6, pp. 529–541, 1996. [9](#)
- [84] P. Zemanek, V. Karasek, and A. Sasso, "Optical forces acting on Rayleigh particle placed into interference field," *Optics Communications*, Vol. 240, No. 4-6, pp. 401–415, 2004. [9](#), [35](#)
- [85] G. Mie, "Articles on the optical characteristics of turbid tubes, especially colloidal metal solutions," *Annalen Der Physik*, Vol. 25, No. 3, pp. 377–445, 1908. [9](#)
- [86] A. Ashkin and J. M. Dziedzic, "Observation of optical resonances of dielectric spheres by light-scattering," *Applied Optics*, Vol. 20, No. 10, pp. 1803–1814, 1981. [9](#), [35](#)
- [87] J. S. Kim and S. S. Lee, "Radiation pressure on a dielectric sphere in a gaussian laser-beam," *Optica Acta*, Vol. 29, No. 6, pp. 801–806, 1982. [9](#), [35](#)
- [88] J. S. Kim and S. S. Lee, "Scattering of laser-beams and the optical-potential well for a homogeneous sphere," *Journal of the Optical Society of America*, Vol. 73, No. 3, pp. 303–312, 1983. [9](#)

- [89] K. F. Ren, G. Gréhan, and G. Gouesbet, “Radiation pressure forces exerted on a particle arbitrarily located in a gaussian-beam by using the generalized Lorenz-Mie theory, and associated resonance effects,” *Optics Communications*, Vol. 108, No. 4-6, pp. 343–354, 1994. [9](#), [35](#)
- [90] O. Moine and B. Stout, “Optical force calculations in arbitrary beams by use of the vector addition theorem,” *Journal of the Optical Society of America B-Optical Physics*, Vol. 22, No. 8, pp. 1620–1631, 2005. [9](#)
- [91] K. Visscher and G. J. Brakenhoff, “Theoretical-study of optically induced forces on spherical-particles in a single beam trap II Mie scatterers,” *Optik*, Vol. 90, No. 2, pp. 57–60, 1992. [9](#)
- [92] J. A. Lock, “Calculation of the radiation trapping force for laser tweezers by use of generalized Lorenz-Mie theory I localized model description of an on-axis tightly focused laser beam with spherical aberration,” *Applied Optics*, Vol. 43, No. 12, pp. 2532–2544, 2004. [9](#)
- [93] B. A. Kemp, T. M. Grzegorzczuk, and J. A. Kong, “Ab initio study of the radiation pressure on dielectric and magnetic media,” *Optics Express*, Vol. 13, No. 23, pp. 9280–9291, 2005. [10](#), [35](#), [85](#)
- [94] T. M. Grzegorzczuk, B. A. Kemp, and J. A. Kong, “Trapping and binding of an arbitrary number of cylindrical particles in an in-plane electromagnetic field,” *Journal of the Optical Society of America A-Optics Image Science and Vision*, Vol. 23, No. 9, pp. 2324–2330, 2006. [10](#), [26](#), [35](#), [85](#)
- [95] B. A. Kemp, T. M. Grzegorzczuk, and J. A. Kong, “Lorentz force on dielectric and magnetic particles,” *Journal of Electromagnetic Waves and Applications*, Vol. 20, No. 6, pp. 827–839, 2006. [10](#), [26](#), [35](#)
- [96] O. Moine, *Modélisation de forces optiques*. PhD thesis, Université Paul Cézanne, 2005. [10](#), [26](#), [35](#), [40](#)
- [97] E. Schonbrun, R. Piestun, P. Jordan, J. Cooper, K. D. Wulff, J. Courtial, and M. Padgett, “3D interferometric optical tweezers using a single spatial light modulator,” *Optics Express*, Vol. 13, No. 10, pp. 3777–3786, 2005. [13](#), [63](#)
- [98] M. P. MacDonald, L. Paterson, K. Volke-Sepulveda, J. Arlt, W. Sibbett, and K. Dholakia, “Creation and manipulation of three-dimensional optically trapped structures,” *Science*, Vol. 296, No. 5570, pp. 1101–1103, 2002. [13](#)



- 
- [99] J. Gluckstad, "Microfluidics - sorting particles with light," *Nature Materials*, Vol. 3, No. 1, pp. 9–10, 2004. 13
- [100] T. Cizmar, V. Garces-Chavez, K. Dholakia, and P. Zemanek, "Optical conveyor belt for delivery of submicron objects," *Applied Physics Letters*, Vol. 86, No. 17, pp. –, 2005. 26
- [101] W. H. Wright, G. J. Sonek, and M. W. Berns, "Parametric study of the forces on microspheres held by optical tweezers," *Applied Optics*, Vol. 33, No. 9, pp. 1735–1748, 1994. 28
- [102] H. Felgner, O. Muller, and M. Schliwa, "Calibration of light forces in optical tweezers," *Applied Optics*, Vol. 34, No. 6, pp. 977–982, 1995. 28
- [103] W. Wang, A. E. Chiou, G. J. Sonek, and M. W. Berns, "Self-aligned dual-beam optical laser trap using photorefractive phase conjugation," *Journal Of The Optical Society Of America B-Optical Physics*, Vol. 14, No. 4, pp. 697–704, 1997. 30
- [104] A. E. Chiou, "Photorefractive phase-conjugate optics for image processing, trapping, and manipulation of microscopic objects," *Proceedings of the Ieee*, Vol. 87, No. 12, pp. 2074–2085, 1999. 30
- [105] D. R. Reyes, D. Iossifidis, P. A. Auroux, and A. Manz, "Micro total analysis systems. 1. introduction, theory, and technology," *Analytical Chemistry*, Vol. 74, No. 12, pp. 2623–2636, 2002. 31, 106
- [106] H. Andersson and A. van den Berg, "Microfluidic devices for cellomics: a review," *Sensors and Actuators B-Chemical*, Vol. 92, No. 3, pp. 315–325, 2003. 31, 106
- [107] C. Q. Yi, C. W. Li, S. L. Ji, and M. S. Yang, "Microfluidics technology for manipulation and analysis of biological cells," *Analytica Chimica Acta*, Vol. 560, No. 1-2, pp. 1–23, 2006. 31, 106
- [108] F. Arai, A. Ichikawa, M. Ogawa, T. Fukuda, K. Horio, and K. Itoigawa, "High-speed separation system of randomly suspended single living cells by laser trap and dielectrophoresis," *Electrophoresis*, Vol. 22, No. 2, pp. 283–288, 2001. 31, 106
- [109] A. Terray, J. Oakey, and D. W. M. Marr, "Fabrication of linear colloidal structures for microfluidic applications," *Applied Physics Letters*, Vol. 81, No. 9, pp. 1555–1557, 2002. 31, 106

- [110] M. Ozkan, M. Wang, C. Ozkan, R. Flynn, A. Birkbeck, and S. Esener, "Optical manipulation of objects and biological cells in microfluidic devices," *Biomedical Microdevices*, Vol. 5, No. 1, pp. 61–67, 2003. 31, 106
- [111] S. Umehara, Y. Wakamoto, I. Inoue, and K. Yasuda, "On-chip single-cell microcultivation assay for monitoring environmental effects on isolated cells," *Biochemical and Biophysical Research Communications*, Vol. 305, No. 3, pp. 534–540, 2003. 31
- [112] J. Enger, M. Goksor, K. Ramser, P. Hagberg, and D. Hanstorp, "Optical tweezers applied to a microfluidic system," *Lab On A Chip*, Vol. 4, No. 3, pp. 196–200, 2004. 31, 106
- [113] P. Jakl, M. Sery, J. Jezek, and P. Zemanek, "How the size of a particle approaching dielectric interface influences its behavior," in *Proceedings of SPIE - The International Society for Optical Engineering*, vol. 5514, pp. 636–642, 2004. 35
- [114] T. Cizmar, M. Siler, M. Sery, P. Zemanek, V. Garces-Chavez, and K. Dholakia, "Optical sorting and detection of submicrometer objects in a motional standing wave," *Physical Review B*, Vol. 74, No. 3, p. 035105, 2006. 35
- [115] W. Mu, Z. L. Li, L. Luan, P. West, H. Kyriazis, G. Spalding, G. Wang, A. Feinerman, and J. B. Ketterson, "Force measurement and optical assisted particle separation in an optical standing wave," in *Optical Trapping and Optical Micromanipulation IV* (G. C. S. K. Dholakia, ed.), vol. 6644, (San Diego), p. 66440R, SPIE, 2007. 42
- [116] M. Moller and W. Lange, "Radiation trapping - an alternative mechanism for chaos in a nonlinear-optical resonator," *Physical Review A*, Vol. 49, No. 5, pp. 4161–4169, 1994. 42
- [117] J. Rohner, J. M. Fournier, P. Jacquot, F. Merenda, and R. P. Salathe, "Multiple optical trapping in high gradient interference fringes," in *Optical Trapping and Optical Micromanipulation III* (G. C. S. K. Dholakia, ed.), vol. 6326, (San Diego), p. 07, SPIE Proc., 2006. 42
- [118] S. Tolansky, "An interferometric procedure for the examination of crystal surfaces," *Nature*, Vol. 152, pp. 722–723, 1943. 42
- [119] S. Tolansky, "Low-order multiple-beam interferometry," *Proceedings of the Physical Society of London*, Vol. 58, No. 330, pp. 654–662, 1946. 42

- [120] S. Tolansky, *An introduction to interferometry*. London: Longman, second ed., 1973. 42
- [121] J. Brossel, "Multiple-beam localized fringes .1. intensity distribution and localization," *Proceedings of the Physical Society of London*, Vol. 59, No. 332, pp. 224–233, 1947. 42
- [122] M. Françon, *Optical interferometry*. New York and London: Academic Press, 1966. 42
- [123] N. Aebischer, *Etudes d'interférences en ondes multiple par une méthode graphique application aux franges d'égale épaisseur*. PhD thesis, Université de Besançon, 1969. 43
- [124] N. Aebischer, "Etudes d'interférences en ondes multiples par diagramme complexe pour visualiser les franges en réflexion," *Nouvelle Revue d'Optique Appliquée*, Vol. 1, No. 4, pp. 233–248, 1970. 43
- [125] J. Holden, "Multiple-beam interferometry - intensity distribution in the reflected system," *Proceedings of the Physical Society of London Section A*, Vol. 62, No. 7, pp. 405–417, 1949. 44
- [126] V. Berger, O. GauthierLafaye, and E. Costard, "Photonic band gaps and holography," *Journal of Applied Physics*, Vol. 82, No. 1, pp. 60–64, 1997. 53
- [127] W. H. F. Talbot, "Facts relating to optical science no. iv," *Philosophical Magazine*, Vol. 9, pp. 401–407, 1836. 60
- [128] L. Rayleigh, "On copying diffraction gratings, and on some phenomena connected therewith," *Philosophical Magazine*, Vol. 11, pp. 196–201, 1881. 61
- [129] J. T. Winthrop and Worthing.Cr, "Theory of fresnel images .i. plane periodic objects in monochromatic light," *Journal of the Optical Society of America*, Vol. 55, No. 4, pp. 373–381, 1965. 61
- [130] K. Patorski, "The self-imaging phenomenon and its applications," *Progress In Optics*, Vol. 27, pp. 3–108, 1989. 61
- [131] P. Latimer and R. F. Crouse, "Talbot effect reinterpreted," *Applied Optics*, Vol. 31, No. 1, pp. 80–89, 1992. 61
- [132] A. W. Lohmann, J. Schwider, N. Streibl, and J. Thomas, "Array illuminator based on phase-contrast," *Applied Optics*, Vol. 27, No. 14, pp. 2915–2921, 1988. 61

- [133] A. W. Lohmann and J. A. Thomas, "Making an array illuminator based on the talbot effect," *Applied Optics*, Vol. 29, No. 29, pp. 4337–4340, 1990. 61
- [134] J. R. Leger and G. J. Swanson, "Efficient array illuminator using binary-optics phase plates at fractional-talbot planes," *Optics Letters*, Vol. 15, No. 5, pp. 288–290, 1990. 61
- [135] T. J. Suleski, "Generation of lohmann images from binary-phase talbot array illuminators," *Applied Optics*, Vol. 36, No. 20, pp. 4686–4691, 1997. 61
- [136] H. Hamam, "Design of talbot array illuminators," *Optics Communications*, Vol. 131, No. 4-6, pp. 359–370, 1996. 61
- [137] P. Xi, C. H. Zhou, E. W. Dai, and L. R. Liu, "Generation of near-field hexagonal array illumination with a phase grating," *Optics Letters*, Vol. 27, No. 4, pp. 228–230, 2002. 61
- [138] A. Kolodziejczyk, Z. Jaroszewicz, R. Henao, and O. Quintero, "The talbot array illuminator: imaging properties and a new interpretation," *Journal Of Optics A-Pure And Applied Optics*, Vol. 6, No. 6, pp. 651–657, 2004. 61
- [139] E. Lau, "Beugungserscheinungen an doppelrastern," *Annalen Der Physik*, Vol. 2, No. 7-8, pp. 417–423, 1948. 61
- [140] J. Jahns and A. W. Lohmann, "Lau effect (a diffraction experiment with incoherent illumination)," *Optics Communications*, Vol. 28, No. 3, pp. 263–267, 1979. 61
- [141] P. Latimer, "Talbot plane patterns - grating images or interference effects," *Applied Optics*, Vol. 32, No. 7, pp. 1078–1083, 1993. 63
- [142] B. Besold and N. Lindlein, "Fractional talbot effect for periodic microlens arrays," *Optical Engineering*, Vol. 36, No. 4, pp. 1099–1105, 1997. 63
- [143] O. Bryngdahl, "Image formation using self-imaging techniques," *Journal of the Optical Society of America*, Vol. 63, No. 4, pp. 416–419, 1973. 63
- [144] J. R. Leger, M. Holz, G. J. Swanson, and W. B. Veldkamp, "Coherent laser beam addition: An application of binary-optics technology," *The Lincoln Laboratory Journal*, Vol. 1, No. 2, pp. 225–244, 1988. 63
- [145] G. S. Spagnolo and D. Ambrosini, "Talbot effect application: measurement of distance with a fourier-transform method," *Measurement Science and Technology*, Vol. 11, No. 1, pp. 77–82, 2000. 63

- [146] D. S. Mehta, S. K. Dubey, C. Shakher, and M. Takeda, “Two-wavelength talbot effect and its application for three-dimensional step-height measurement,” *Applied Optics*, Vol. 45, No. 29, pp. 7602–7609, 2006. 63
- [147] S. Jeon, V. Malyarchuk, J. A. Rogers, and G. P. Wiederrecht, “Fabricating three dimensional nanostructures using two photon lithography in a single exposure step,” *Optics Express*, Vol. 14, No. 6, pp. 2300–2308, 2006. 63
- [148] R. Newell, J. Sebby, and T. G. Walker, “Dense atom clouds in a holographic atom trap,” *Optics Letters*, Vol. 28, No. 14, pp. 1266–1268, 2003. 63
- [149] Y. Y. Sun, X. C. Yuan, L. S. Ong, J. Bu, S. W. Zhu, and R. Liu, “Large-scale optical traps on a chip for optical sorting,” *Applied Physics Letters*, Vol. 90, No. 3, 2007. 63
- [150] M. Liebling, *On fresnelets, interference fringes, and digital holography*. PhD thesis, Ecole Polytechnique Fédérale de Lausanne, 2004. 66
- [151] J. W. Goodman, *Introduction to Fourier optics*. Engelwood: Roberts, 3rd ed. ed., 2005. 66
- [152] V. Arrizon and E. Lopezolazagasti, “Binary phase grating for array generation at 1/6 of talbot length,” *Journal of the Optical Society of America A-Optics Image Science and Vision*, Vol. 12, No. 4, pp. 801–804, 1995. 72
- [153] F. Depasse and J. M. Vigoureux, “Optical binding force between 2 Rayleigh particles,” *Journal Of Physics D-Applied Physics*, Vol. 27, No. 5, pp. 914–919, 1994. 84
- [154] P. C. Chaumet and M. Nieto-Vesperinas, “Optical binding of particles with or without the presence of a flat dielectric surface,” *Physical Review B*, Vol. 6403, No. 3, 2001. 84, 85
- [155] S. K. Mohanty, J. T. Andrews, and P. K. Gupta, “Optical binding between dielectric particles,” *Optics Express*, Vol. 12, No. 12, pp. 2746–2753, 2004. 84
- [156] M. Guillon, O. Moine, and B. Stout, “Longitudinal optical binding of high optical contrast microdroplets in air,” *Physical Review Letters*, Vol. 96, No. 14, p. 143902, 2006. 84
- [157] M. Guillon, “Field enhancement in a chain of optically bound dipoles,” *Optics Express*, Vol. 14, No. 7, pp. 3045–3055, 2006. 84

- 
- [158] S. A. Tatarkova, A. E. Carruthers, and K. Dholakia, "One-dimensional optically bound arrays of microscopic particles," *Physical Review Letters*, Vol. 89, No. 28, 2002. 84
- [159] W. Singer, M. Frick, S. Bernet, and M. Ritsch-Marte, "Self-organized array of regularly spaced microbeads in a fiber-optical trap," *Journal Of The Optical Society Of America B-Optical Physics*, Vol. 20, No. 7, pp. 1568–1574, 2003. 84, 95
- [160] V. Karasek, K. Dholakia, and P. Zemanek, "Analysis of optical binding in one dimension," *Applied Physics B-Lasers and Optics*, Vol. 84, No. 1-2, pp. 149–156, 2006. 84
- [161] N. K. Metzger, E. M. Wright, W. Sibbett, and K. Dholakia, "Visualization of optical binding of microparticles using a femtosecond fiber optical trap," *Optics Express*, Vol. 14, No. 8, pp. 3677–3687, 2006. 84
- [162] D. McGloin, A. E. Carruthers, K. Dholakia, and E. M. Wright, "Optically bound microscopic particles in one dimension," *Physical Review E*, Vol. 69, No. 2, 2004. 84
- [163] T. M. Grzegorzczuk, B. A. Kemp, and J. A. Kong, "Stable optical trapping based on optical binding forces," *Physical Review Letters*, Vol. 96, No. 11, p. 113903, 2006. 84
- [164] J. Ng, Z. F. Lin, C. T. Chan, and P. Sheng, "Photonic clusters formed by dielectric microspheres: Numerical simulations," *Physical Review B*, Vol. 72, No. 8, p. 085130, 2005. 84
- [165] T. M. Grzegorzczuk, B. A. Kemp, and J. A. Kong, "Passive guiding and sorting of small particles with optical binding forces," *Optics Letters*, Vol. 31, No. 22, pp. 3378–3380, 2006. 85
- [166] D. Maystre and P. Vincent, "Making photonic crystals using trapping and binding optical forces on particles," *Journal of Optics a-Pure and Applied Optics*, Vol. 8, No. 12, pp. 1059–1066, 2006. 85
- [167] A. Dereux, C. Girard, O. J. F. Martin, and M. Devel, "Optical binding in scanning probe microscopy," *Europhysics Letters*, Vol. 26, No. 1, pp. 37–42, 1994. 85
- [168] M. Guillon, "Optical trap shaping for binding force study and optimization," in *Proceedings of SPIE - The International Society for Optical Engineering*, vol. 6483, 2007. 88, 90, 91

- [169] J. Ng, Z. Hang, Z. Lin, P. Sheng, and C. Chan, "Theoretical study of optical forces and bindings," in *Optical Trapping for Molecular Interactions*, (Lausanne. Switzerland), 2007. 88, 90
- [170] S. C. Terry, *A gas chromatography system fabricated on a silicon wafer. using integrated circuit technology*. PhD thesis, Stanford Univ., CA, 1975. 106
- [171] M. A. Unger, H. P. Chou, T. Thorsen, A. Scherer, and S. R. Quake, "Monolithic microfabricated valves and pumps by multilayer soft lithography," *Science*, Vol. 288, No. 5463, pp. 113–116, 2000. 106
- [172] S. R. Quake and A. Scherer, "From micro- to nanofabrication with soft materials," *Science*, Vol. 290, No. 5496, pp. 1536–1540, 2000. 106
- [173] T. Thorsen, S. J. Maerkl, and S. R. Quake, "Microfluidic large-scale integration," *Science*, Vol. 298, No. 5593, pp. 580–584, 2002. 106
- [174] J. Leach, H. Mushfique, R. di Leonardo, M. Padgett, and J. Cooper, "An optically driven pump for microfluidics," *Lab on a Chip*, Vol. 6, No. 6, pp. 735–739, 2006. 106
- [175] R. W. Applegate, J. Squier, T. Vestad, J. Oakey, and D. W. M. Marr, "Optical trapping, manipulation, and sorting of cells and colloids in microfluidic systems with diode laser bars," *Optics Express*, Vol. 12, No. 19, pp. 4390–4398, 2004. 106
- [176] P. Mitchell, "Microfluidics - downsizing large-scale biology," *Nature Biotechnology*, Vol. 19, No. 8, pp. 717–721, 2001. 106
- [177] D. N. Breslauer, P. J. Lee, and L. P. Lee, "Microfluidics-based systems biology," *Molecular Biosystems*, Vol. 2, No. 2, pp. 97–112, 2006. 106
- [178] E. Eriksson, J. Enger, B. Nordlander, N. Erjavec, K. Ramser, M. Goksor, S. Hohmann, T. Nystrom, and D. Hanstorp, "A microfluidic system in combination with optical tweezers for analyzing rapid and reversible cytological alterations in single cells upon environmental changes," *Lab on a Chip - Miniaturisation for Chemistry and Biology*, Vol. 7, No. 1, pp. 71–76, 2007. 106
- [179] D. C. Duffy, J. C. McDonald, O. J. A. Schueller, and G. M. Whitesides, "Rapid prototyping of microfluidic systems in poly(dimethylsiloxane)," *Analytical Chemistry*, Vol. 70, No. 23, pp. 4974–4984, 1998. 107





---

# Curriculum vitae

## JOHANN ROHNER

October, 31<sup>st</sup> 1978

Nationality: Swiss

johann.rohner@a3.epfl.ch

### EDUCATION

<b>PhD Thesis</b> at the Swiss Federal Institute of Technology (EPFL), Lausanne (thesis advisor: R.P. Salathé) Institute of Applied Optics	2003-2007
<b>Swiss Federal Institute of Technology</b> (EPFL), Lausanne Engineer diploma Microengineering Orientation: Production's techniques and robotics <i>Prize: Hilti Mechatronic, 2002</i>	1997-2002
<b>Technische Universität Darmstadt</b> (D), Erasmus student	1999-2000
<b>Gymnase de la Cité</b> (Lausanne): Federal maturity (University ad- mission) Section XB (Latin - English - Mathematics) <i>Prizes : Latin and antique culture, Physics, Sport</i>	1994-1997

### EXPERIENCE

<b>Researcher</b> and <b>Assistant</b> at the Institute for Applied Optics (EPFL)	2003-2007
One Year <b>civil service</b> in Basel in a house for Drugs addict people (Haus Elim)	2002-2003
Creation of <b>Web Sites</b> solutions for the Protestant Church	2001-2006
<b>Assistant</b> at the Microcontroller course	2001
Two practical training's in the computer science laboratory of the EPFL , domain: microcontroller; Achievement of assemblers for varied processors	1999 / 2000
Practical training on machines (one month) at the Ecole des métiers (ETML), Lausanne	1999
Two month work at the company Dubois-Dépraz (Le Lieu): watch assembly	1997

## PROJECTS

- |   |           |
|---|-----------|
| PhD Thesis on Light structuring for massively parallel <b>optical trapping</b>  | 2003-2007 |
| <b>Modeling and control of an orthosis</b> for rehabilitation of paraplegic; biomechanical studies, human movements simulation (diploma work)                 | 2002      |
| <b>Electrical muscles stimulation system</b> for the mentioned orthosis: creation of a program for microcontroller and PC program for command (semester work) | 2001      |

## LANGUAGES

- |               |   |
|---------------|---|
| French :      | Mother language   |
| German :      | Spoken and written fluently (two years spent in Germany and in Basel) |
| English :     | Spoken and written level <i>First</i>                                 |
| Swiss German: | Oral comprehension  |
| Spanish :     | Oral knowledge  |

## COMPUTER KNOWLEDGE

- |   |
|---|
| Very Good knowledge of MS Windows and software: Word, Excel, Power-Point, Adobe Photoshop       |
| Knowledge of UNIX/LINUX operating systems. Adobe Premiere and Illustrator                       |
| Basic Knowledges of Labview, Pro-Engineer, L-Edit, MS Access, MS Project, Adobe Premiere, Flash |
| Technical drawing with I-Deas, Ashlar Vellum  |
| Programming in C, assembler, Matlab, $\text{\LaTeX}$ , PHP, HTML and web design                 |

## OTHER FORMATIONS

- |  |
|--|
| Accounting and financial management course                     |
| Certificate of instructor for young people in ski hiking (J+S) |
| Formation of leader for catechumen (JACK)                      |

## HOBBIES

Climbing and mountain sports: member of the Swiss alpine club (CAS)  
 Sport: alpine ski, cross-country ski, ski hiking, bike trips, member of the gymnastic society (FSG)  
 President of State Council for Youth of Protestant Church and member of the Department Council for Formation  
 Trumpeter at the symphonic *Orchestre de Ribeaupierre*

## PUBLICATIONS

- J. Rohner, J. M. Fournier, P. Jacquot, F. Merenda and R. P. Salathe (2006). Multiple Optical Trapping in High Gradient Interference Fringes. Optical Trapping and Optical Micromanipulation III, San Diego, Proc. SPIE.
- F. Merenda, J. Rohner, J. -M. Fournier, and R. -P. Salathé (2007), Miniaturized high-NA focusing-mirror multiple optical tweezers, Opt. Express 15, 6075-6086.
- F. Merenda, G. Boer, J. Rohner, G. Delacretaz and R. P. Salathe (2006). Escape trajectories of single-beam optically trapped micro-particles in a transverse fluid flow. Optics Express 14(4): 1685-1699.
- J.M. Fournier, J. Rohner, P. Jacquot, R. Johann, S. Mias and R. P. Salathe (2005). Assembling mesoscopic particles by various optical schemes. Optical Trapping and Optical Micromanipulation II, San Diego, Proc. SPIE.
- J. M. Fournier, G. Boer, G. Delacrétaz, P. Jacquot, J. Rohner and R. P. Salathé (2004). Building Optical Matter with Binding and Trapping Forces. Optical Trapping and Optical Micromanipulation, Denver, Proc. SPIE.

## PRESENTATIONS

- Parallel bioanalytics monitored on multiple laser-trapped beads in a micro-fluidic system. Latsis symposium, Lausanne, 2007
- Parallel bioanalytics monitored on multiple laser-trapped beads in microfluidics, BMPN, Zuerich, 2007
- Optical manipulation of large number of particles. Invited speaker, LCPPM Winterschool, Loeche, 2007
- Multiple Optical Trapping in High Gradient Interference Fringes. SPIE conference San Diego 2006
- Optical Trapping in High Gradient Interference Fringes. Solid State and Photonics Lab. Stanford University
- Beam shaping for large assemblies of optical traps. Munich 2005